NASA CONTRACTOR
REPORT

Report No. 61285

ACOUSTIC LOADS AT THE BASE OF
ENGINE CLUSTERS

By D. O. Barnett and H. A. Cikanek

Northrop-Huntsville,
Huntsville, Alabama

May 1969

Prepared for

NASA-GEORGE C. MARSHALL SPACE FLIGHT CENTER
Marshall Space Flight Center, Alabama 35812

1. Report No. NASA CR-61285	2. Government Accession No.	3. Recipient's Catalog No.
4. Title and Subtitle ACOUSTIC LOADS AT THE BASE OF ENGINE CLUSTERS		5. Report Date May 1969
		6. Performing Organization Code
7. Author(s) D. O. Barnett and H. A. Cikanek		8. Performing Organization Report No. TR-794-9-536
9. Performing Organization Name and Address Northrop-Huntsville Huntsville, Alabama		10. Work Unit No.
		11. Contract or Grant No. NAS8-20082
		13. Type of Report and Period Covered
12. Sponsoring Agency Name and Address Marshall Space Flight Center, NASA Aero-Astrodynamics Laboratory Huntsville, Alabama 35812		
		14. Sponsoring Agency Code
15. Supplementary Notes		

16. Abstract

SEE THE REVERSE SIDE OF THIS PAGE

17. Key Words acoustic and hydromechanically induced loads, flow geometry, plume clusters	18. Distribution Statement FOR PUBLIC RELEASE: E. D. GEISSLER Dir, Aero-Astrodynamics Lab, MSFC		
19. Security Classif. (of this report) Uncl	20. Security Classif. (of this page) U	21. No. of Pages 98	22. Price

ABSTRACT

The first phase of a program to determine acoustic and hydromechanically induced dynamic loads at the base of Saturn configured vehicles is covered in this report. An experimental program was conducted in support of this goal using a clustered rocket model and the Cold Flow Duct of the Marshall Space Flight Center Thermal Acoustic Jet Facility. The total experiment consisted of several separate investigations. Schlieren and shadowgraph photography were used to determine the flow geometry and shock structure of plume clusters. In those regions determined of interest from the photographic data, pitot pressure distribution across the plumes were measured. Finally, the static and dynamic pressure distributions were measured on a rigid baseplate for simulated rocket clusters of one to five engines exhausting over a range of stagnation-to-ambient pressure ratios.

Data are reported on distributions of mean static pressures and root-mean-square levels, power spectral densities, and space-time correlations of the fluctuating pressures at the base of engine clusters. Additionally, the distributions of velocities and pressures across the jets and the extent of the shear layer are given.

An attempt is made to define those factors influential to the dynamic loads at the base of engine clusters in terms of acoustic and hydromechanical components. The base loading characteristics of the lower stages of the Saturn vehicle are then discussed on the basis of these conclusions. Finally, recommendations are made for future studies for the determination of scaling factors of dynamic loads.

FOREWORD

This report presents the results of an exploratory investigation into the nature of acoustic loadings at the base of engine clusters. The subject study was performed under the direction of Dr. F. Krause and Mr. Ira Jones of the Fluid Mechanics Research Office of the Aero-Astrodynamics Laboratory of Marshall Space Flight Center under Contract NAS8-20082, Appendix B, Schedule Order No. 127.

Several persons contributed to the completion of this study. In addition to the aforementioned NASA Program Managers, special mention is due Drs. M. J. Fisher and J. M. Clinch of I.I.T. Research Institute who arranged for reduction of much of the spectral data to be discussed and who offered many helpful comments on the test procedures and instrumentation used.

TABLE OF CONTENTS

LIST OF ILLUSTRATIONS

LIST OF ILLUSTRATIONS (Continued)

LIST OF ILLUSTRATIONS (Concluded)

LIST OF TABLES

NOMENCLATURE

Symbol	Definition	Units
A^*	Throat Area	in^2
C_a	Ambient Acoustic Speed	ft/sec
D	Nozzle Exit Diameter	in.
D^*	Throat Diameter	in.
f	Frequency	Hz
f_c	Centerband Frequency	Hz
f_u	Upper Cut-off Frequency	Hz
$f(\theta)$	Distribution Function	
Δf	Filter Bandwidth	Hz
F	Jet Thrust	lb_f
g	Gravitational Constant	$32.176 \ ft/sec^2$
$G(\omega)$	Power Spectral Density	$psi^2/rad/sec$
I	Sound Pressure Level	dB
k_o	Wave Number	ft^{-1}
$K(f)$	Dimensionless Power Spectral Density	
m	Exponent	
M	Mach Number	
$p(x,t)$	Instantaneous Static Pressure	psi
$p'(x,t)$	Fluctuating Component of Static Pressure	psi
$\bar{p}(x)$	Mean Static Pressure	psi
$\overline{p^2(x)}$	Mean Square Static Pressure	psi^2
$\left\langle p'^2(x) \right\rangle$	Mean Square Dynamic Pressure, Variance	psi^2
$\left\langle p'^2 \right\rangle^{1/2}$	Root-Mean-Square Dynamic Pressure, Standard Deviation	psi

NOMENCLATURE (Continued)

Symbol	Definition	Unit
P_o	Pressure Amplitude of Acoustic Wave	psi
P_a	Ambient Pressure	psia
P_o	Stagnation Pressure	psia or psig
$\overline{P}_b$	Mean Base Pressure	psi
P_{o_Y}	Measured Pitot Pressure At "Y"	psig
r	Baseplate Radial Coordinate (Table 3-2)	in.
r/D	Dimensionless Distance From Nozzle Centerline	
$R(\xi,\tau)$	Cross-Correlation Coefficient	
$R(\xi,0)$	Space Correlation Coefficient	
$R(0,\tau)$	Autocorrelation Coefficient	
S	Strouhal Number	
$S(f)$	Power Spectral Density	psi^2/Hz
T_a	Ambient Temperature	°R
T_o	Stagnation Temperature	°R
u	Shear Layer Velocity	ft/sec
U_o	Velocity At Inner Edge of Shear Layer	ft/sec
U_c	Convection Speed	ft/sec
U_j	Jet Velocity	ft/sec
V_e	Nozzle Exit Velocity	ft/sec
$\overline{V}$	Mean Velocity in Shear Layer	ft/sec
x,y	Coordinates in Figure 2-2	
X,Y,Z	Coordinate System for Pitot Data Acquisition (Figure 3-11)	in.

NOMENCLATURE (Concluded)

Symbol	Definition	Unit
γ	Specific Heat Ratio	
δ	Shear Layer Thickness	in.
η	Dimensionless Location in Shear Layer	
θ	Angular Polar Coordinate on Baseplate (Table 3-2)	deg
λ	Wavelength	ft
ξ	Separation Distance	in.
τ	Time Delay	millisec
ϕ	Scaling Parameter, Equation 4-2	
ω	Frequency	rad/sec
$\Delta\omega$	Frequency Bandwidth	rad/sec

Subscripts

m	Measured
t	True

Section I

INTRODUCTION

An exploratory study of loads induced at the base of clustered exhausts has been performed as part of the Crossed-Beam Aerodynamics Program (Contract NAS8-20082, Appendix B, Schedule Order 127). Such a study was required to obtain data on the magnitude and characteristics of dynamic base loads and to determine if such loads are acoustic or hydromechanical in origin. Accordingly, experiments were designed to determine both the structure of flow in clustered exhausts and the distribution of mean and dynamic loads on the baseplate of a Saturn configured model.

The Saturn Cluster Model used for these studies allowed simulation of plume shapes generated in flight by the Saturn S-II stage by ambient temperature jets exhausting to a pressure of one atmosphere. Stagnation-to-ambient pressure ratios in the range of 35 to 105 atmospheres were studied for nozzle combinations of one through five engines exhausting.

The total experiment included five tests in the MSFC Thermal Acoustic Jet Facility:

- Tests TAJF-008 and TAJF-009 used Schlieren and shadowgraph photography to determine the flow geometry and shock structure of plume clusters.

- Tests TAJF-010 and TAJF-011 measured pitot pressure distributions across regions of the plume determined of interest from the preceding tests.

- Test TAJF-013 determined the static and dynamic pressure loadings on the baseplate of the Cluster Model as well as sound pressure levels downstream of the nozzle exit plane.

Existing scaling laws and a model of the base pressure resulting from oblique acoustic waves of random incidence are used to analyze the data. It is concluded that base loads may be scaled by the conventional relations only for simple geometries. From the developed acoustic model, it was found that the present experimental results can be explained as due to sound waves reverberating between the engine bells. In the single case where significant convection existed, however, it is inferred that hydromechanical loads present

a more severe loading condition than the acoustic loads. A sample calculation for the base loading of the S-IC stage is presented which indicates that transient narrow-band excitation of the heat shield may exist of the order of 5000 pounds at a dominant frequency of 12 Hz.

Section II of the report discusses the nature of loads at the base of missiles in terms of acoustic and hydromechanical components. Section III gives information on the experimental equipment and procedures while Section IV presents the results of the experimental program. Pertinent results of the study are summarized in Section V along with a discussion of some implications that may be drawn for base loads on Saturn vehicles. In Section VI recommendations are made for future studies of the base loading problem.

Section II

HYDROMECHANICAL AND ACOUSTIC LOADS AT THE BASE OF MISSILES

The experimental studies that are the subject of this report were undertaken to investigate the statistical properties of the random pressure fields created at the base of a simulated missile. Such studies were warranted in view of the lack of such data obtained under controlled conditions. A secondary objective of the program was to establish the effectiveness of the Marshall Space Flight Center Thermal Acoustic Jet Facility (TAJF) for studies of acoustically induced base loads. Finally, the investigation was to serve as the starting point for a longer range program that will determine the means for scaling base loads from model to prototype values.

Statistical averages of random pressure fields that are of principal interest to this study are reviewed in subsection 2-1. Subsection 2-2 reviews some characteristics of hydromechanical or flow induced pressure fields at the base of engine clusters. Finally, in subsection 2-3 a discussion of acoustically induced loads is presented along with an acoustic model of base pressure loadings that will be used for comparison to the results.

2.1 STATISTICAL CHARACTERISTICS OF RANDOM PRESSURE FIELDS

The structure of aerospace vehicles is subject to excitation from many sources. Certain of these sources, such as turbulent boundary layers, oscillating shocks, and engine exhaust noise, behave in a highly irregular fashion and may be regarded as random exciters of structure. Techniques commonly used in the analysis of the random vibration of, for example, the skin of a missile requires knowledge of certain statistical characteristics of the imposed pressure field. Once these averages are known along with certain response or transfer functions of structure, analyses may be performed to ascertain the vibratory system response. (Such analyses are discussed in reference 1, 2, and 3). In this section those averages of the random pressure field that were deemed most important to the present study will be discussed.

For simplicity, the pressure field may be regarded as a function of a single space variable, x, and time, t. The mean value of this pressure is given by

$$\bar{p}(x) = \lim_{T \to \infty} \frac{1}{T} \int_0^T p(x,t)dt \qquad (2\text{-}1)$$

The mean square value of the pressure is defined similarly by

$$\overline{p^2}(x) = \lim_{T \to \infty} \frac{1}{T} \int_0^T p^2(x,t)dt \qquad (2\text{-}2)$$

Also, one may consider departures of the pressure from the mean in terms of a fluctuating or dynamic component of pressure, p'(x,t) defined by

$$p'(x,t) = p(x,t) - \bar{p}(x) \qquad (2\text{-}3)$$

The mean square of the dynamic component (or variance) is given by

$$\left\langle p'^2(x) \right\rangle = \lim_{T \to \infty} \frac{1}{T} \int_0^T [p-\bar{p}]^2 \, dt \qquad (2\text{-}4)$$

In view of equation (2-2), the variance differs from the mean square pressure by the square of the mean pressure, i.e.,

$$\left\langle p'^2(x) \right\rangle = \overline{p^2}(x) - \bar{p}(x)^2 \qquad (2\text{-}5)$$

For those data to be presented in the body of this report, only fluctuations around the mean were recorded. In view of equation (2-4), this procedure was equivalent to taking data with a zero mean value. Distinctions between the mean square and variance vanish for such data. Mean square, as used in this report, then will refer to the variance, that is, the mean square of the dynamic pressure. The term root-mean-square will be reserved for what is normally termed the standard deviation, i.e.

$$\left\langle p'^2(x) \right\rangle^{1/2} = \sqrt{\overline{p'^2}(x)} \qquad (2\text{-}6)$$

Mean square properties defined by equations (2-4) and (2-6) give the amplitude characteristics of the dynamic pressure. Temporal variation is given by the autocorrelation coefficient

$$R(\tau) = \lim_{T \to \infty} \frac{1}{T} \int_0^T \frac{p'(x,t)\ p'(x,t+\tau)}{\left\langle p'^2(x) \right\rangle}\ dt \qquad (2-7)$$

while frequency characteristics are obtained from the power spectral density

$$G(\omega) = \frac{1}{2\pi} \int_{-\infty}^{\infty} R(\tau)\ e^{-i\omega\tau}\ d\tau \qquad (2-8)$$

The power spectral density, which may be regarded as the concentration of power in a narrow band $\Delta\omega$ around the frequency ω, is essentially the Fourier transform of the autocorrelation function. The power spectra reported here will be given in terms of circular frequencies, f, rather than the angular value ω. The relationship to equation (2-8) is simply (ref. 4)

$$S(f) = 4\pi\ G(\omega) \qquad (2-9)$$

It is noted further that

$$\left\langle p'^2 \right\rangle = \int_0^\infty S(f)df$$

Knowledge of the frequency decomposition provided by the spectrum thus gives the amplitude characteristics (mean square and root-mean-square) of the random signal.

The autocorrelation function, defined by equation (2-7), specifies the correlation history at a single point in space. A more general relationship is the cross-correlation function, which describes variation in both space and time. This space-time correlation may be written for a homogeneous, stationary pressure field as

$$R(\xi,\tau) = \lim_{T \to \infty} \frac{1}{T} \int_0^T \frac{p'(x,t)\ p'(x+\xi,\ t+\tau)}{\left\langle p'^2(x,t) \right\rangle^{1/2} \cdot \left\langle p'^2(x+\xi,\ t+\tau) \right\rangle^{1/2}}\ dt \qquad (2-11)$$

The specific cases $R(o,\tau)$ and $R(\xi,o)$ correspond, respectively, to the auto-correlation and space correlation functions.

A result of major interest in the present study was the possible convection of the pressure field by a mean flow component. If such a situation exists, the cross-correlation function for different separation distances ξ_1 and ξ_2 will be characterized by peak correlations occurring at different time delays τ_1 and τ_2. This situation is depicted in Figure 2-1. A measure of the mean convection speed is then provided by (ref. 5).

$$U_c = \frac{\xi_2 - \xi_1}{\tau_2 - \tau_1} \qquad (2\text{-}12)$$
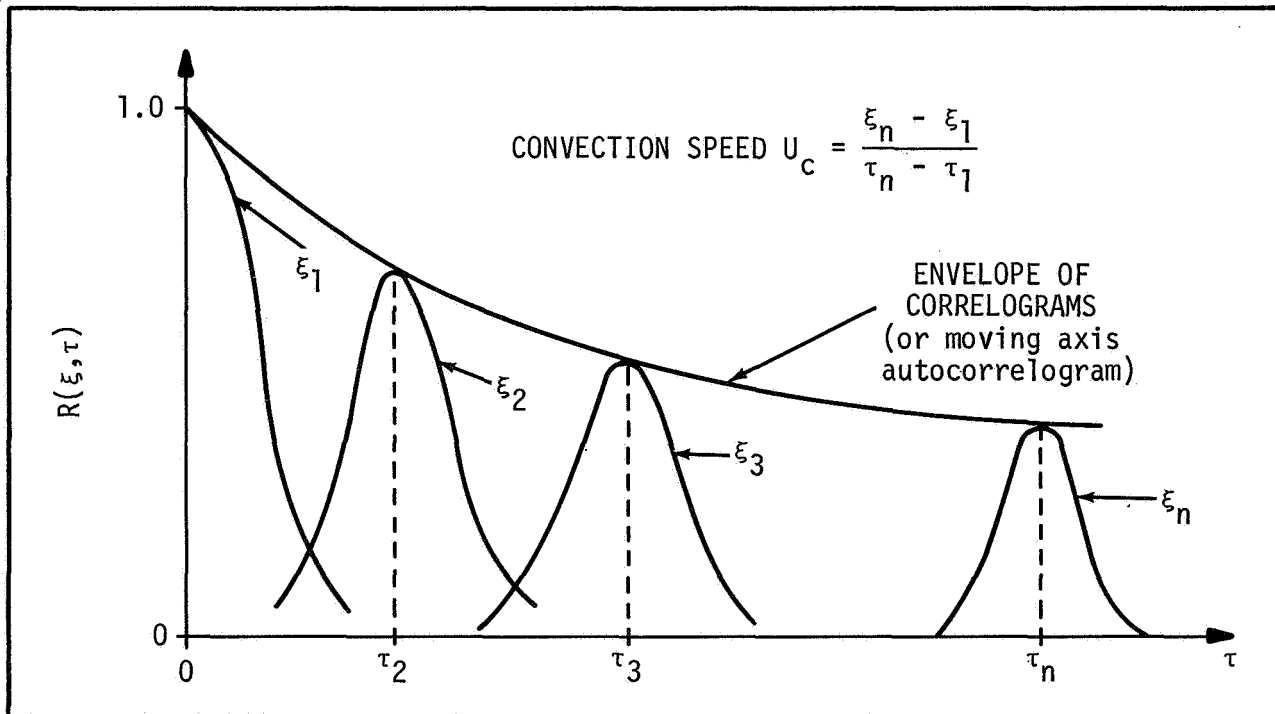

Figure 2-1.   ESTIMATION OF CONVECTION SPEED BY USE
OF CROSS-CORRELATION FUNCTIONS

The zero-separation result is simply the autocorrelation function which always peaks at $\tau = 0$. It is convenient in the application of equation (2-12) to choose $\xi_1 = \tau_1 = 0$.

Those averages of pressure that will be considered specifically in this report are the mean value, equation (2-1); mean square, equation (2-4); root-mean-square, equation (2-6); power spectral density, equation (2-9); and cross-correlation function, equation (2-11). The cross-spectral density function will not be considered in this study because most characteristics of the data were realizable from other parameters.

2.2 GENERATION OF HYDROMECHANICAL LOADS

Consideration of the environment produced at the base of a missile during flight has received much attention over the past twenty years. (See reference 6 for a bibliography.) A prime consideration in such studies has been the mean pressure acting on the base as an input to vehicle drag calculations. Other factors of interest have been the establishment of convective heat transfer rates and the establishment of conditions for the existence of base "burning". Such studies, however, lack sufficient detail to serve as an input to a structural analysis of the base region.

A mechanism by which flow can be directed toward the vehicle base is provided by the analytical techniques pioneered by Korst (ref. 7). In that two-dimensional problem, consideration was given to the interaction region of impinging supersonic streams. It was subsequently established that the stagnation pressure of a portion of the flow in a free shear layer is too low for fluid particles outside a certain "discriminating" streamline to cross the shock resulting from impingement; thus, conservation of momentum requires a redirection of the flow toward the vehicle base.

The physical situation described is similar to that encountered when jet or rocket exhausts impinge with one another or an enveloping free stream flow. Such a three-dimensional analogue to the original Korst analysis possesses additional degrees of freedom; that is, momentum can be conserved by flows that are not directed toward the base. Therefore, for recirculation to exist at the base of an engine cluster, an additional closure criterion must be satisfied.

Goethert (ref. 8 and 9) experimentally studied the existence of re-circulation at the base of a symmetric four jet cluster over a range of chamber-to-ambient pressure ratios. The study showed that at low P_o/P_a values the jets acted as a pump drawing flow from the base region. As the pressure ratio was increased the base flow experienced a transition from an aspirating flow mode to the reverse flow expected from impinging supersonic flows. At the highest pressure ratios, such flows were found to be "choked" in the vicinity of the engine bells.

From these observations several conclusions can be drawn as to some of the important factors contributing to the existence of recirculatory flows. For the flow approaching an interaction region the velocity distribution across the shear layer and the thickness of the shear layer affect the mass flow di-rected toward the base. Secondly, for a specified fluid, nozzle geometry, and nozzle separation distance, the stagnation-to-ambient pressure ratio dictates the point at which impingment occurs. Finally, the geometric arrangement of the interacting jets and the distance from the intersection point to the base-plate of an engine cluster are influential in dictating whether recirculation affects the base since the former factor specifies whether closure is attained and the latter factor specifies the approach velocity to the base.

For the model used in this investigation it was possible to assess several of these factors as will be shown. The influence of recirculation on the sta-tistical character of random pressure loadings at the base could only be judged qualitatively because measurements of turbulence in the impinging jets were not made.

2.3 GENERATION OF ACOUSTIC LOADS

In addition to excitation from flow induced pressure fluctuations, the base region is acted on by acoustic radiation from rocket or jet exhausts. From Lighthill's fundamental work on aerodynamically generated sound (ref. 10 and 11), it is known that significant noise results in those regions of a jet where high shear velocities are coupled with intense turbulence. Figure 2-2 schematically represents an underexpanded jet of the type used in the present
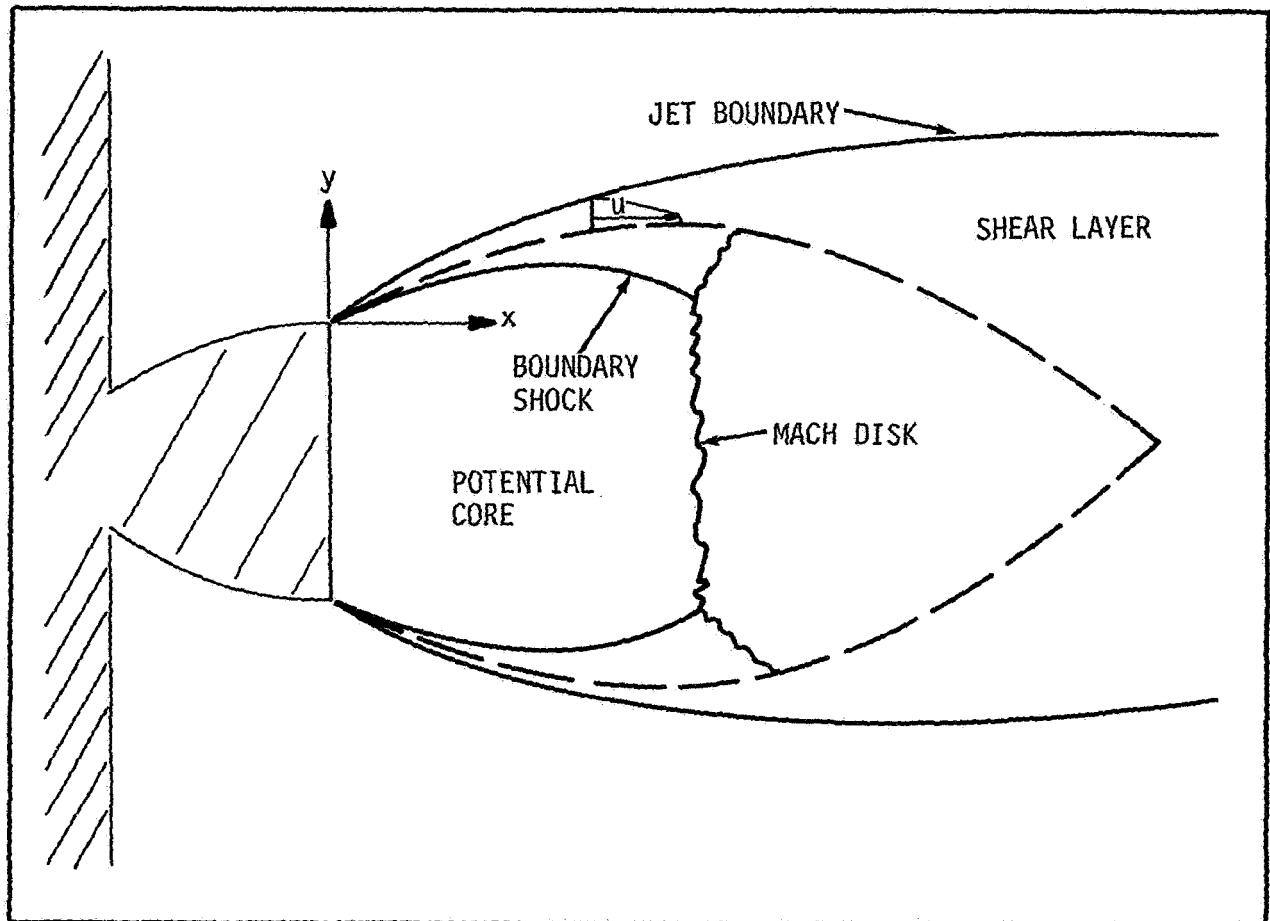
Figure 2-2. SCHEMATIC OF UNDEREXPANDED JET

experimental study. Two regions that meet the criteria for noise generation are the shear layer of the jet ($\frac{\partial u}{\partial y}$ large) and the interaction region of the shock cell with the shear layer ($\frac{\partial u}{\partial x}$ large). An additional potential source of acoustic radiation is afforded by the shock cell since any longitudinal unsteadiness of this system can result in highly efficient radiation (ref. 12). Of particular concern in this latter regard is the development of feed-back systems which are selective in frequency and may be coincident, in flight applications, to the natural frequency of skin panels (ref. 13).

Analysis of acoustic propagation by the above mechanisms is extremely difficult since empirical data are required that are not accessible, in general, to conventional instrumentation. Many characteristics of jet noise have been

determined by dimensional arguments and experiments. Several facets of the sound field that will be investigated later are the relationship of sound pressure level to jet thrust, the general characteristics of the spectra of both single and clustered exhausts, and the cross-correlation of pressures resulting at the base of clusters due to radiation. For this purpose it is convenient to develop a mathematical model that will relate the base pressure data obtained to a pressure loading due to acoustic radiation.

Consider the family of plane waves obliquely incident on the surface of Figure 2-3. The (one-dimensional) loading of the surface due to this family of waves is (ref. 14)

$$p'(x,\theta,t) = p_o \cos(\omega t - k_o x \sin \theta) \tag{2-13}$$
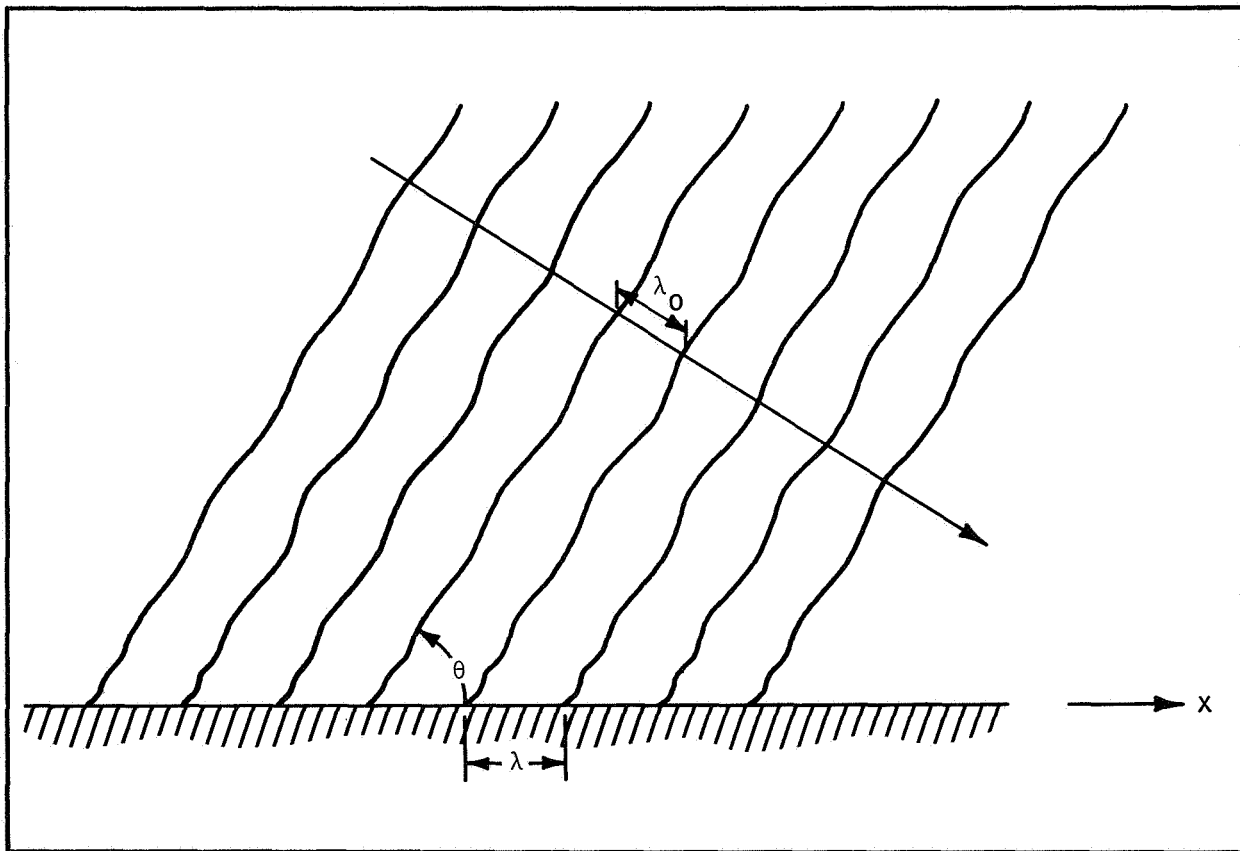

Figure 2-3. ACOUSTIC WAVE TRAIN OBLIQUELY INCIDENT ON PLANE SURFACE

From equations (2-2) and (2-6) the root-mean-square pressure at the surface
is simply

$$\left\langle p'^2 \right\rangle^{1/2} = \frac{P_o}{\sqrt{2}} \tag{2-14}$$

This value is independent of location on the surface and depends only on the
factor p_o which may be regarded as jet induced. The cross-correlation function
is defined by equation (2-11) for a homogeneous, stationary field and gives

$$R(\xi,\theta,\tau) = \cos\omega\tau \cos(k_o \xi \sin\theta) + \sin\omega\tau \sin(k_o \xi \sin\theta) \tag{2-15}$$

This result is valid for any angle of incidence θ. To extend this result to
waves striking the surface at all angles of incidence, one may define the
cross-correlation of the assembly by

$$R(\xi,\tau) = \int_o^\pi R(\xi,\theta,\tau) \ f(\theta) \ d\theta \tag{2-16}$$

where the probability distribution function, $f(\theta)$, has the property that

$$\int_o^\pi f(\theta) \ d\theta = 1 \tag{2-17}$$

For the simple case of all directions equally probable, $f(\theta) = \frac{1}{\pi}$. It follows
from equations (2-15) and (2-16) that

$$R(\xi,\tau) = \frac{\cos\omega\tau}{\pi} \int_o^\pi \cos(k_o \xi \sin\theta) \ d\theta$$

$$+ \frac{\sin\omega\tau}{\pi} \int_o^\pi \sin(k_o \xi \sin\theta) \ d\theta \tag{2-18}$$

The first of these integrals is a form of Bessel's integral while the
second can be interpreted in terms of a summation of Bessel functions. Per-
forming the indicated integrations,

$$R(\xi,\tau) = J_o(k_o\xi)\,\cos\omega\tau + \frac{4}{\pi}\,\sin\omega\tau \sum_{n-o}^{\infty} \left(\frac{J_{2n+1}(k_o\xi)}{2n+1} \right) \qquad (2\text{-}19)$$

Cancellation results for the assembly of waves because

$$\lim_{\xi\to\infty} R(\xi,\tau) = 0 \qquad (2\text{-}20)$$

Furthermore, the space correlation is simply

$$R(\xi,0) = J_o(k_o\xi) \qquad (2\text{-}21)$$

These results will be employed in the data analysis of Section IV.

Section III

DATA ACQUISITION

The experimental program performed to obtain the distribution of loads at the base of engine clusters consisted of five separate tests in the Marshall Space Flight Center Thermal Acoustic Jet Facility (TAJF). A base flow model was used which is termed the Saturn Cluster Model due to its geometric similarity to the lower stages of the Saturn vehicle. Tests TAJF-008 and TAJF-009 were photographic studies of the structure of, and interactions between, underexpanded plumes. In Tests TAJF-010 and TAJF-011 pitot traverses were made across clustered plumes to allow estimation of velocity profiles and shear layer thickness. Dynamic pressure measurements at the base of the Cluster Model were made in Test TAJF-013 for several stagnation pressures and combinations of nozzles exhausting.

In the following subsections, a brief discussion is presented on the test facility, Saturn Cluster Model, instrumentation systems, and test procedures. Also included in this section are a description of the data acquisition system and the data reduction procedures followed.

3.1   THERMAL ACOUSTIC JET FACILITY'S COLD FLOW DUCT

The Thermal Acoustic Jet Facility consists of two blowdown units which provide gas flows over a wide range of chamber pressures and mass flow rates. Studies may be conducted at either ambient temperatures using a Cold Flow Duct, or at elevated temperatures using the Heated Flow Duct. Figure 3-1 shows a view of the TAJF. All tests discussed in this report used the Cold Flow Duct so that data corresponding to unheated jets were obtained.

The Cold Flow Duct consists of a high and low mass flow circuit. The high mass flow circuit includes a safety valve, a control valve and a by-pass valve with a maximum flow of 180 lbs/sec. The low mass circuit, designed for flows of 8 percent of maximum, or less, was not used in the present tests. Chamber pressure is controlled in the high mass flow circuit by adjusting the control valve and positioning the by-pass valve. The by-pass valve is used to obtain

Figure 3-1. THERMAL ACOUSTIC JET FACILITY

optimum control and maximum flow rates. A schematic diagram of the piping arrangement of the facility is given as Figure 3-2.

Compressed air is supplied to the facility from either a 3500 cubic feet bottle farm 600 feet distant from the test site or a bottle farm of 4800 cubic feet capacity located at the facility. The former storage facility has a maximum working pressure of 3500 psi while the latter is limited to 1850 psi. In either case, the ambient temperature air used in the Cold Flow Duct was supplied at a dew point of better than $-70°F$.

After air leaves the high mass flow circuit, it enters a turbulence control assembly. Here the air passes through a honeycomb flow straightener, a series of screens and enters a settling chamber as may be seen in Figure 3-3. The screens, mounted in the constant area section of the settling tank, are designed to remove upstream disturbances. The flow then enters a converging section, where screens may be added to promote turbulence, and exhausts to the atmosphere through any of various single or multiple nozzles attached to the exit end of the control assembly. Further discussions of the Cold Flow Duct can be found in references 15 and 16.

3.2 SATURN CLUSTER MODEL

The Saturn Cluster Model (Figure 3-4) consists basically of five identical nozzles and an instrumented baseplate. The nozzles may be individually closed to provide posible exhaust combinations of one to five nozzles. The center engine, moreover, may be removed and a baseplate adapter added to allow simulation of a symmetric four jet cluster.

A primary consideration in the design of the cluster nozzles was simulation of Saturn S-II Stage exhaust plumes and plume intersections at the "max q" flight condition. To accomplish this objective with ambient temperature air exhausting to one atmosphere, it was necessary to use a nozzle having an extremely high divergence angle at the throat. This can be seen in Figure 3-5 which presents the nozzle contours. The success of the design in obtaining the desired
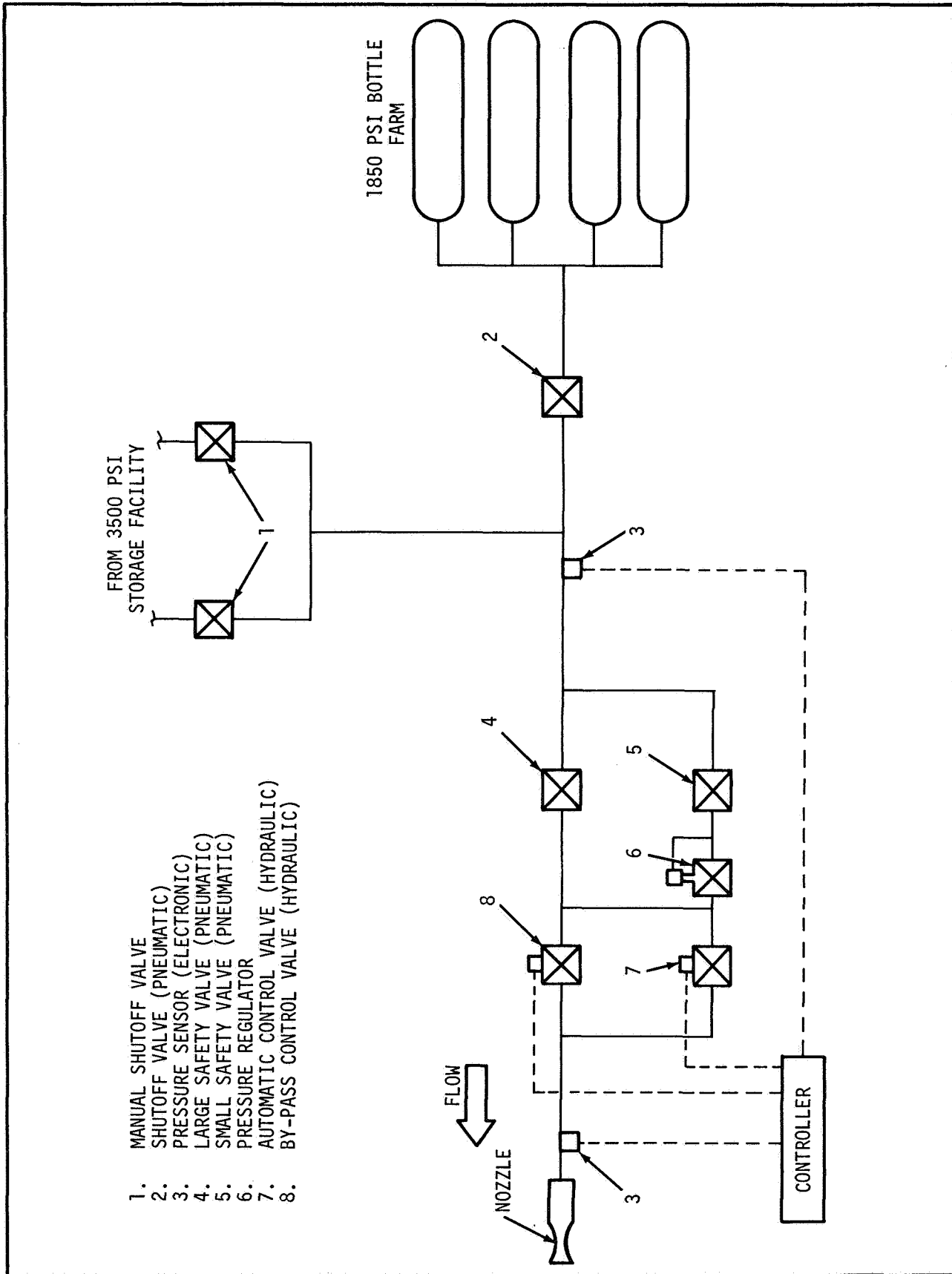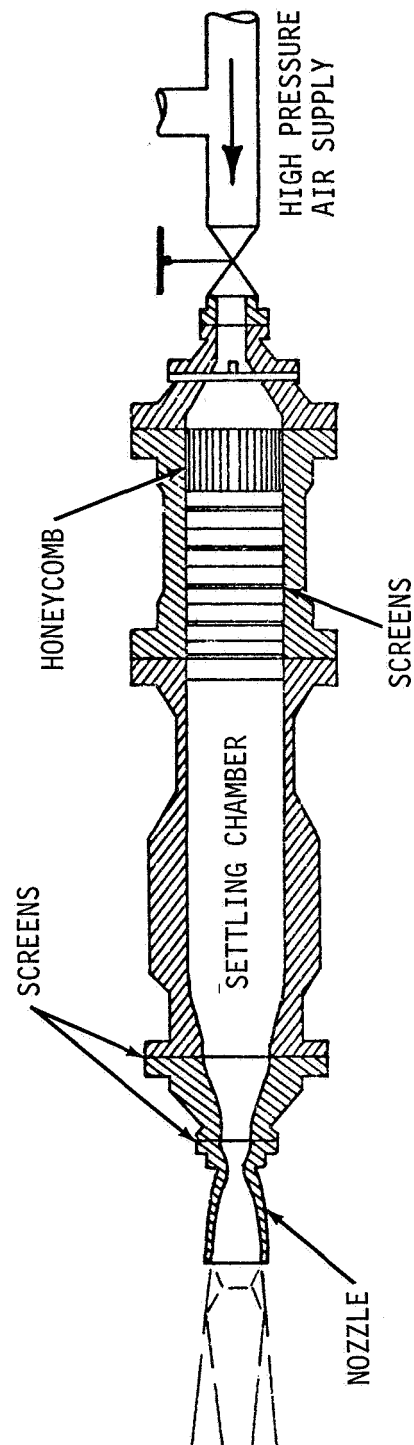
Figure 3-2. SCHEMATIC DIAGRAM OF COLD FLOW DUCT

1. MANUAL SHUTOFF VALVE
2. SHUTOFF VALVE (PNEUMATIC)
3. PRESSURE SENSOR (ELECTRONIC)
4. LARGE SAFETY VALVE (PNEUMATIC)
5. SMALL SAFETY VALVE (PNEUMATIC)
6. PRESSURE REGULATOR
7. AUTOMATIC CONTROL VALVE (HYDRAULIC)
8. BY-PASS CONTROL VALVE (HYDRAULIC)

Figure 3-3. SCHEMATIC OF COLD FLOW DUCT

NORTHROP·HUNTSVILLE ——————————————
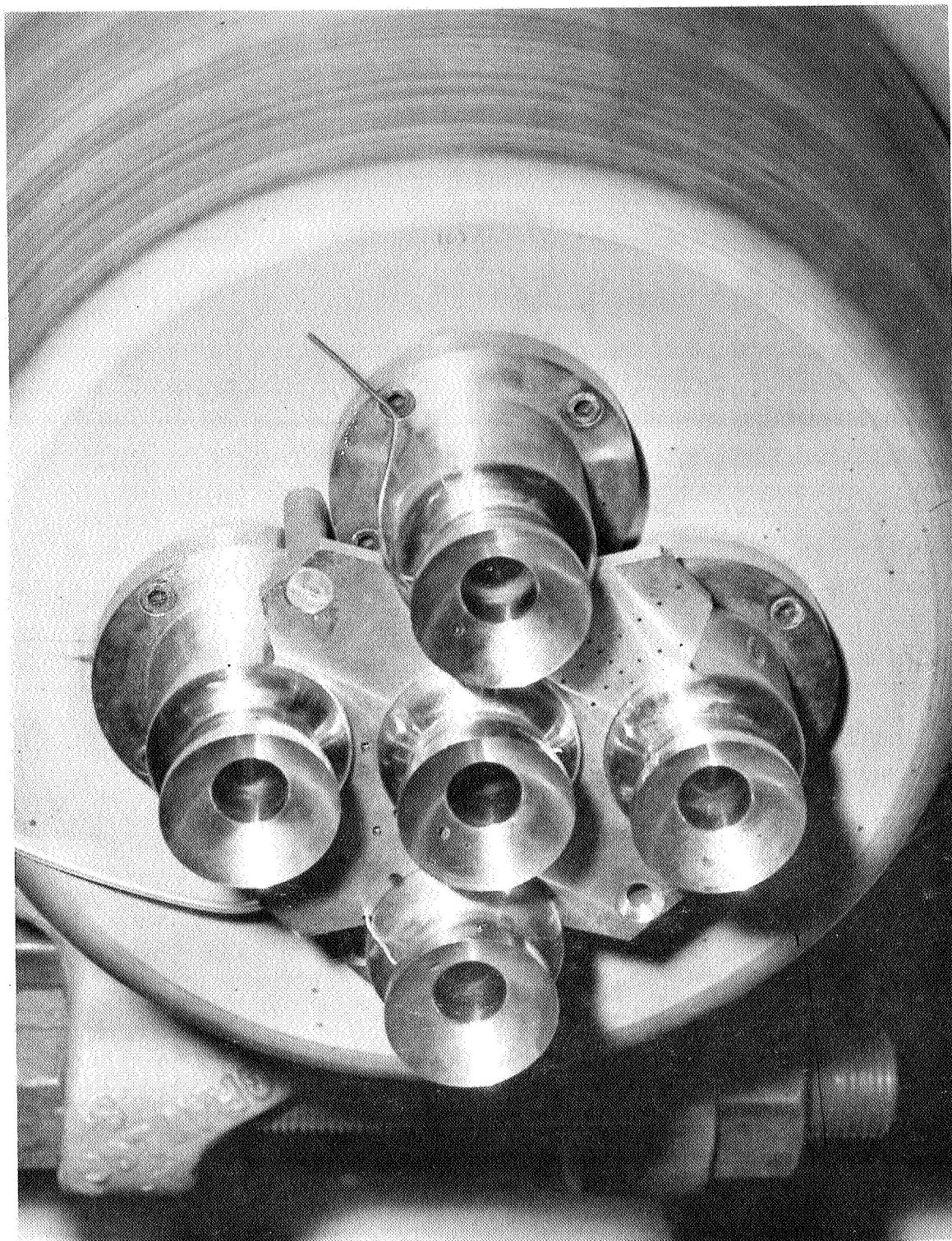
Figure 3-4. SATURN CLUSTER MODEL

| Internal Contour		External Contour	
X	Y	X	Y
0	.9000	0	.900
.0210	.8778	.180	.893
.0417	.8556	.360	.866
.0521	.8443	.540	.815
.0790	.8147	..720	.756
.0813	.8121	.880	.668
.0984	.7927	.911	.869
.1154	.7733	1.012	.970
.1322	.7538	1.112	1.021
.1488	.7341	1.213	1.048
.1652	.7143	1.314	1.049
.1813	.6943	1.350	1.051
.1976	.6741		
.2136	.6537		
.2296	.6330		
.2454	.6119		
.2612	.5906		
.2768	.5688		
.2924	.5467		
.3080	.5240		
.3234	.5009		
.3388	.4772		
.3541	.4528		
.3694	.4277		
.3845	.4018		
.3995	.3750		
.4495	.3755		
.4995	.3770		
.5495	.3793		
.5995	.3827		
.6495	.3870		
.6995	.3922		
.7495	.3985		
.7995	.4057		
.8495	.4139		
.8995	.4231		
.9995	.4445		
1.0995	.4701		
1.1995	.4999		
1.2995	.5342		
1.3995	.5682		
1.4995	.5972		
1.5995	.6213		
1.6995	.6404		
1.7995	.6545		
1.8995	.6636		
2.0327	.6680		
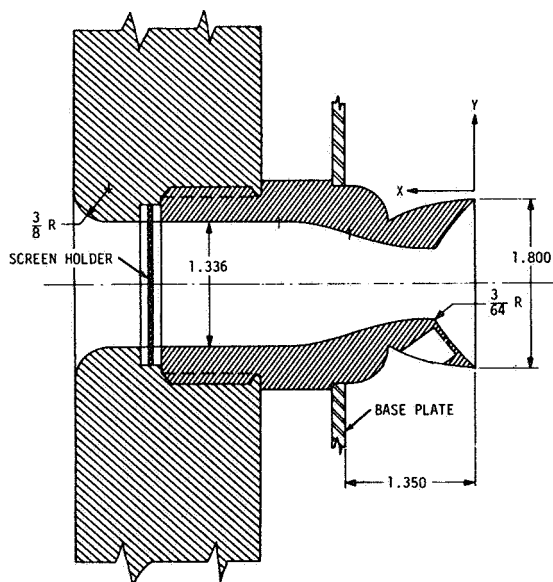
Figure 3-5.   SATURN CLUSTER MODEL NOZZLE GEOMETRY

match may be judged from Figure 3-6 which compares the plume shape at the design stagnation pressure (P_o = 1500 psig) to the desired method of characteristics results (ref. 17).

The baseplate used on this study represents a compromise between a missile heat shield and the mounting requirements of the various pressure sensors and taps. The design used and relative locations of the nozzles are shown in Figure 3-7. The baseplate was fabricated of 0.25-inch thick 316 stainless steel and is attached to the Cold Flow Duct adapter assembly at two points. This attachment, along with the constraints supplied by a force fit between the cluster nozzles is sufficient to insure rigidity of the plate during testing. The set-back distance of the baseplate from the nozzle lip, shown in Figure 3-6, was not varied during these tests.

Further information on individual components and equipment available with the Cluster Model may be obtained from the NASA/MSFC drawings identified in Table 3-1.

Table 3-1. MODEL DESIGN DRAWING NUMBERS

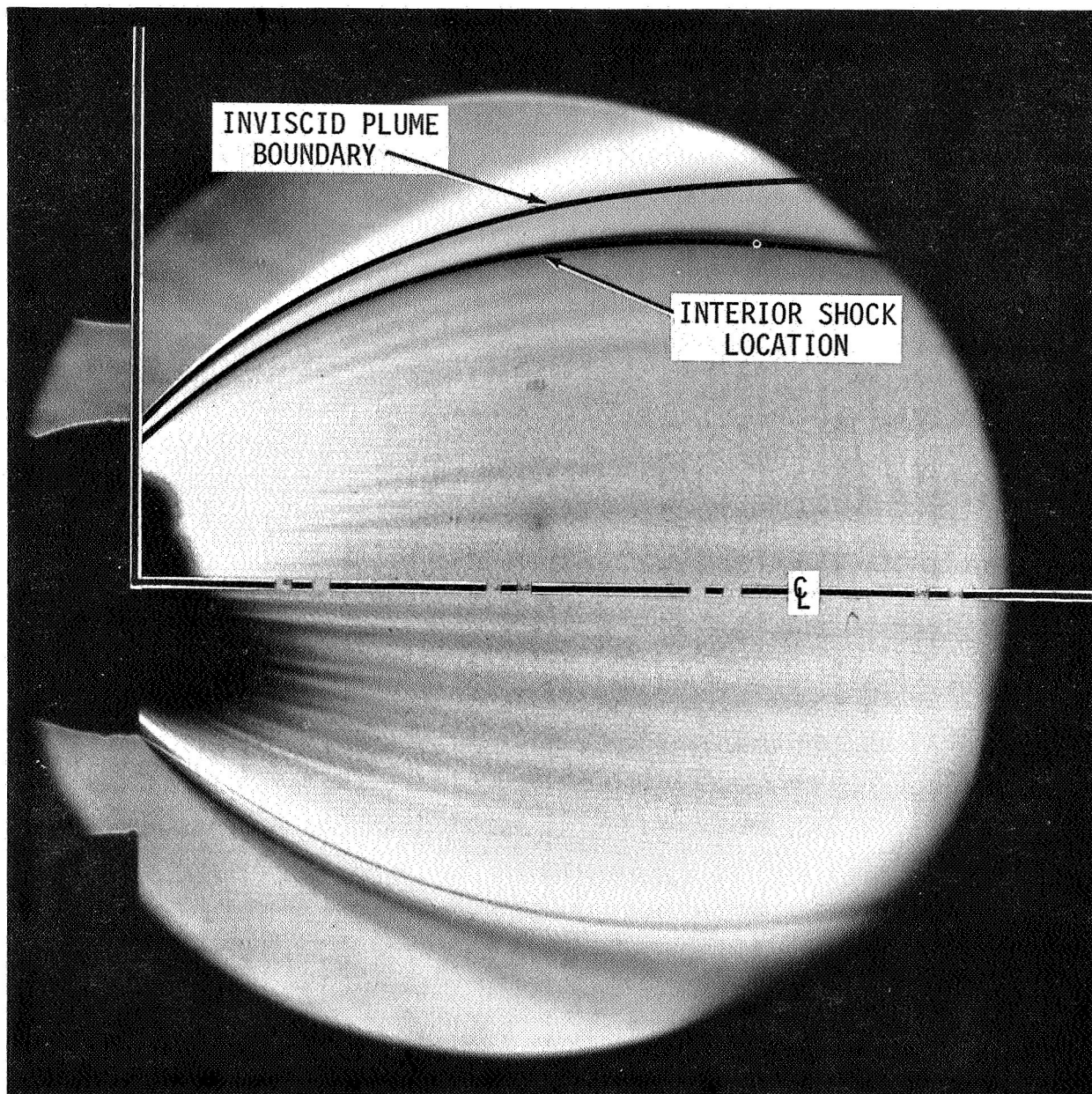| PART	QUANTITY	DRAWING NUMBER
S-II Nozzle Cluster		
Adapter	1	NASA/MSFC 80M 50928
Nozzle	2	80M 41911
Nozzle	1	80M 41913
Nozzle	1	80M 41916
Nozzle	1	80M 41917
Spacer	5	80M 32029
Spacer	5	80M 32032
Baseplate	1	80M 41915
Filler Plate	1	80M 32116
Plug	1	80M 32117

Figure 3-6. COMPARISON OF CHARACTERISTICS SOLUTION TO SINGLE JET FLOWFIELD (P_o = 1500 psig)
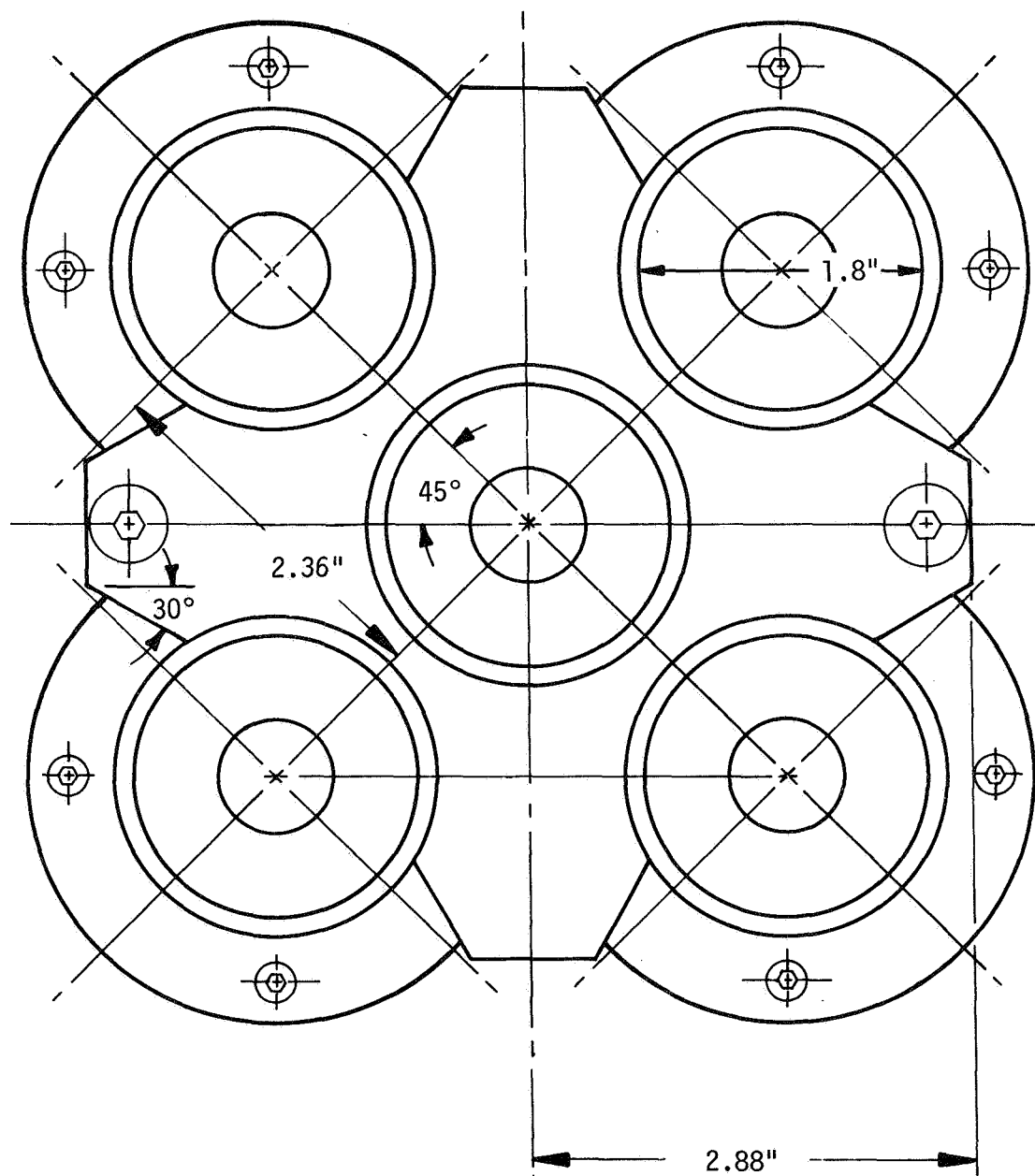
Figure 3-7. SATURN CLUSTER MODEL BASE GEOMETRY

3.3 INSTRUMENTATION

3.3.1 Facility Measurements

Although several facility parameters were measured, only stagnation pressure, stagnation temperature, and atmospheric conditions will be discussed in this report. Stagnation pressure and temperature were measured by total probes located in the settling chamber of the turbulence control assembly. Barometric pressure was measured by a barometer located at the test site. Other atmospheric parameters such as ambient temperature and relative humidity were measured at the Atmospheric Research Facility of MSFC's Aerospace Environment Division.

3.3.2 Plume Measurements

The photographic studies of the plumes (Tests TAJF-008 and TAJF-009) used conventional shadowgraph and Schlieren systems available at the facility. Since the Unertl Schlieren System has a field of view of only 6 inches, Schlieren coverage was limited to the initial three diameters of the jet. Coverage was extended by use of the shadowgraph system which included approximately ten diameters of the clustered exhausts.

Two types of pitot probes were used in the study of total pressure distributions across the plumes. The first, a twenty-probe rake used in Test TAJF-010 (ref. 18), is depicted in Figure 3-8. This rake has 20 individual probes spaced 0.15 inches apart and can measure a 2.85-inch vertical traverse without relocation of the rake in the plume. The second probe consisted of a single pitot tube and is shown in Figure 3-9. This probe, used in test TAJF-011, was mounted on a pneumatically operated, hydraulically damped, vertical-traversing drive mechanism shown in Figure 3-10. A potentiometer measured the location of the probe with respect to a fixed reference point, and synchronized probe location at each instant data was sampled. The traversing rate of the probe was approximately 0.1-inch per second.

The multi-probe rake and the single probe drive mechanism was attached to a massive probe cart (Figure 3-10). Axial location was varied between runs by
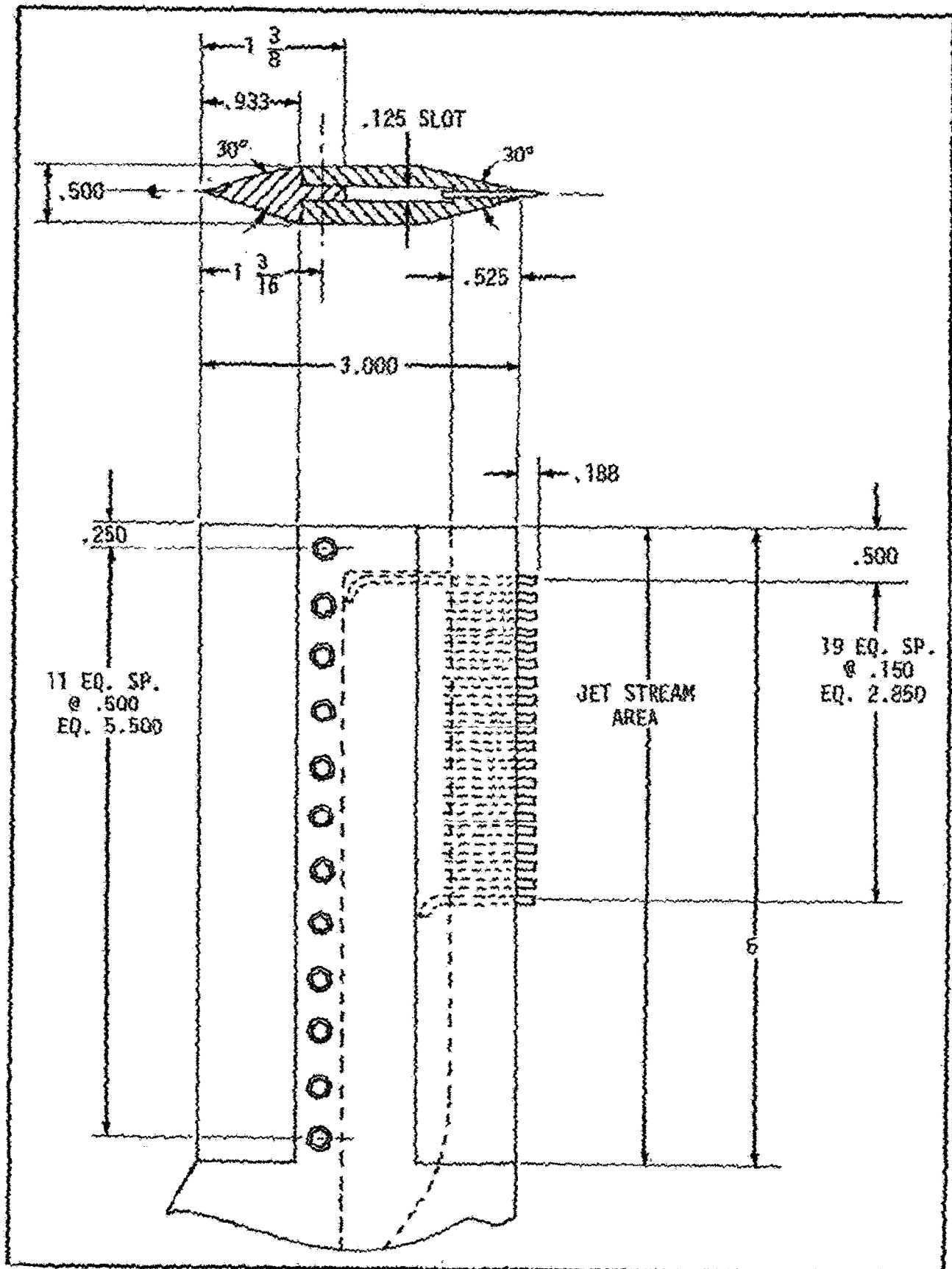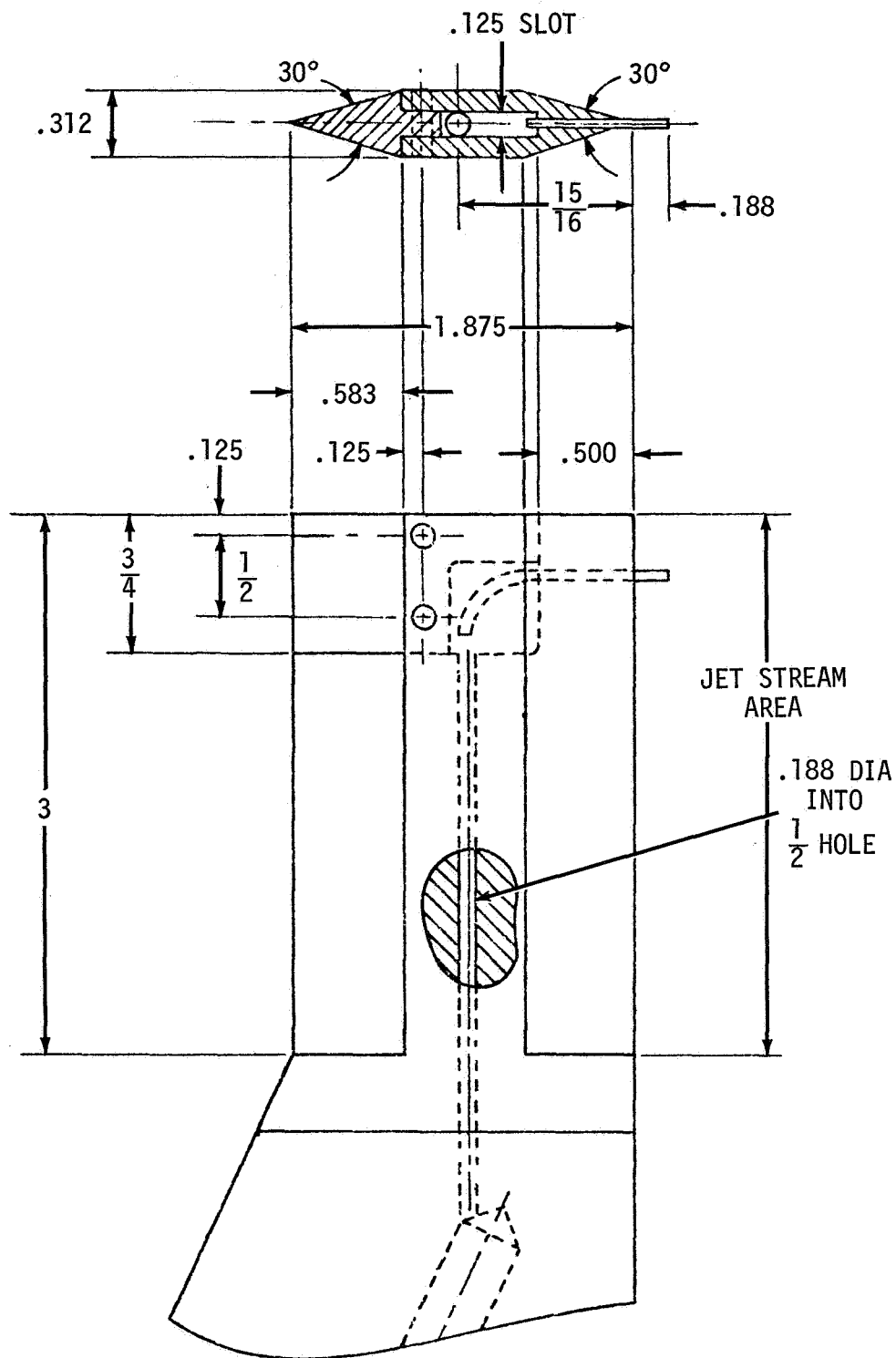
Figure 3-8. TWENTY-PROBE PRESSURE RAKE

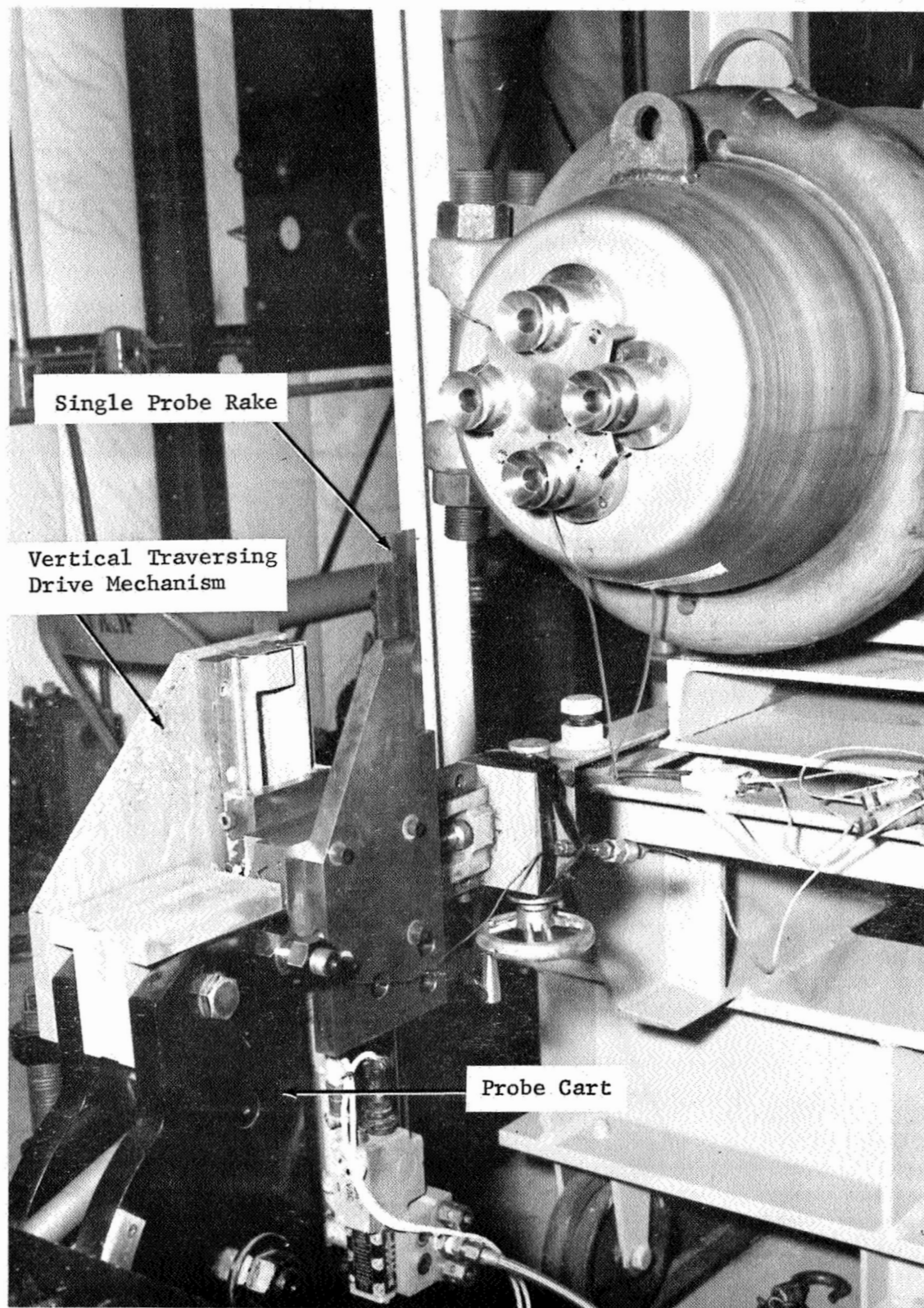Figure 3-9. TRAVERSING PROBE PRESSURE RAKE

Figure 3-10. MODEL INSTALLATION

moving the probe cart along rails running parallel to the direction of jet discharge. The rigidity of the assembly during testing was insured by inter-locking the cart to the rails.

Each probe of the multiple tube rake was routed to a scanivalve and indi-vidual probe measurements were made with a Statham strain gage pressure trans-ducer having a range of 0 to 600 psig. The same transducer was used with the traversing rake, however, the scanivalve was not used. Probe locations are given in terms of a model referenced coordinate system shown in Figure 3-11.

A single microphone, located at X = 12", Y = 0", Z = -30" of the above coordinate system, was used to measure acoustic pressures created by the jets. The instrument used was a Bruel and Kjaer, 0.25-inch condenser microphone. The microphone dynamic range extends to 174 dB (referenced to 0.0002 μ bar) for frequencies from 0.2 kHz to 30 kHz.

3.3.3   Base Load Measurements

The nominal number of measurements taken at the base of the engine clusters varied with the configuration tested. For those tests in which all five nozzles of the Cluster Model were installed, base measurements consisted of 22 mean and 5 fluctuating static pressure measurements. Removal of the center engine to allow simulation of a symmetric four engine configuration in-creased the number of measurements to 29 mean and 10 dynamic measurements. The relative location of these sensing stations are shown in Figure 3-12. Dynamic measurements are indicated by the prefix "F" before the probe number. The suffix "R" is used to denote the reference static pressure tap for each fluctuating probe. Additional dynamic pressure measurements, prefixed by the letter "E", were made in three of the nozzles. These measurements were used to substantiate certain facility characteristics and will not be considered further in this report. The exact position of each sensor is given in Table 3-2.

Due to the large number of static pressures recorded, it was convenient to use the scanivalve system referred to in the discussion of plume pitot data. In the case of base static measurements, however, a ± 12.5 psid (referenced to atmosphere) transducer was used. This effectively limits the accuracy of the mean static pressures to ± 0.1 psid.
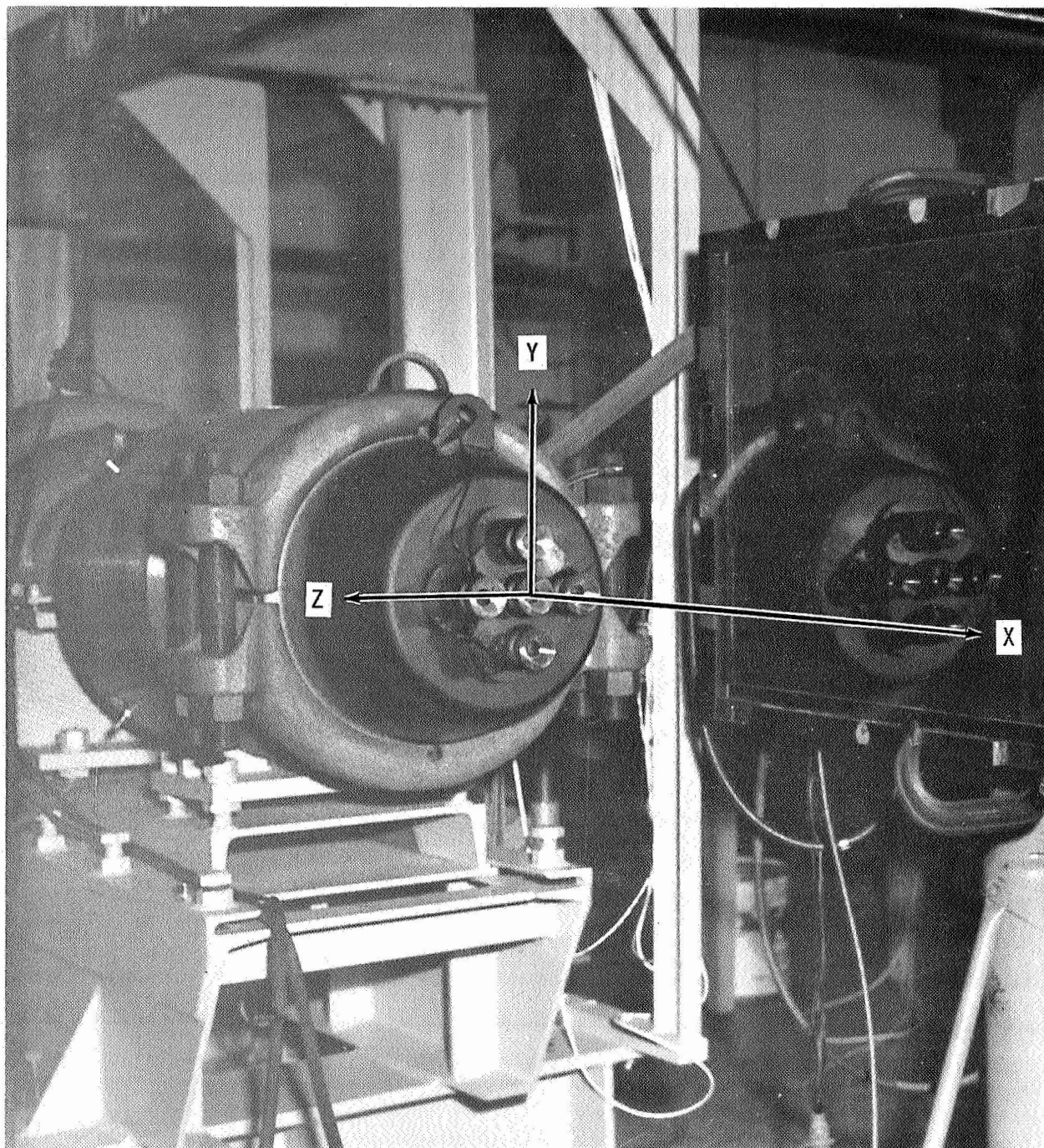
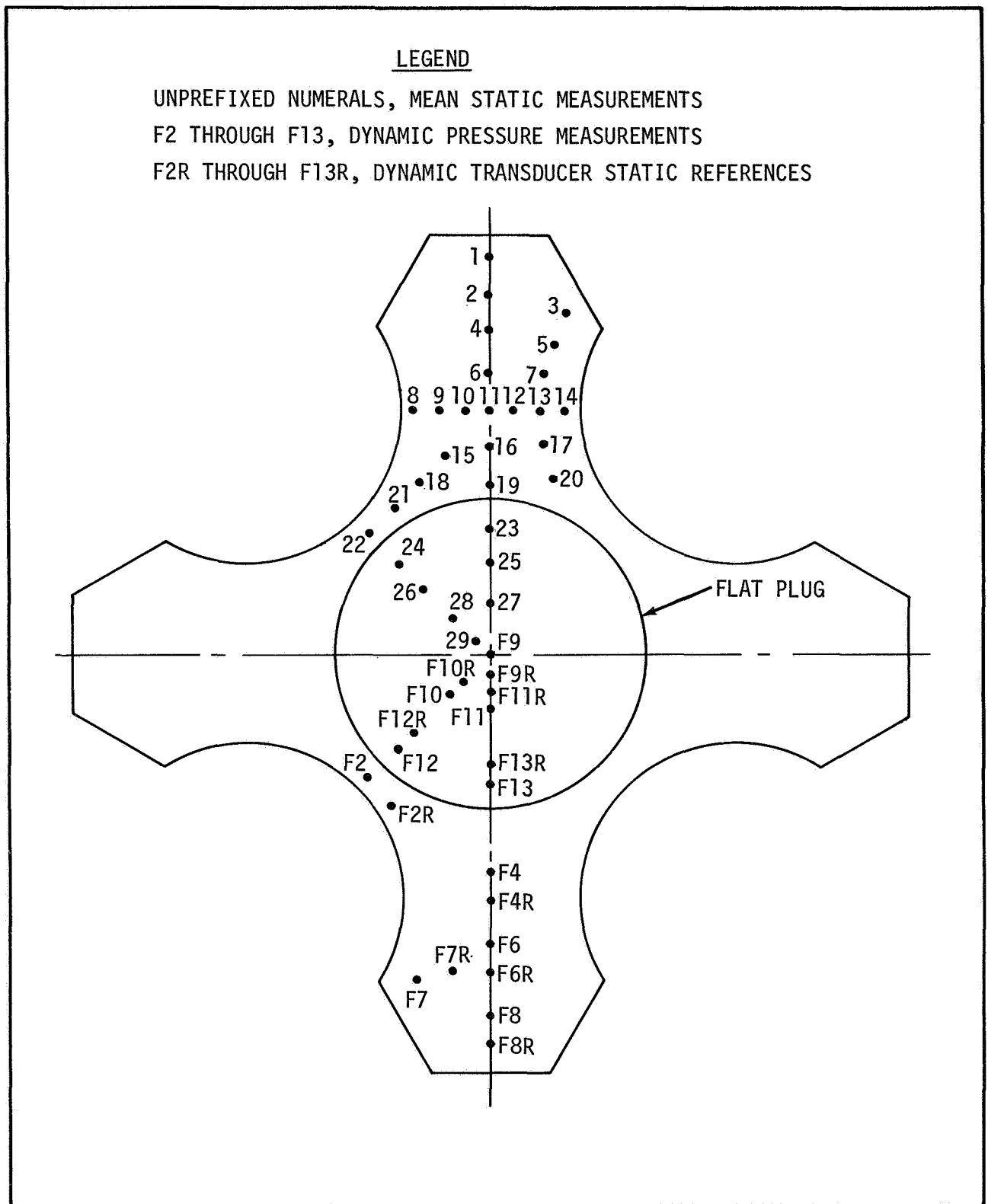Figure 3-11. MODEL REFERENCED COORDINATE SYSTEM

Figure 3-12.   STATIC AND DYNAMIC PRESSURE INSTRUMENTATION LOCATIONS ON
THE SATURN MODEL BASEPLATE

Table 3-2. POLAR COORDINATES OF INSTRUMENTATION LOCATIONS ON BASE OF SATURN CLUSTER MODEL

STATIC PRESSURE PROBE COORDINATES			FLUCTUATING PRESSURE PROBE COORDINATES			LOCATION OF STATIC REFERENCES FOR FLUCTUATING PROBES		
IDENTIFYING SYMBOL	RADIAL LOCATION (INCHES)	θ, ANGULAR LOCATION (DEGREES)	IDENTIFYING SYMBOL	RADIAL LOCATION	θ, ANGULAR LOCATION	IDENTIFYING SYMBOL	RADIAL LOCATION (INCHES)	θ, ANGULAR LOCATION (DEGREES)
1	2.763	0.0	F2	1.181	225.0	F2R	1.210	213.0
2	2.490	0.0	F4	1.420	180.0	F4R	1.670	180.0
3	2.390	12.5	F6	1.920	180.0	F6R	2.170	180.0
4	2.217	0.0	F7	2.230	192.0	F7R	2.183	186.6
5	2.190	11.2	F8	2.420	180.0	F8R	2.670	180.0
6	1.944	0.0	F9	0.0	0.0	F9R	0.125	180.0
7	1.938	10.7	F10	0.375	225.0	F10R	0.250	225.0
8	1.746	343.0	F11	0.375	180.0	F11R	0.250	180.0
9	1.706	348.5	F12	0.875	225.0	F12R	0.750	225.0
10	1.680	354.2	F13	0.875	180.0	F13R	0.750	180.0
11	1.671	0.0						
12	1.680	5.8						
13	1.706	11.5						
14	1.746	17.0						
15	1.401	347.4						
16	1.421	0.0						
17	1.484	14.1						
18	1.284	338.0						
19	1.171	0.0						
20	1.286	19.1						
21	1.210	327.0						
22	1.181	315.0						
23	0.875	0.0						
24	0.875	315.0						
25	0.625	0.0						
26	0.625	315.0						
27	0.375	0.0						
28	0.375	315.0						
29	0.125	315.0						

POLAR COORDINATE SYSTEM

Two types of piezoelectric pressure transducers were used to make the dynamic pressure measurements. The transducers used were 1/8-inch in diameter and were similar in design. The characteristics of these Bytrex and Hidyne transducers are given in Table 3-3.

Table 3-3. TRANSDUCER CHARACTERISTICS

Transducer Idensitication	Type	Sensitivity Range	Sensitive Area	Resonant Frequency	Temperature Sensitivity
Bytrex	HFD-2	0-2 psi .5% linearity	.0123 in.^{2}	60 kHz	0.01% per °F
Hidyne	PHF	0-5 psi @ 3mv/psi (Ref to 3V Bridge)	.0123 in.^{2}	70 kHz	0.25%/°F

Due to attrition and a limited supply of transducers it was sometimes necessary during the run sequence to interchange transducer types at a location. No difference in results was noted due to this interchanging of Hidyne or Bytrex transducers.

3.4 PROCEDURE

All runs performed during the tests of this report followed the same general procedure. Since the only controlled variables of the program were a choice of model configuration and stagnation pressure for an associated run, these were predetermined following a format outlined in the pretest reports of references 18 through 20. A class of measurements, such as photographic or pitot data, were then made for the entire range of test variables. Other measurements were then made in reruns at the same set of conditions. Such a method simplified instrumentation set-up and check-out procedures although exact duplication of test conditions was sacrificed since no control over ambient conditions could be exerted.

During a typical run, chamber pressures were controlled within 1 percent of the nominal value using the facility pressure regulation system described. earlier. When the desired test condition was obtained within this tolerance,

data recording was initiated. Stagnation temperatures were not controlled but were recorded throughout a run. A steady-state condition, determined by conformance to the desired stagnation pressure, was maintained throughout a run. A nominal run time of 30 seconds duration was used.

The Schlieren and shadowgraph studies of TAJF-008 and TAJF-009 required no additional procedures except conformance to general practices for photo-visual studies. One precaution taken was that all photographic studies were performed at night to avoid interference from extraneous natural light. This was necessary since the TAJF is essentially an open facility (Figure 3-1).

Preparation for the pitot tube traverse studies of tests TAJF-010 and TAJF-011 included periodic complete pressure transducer checks as well as instrumentation calibration checks prior to each run. The axial and vertical location of the multiple probe rake and the initial position of the traversing probe were set prior to each run and the probe cart then secured to insure no axial shift during facility operation. Post-run checks were also made to verify probe location. Since an optical cathetometer was used for this purpose the probe position was set to within 0.01 inch of the nominal location for all runs. A complete run schedule for those tests is given in reference 16.

In traverses made near the nozzle exit plane, the pitot probes were often at a high angle of attack relative to local flow streamtubes. To determine the possible influence of this angularity, runs were made in which the pitot tube was varied 30 degrees from the vertical. No measurable difference in results were obtained so that the pitot data is presumed unaffected by flow angularity.

Base pressure loads were measured in test TAJF-013. A summary of configuration, chamber pressures, and associated run numbers for the study is given as Table 3-4. In the remainder of this report, the number of engines exhausting and geometric arrangement of the nozzles will be identified by the nomenclature used in the table.

Some runs of a particular configuration were duplicated. This was done because it was determined that the initial dynamic transducer full scale settings

Table 3-4.   RUN SUMMARY FOR BASE LOADING TEST (TAJF-013)

IDENTIFYING SYMBOL	CONFIGURATION WHERE: ● = NOZZLE BLOWING ◁ = DYNAMIC INSTRUMENTATION	RUN NUMBERS		
		P_o = 1500 PSIG	P_o = 900 PSIG	P_o = 500 PSIG
I		3/1, 55/0	2/0, 56/0	1/1, 57/0
IIA		9/0	8/0	7/0
IIA^{-1}		6/1	5/1	4/1
IIB		30/0	29/0	28/0
IIC		52/0	53/0	54/0
IIC^{-1}		49/0	50/0	51/0
IIIA		12/0	11/0	10/0
IIIA^{-1}		15/0	14/0	13/0
IIIB		25/0, 37/0	26/0, 38/0	27/0, 39/0
IIIB^{-1}		22/0, 34/0	23/0, 35/0	24/0, 36/0
IVA		19/0, 33/0	20/0, 32/0	21/0, 31/0
IVB		40/0	41/0	42/0
IVB^{-1}		46/0	47/0	48/0
V		16/0, 43/0	17/0, 44/0	18/0, 45/0

of ± 0.3 psi were in excess of the dynamic loads measured. To improve the accuracy of the readings, the transducer gains were adjusted to ± 0.1 psi following Run 29/0. Discussion will be confined to these latter data which have an estimated overall root-mean-square accuracy of ± 0.03 psi, unless otherwise specified. The number following the run number indicates the attempt to obtain the desired test condition. For example, Run 3/1 indicates the second attempt to obtain data at the conditions of Run 3.

Except for recording, run procedures for this test were identical to the other tests described. All sensors were calibrated periodically. Due to frequent break-downs of piezoelectric transducers such calibration were more frequent than in other tests.

3.5   DATA RECORDING AND PROCESSING

Settling chamber total conditions, pitot data, and base mean static pressures were recorded using a solid state, digital data acquisition system available at the facility. Transducer outputs were converted from analog to digital signals and recorded on Hollerith cards through the SEL (Systems Engineering Laboratory) data acquisition and card punch system. Reduction of these data to physical units was then affected using the measured transducer calibration constants and a data reduction program written for an IBM 1130 Computer.

The data acquisition system for the piezoelectric pressure transducers and condenser microphone is illustrated in the schematic of Figure 3-13. Basically, signals from the piezoelectric transducers are fed to an ENDEVCO 4402 signal conditioning module which supplies three legs of a wheatstone bridge and the D.C. excitation. The signal then goes to a TEKTRONIX differential amplifier (gain = 1 volt rms), and then to the voltage control oscillator (VCO) manufactured by Data Control System. Here, nine channels of the data were accepted simultaneously and multiplexed to preserve phase information and, thus, facilitate cross-correlation of the data. The multiplexed data were then sent through a coaxial cable and recorded on a Consolidated Electrodynamics Corporation VR 3600 tape recorder at 120 ips. This system effectively restricts the data obtained to frequencies between 0.1 and 20 kHz. Recording errors estimated from reference 21 are given in Table 3-5 for the data acquisition system.
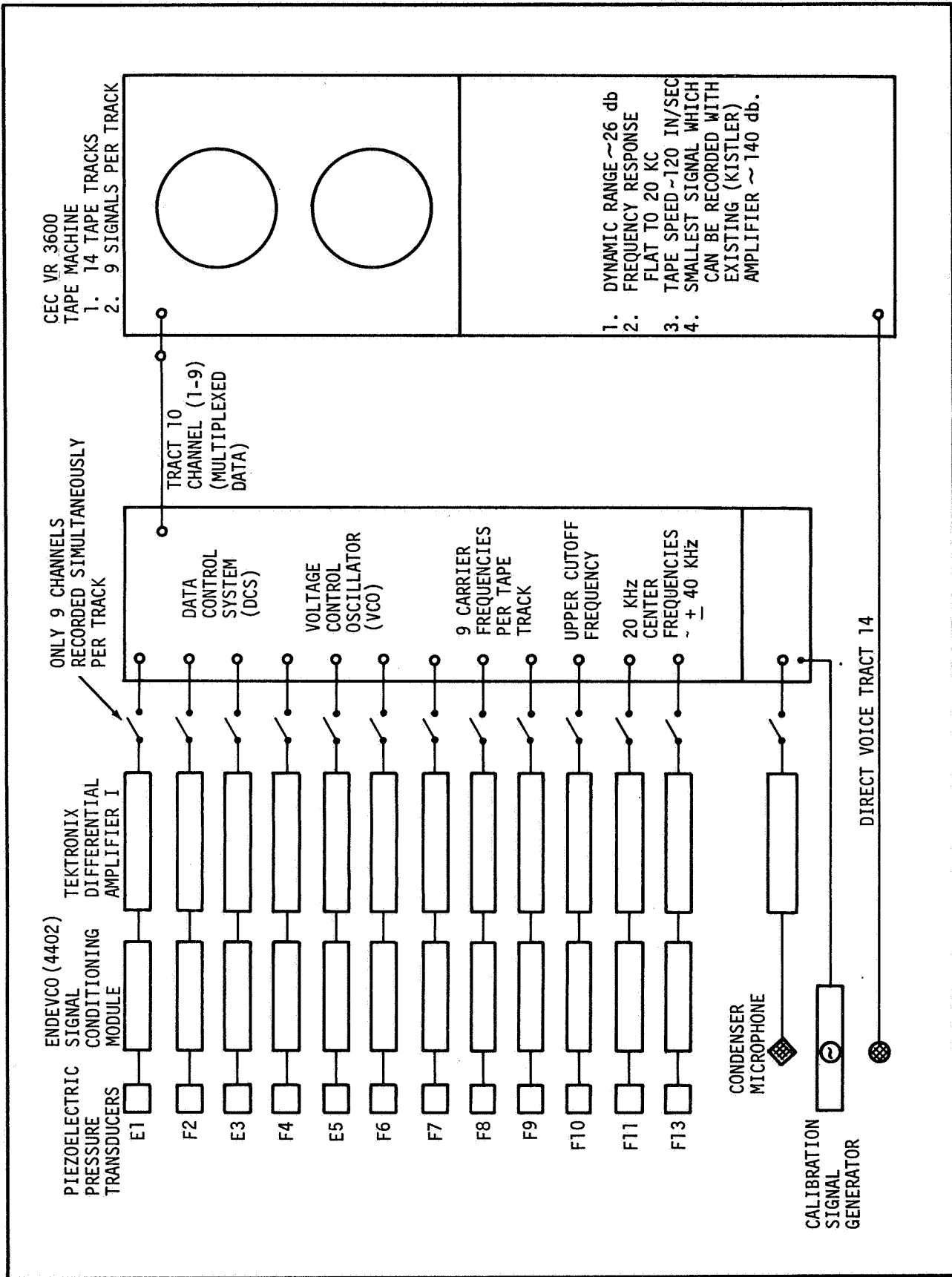
Figure 3-13. DYNAMIC INSTRUMENTATION DATA ACQUISITION SYSTEM

Table 3-5. ESTIMATED RECORDING ERRORS

INSTRUMENT	PHASE ANGLE ERROR	AMPLITUDE ERROR(%)	FREQUENCY ERROR(%)
VCO DCS Multiplex System	0 - 12°	0.50	0.25
CEC VR 3600 Tape Recorder	0 - 6°	0.50	0.25
Accumulative Worst Case Estimate	15° at	1.00	0.50

Dynamic data reduction was accomplished primarily using analog equipment. A few runs were also selected and computed using the CORFUN digital program of reference 22. Corroboration of the analog results was obtained for those runs. Instruments used for this study included an analog correlator and a one-third octave frequency analyzer.

The correlator used was a Honeywell, Model 9410, Time Delay Correlator. This instrument computes auto- or cross-correlation functions of periodic or random data from 0.05 kHz to 250 kHz. Specifications, range, sensitivity, and operating details of this instrument are given in reference 23.

The individual operations performed by the correlator are:

● Signals received by the correlator are delayed in time with respect to each other and multiplied to form a product.

● The instantaneous product is averaged by integration over a period of time. Implicit in the operation is the selection of integration time sufficiently long to obtain meaningful averages.

● These steps (delay, multiply, and average) are repeated for additional discrete time delays until a correlogram is generated.

To reduce the transducer and microphone data, the data tape was played back on the VR 3600 Recorder at 120 ips and passed through an appropriate demodulating system. Gains were adjusted to overcome the noise threshold of the correlator, but sufficiently low to preclude clipping. Most raw data were

adjusted to about 2 volts peak-to-peak where possible. Autocorrelations were first calculated by re-running the tape at 120 ips and correlations were obtained one point at a time. An integration time of 5 sec was pre-selected for each case, since about four times this amount of steady state data was available on tape. When all autocorrelograms of the desired data were completed, pairs of these ramdom signals were cross-correlated in a similar manner without readjustment of any gain settings previously determined during autocorrelation. Negative values for the correlograms were determined by reversing the channels of input data. This dimensionless function was then plotted as a function of time delay to form the correlograms presented in this report.

Power spectra and most root-mean-square values were determined by use of a Bruel and Kjaer 1/3 Octave Frequency Spectrometer, Type 2112. The selective frequency range for this instrument is 22 to 45,000 Hz. Frequency analysis with this instrument may be based on standard 1/1 or 1/3 Octave band-pass filters. Only one-third octave analysis was used in this study. Additional information on the spectrometer is given in reference 24.

Tape handling procedures for the spectral analysis of dynamic data were similar to those used with the correlator. One exception to be noted is that demodulator gains were not adjusted as in the case of the correlation determinations. As the tape was played, the root-mean-square value in the frequency band selected was recorded. The tape was then replayed until the entire 0.1 to 20 kHz range was covered. The overall root-mean-square value was also read from this instrument. Power spectral density was then calculated by the relation

$$S(f_c) = \frac{<p'^2>}{\Delta f} \qquad (3\text{-}1)$$

where f_c is the centerband frequency of the 1/3 octave band of width Δf.

Section IV

PRESENTATION OF RESULTS

Data obtained in the preceding tests are presented in this section. Sub-section 4.1, considers characteristics of the flow in the clustered jets of the investigation and the limited acoustic data taken on these jets. In subsection 4.2 the mean and dynamic variation of static pressures on the Cluster Model baseplate is presented.

4.1 CHARACTERISTICS OF CLUSTERED JETS

The detailed pitot traverses made in this investigation were required to determine the operating characteristics of the clustered nozzles studied, to allow estimation of shear layer location and thickness, and for comparisons with results of other model tests. These mean data have been reported pre-viously in reference 17.

For all stagnation pressures used in these experiments (P_o = 500, 900, or 1500 psig), the nozzles were operating in a highly under-expanded mode. As a result the accommodation of the static pressures in the plume core to the am-bient pressure (nominally P_a = 14.4 psia) was by a multiple shock system such as shown in Figure 4-1. Flows near the plume boundary were thus characterized by an inner boundary shock originating within the nozzle and an outer boundary shock arising at the nozzle lip. It appears from the photographic data that the shear layer lies mostly outside the lip shock.

In regions where jet interactions occurred, additional complexities in the shock structure resulted. Such a situation is depicted in Figure 4-2 where it is seen that impingement of adjacent plumes generates interaction shocks resulting from the coalescence of an impingment shock and the boundary shocks present in the individual plumes. An increase in the number of jets exhausting, then, increases the number of interactions that occur, as well as creating regions where three or even four plumes interact coincidentally.

Proceeding downstream, a normal shock or Mach disc terminates the super-sonic portion of the jet. The location of this shock is dictated for a given
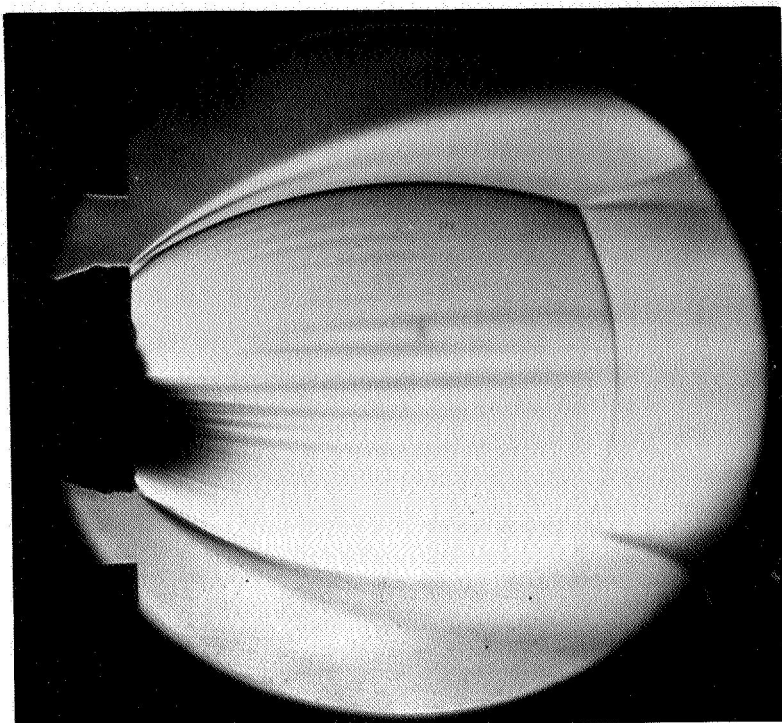
Figure 4-1. SINGLE NOZZLE EXHAUSTING FROM A
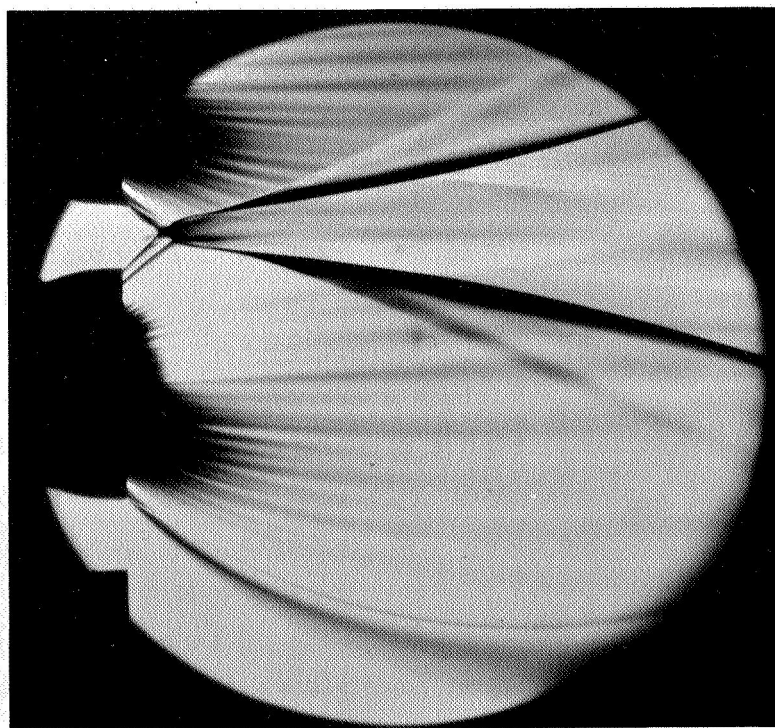STAGNATION PRESSURE OF 900 PSIG

Figure 4-2. JET INTERACTION REGION FOR A TWO-
JET CONFIGURATION (P_o = 1500 psig)

nozzle, by the stagnation-to-ambient pressure ratio (ref. 25). As may be seen from Figure 4-3, the interaction between a Mach disc and plume interaction shock creates additional interaction regions and Mach discs.

Representative pitot pressure profiles are presented in Figure 4-4 for a two-jet cluster. Two unusual aspects of the pitot pressure profiles are the significantly higher pressure recoveries observed in the core of the individual jets at low X/D ratios and the rise noted near the edge of the plumes and in interaction zones. The former effect is due to the extreme Mach number variation across these jets. Typical values ranged from M = 2.7 at the centerline to M = 4.4 immediately within the interior shock for a chamber pressure of P_o = 500 psig at X/D = 0.22. For P_o = 1500 psig the variation is from M = 2.7 to M = 6.0 at the same locations. The latter effect is believed due to a more efficient pressure recovery by the pitot tube in the vicinity of the two shock system formed by the plume bounding oblique shock and pitot bow shock.

Attempts to determine velocity distributions across the plume from these data were only partially successful. In the initial expansion region of the plume, that is, in the shock cell formed by the Mach disc and interior shock, the flow is essentially isentropic. Applying one-dimensional flow relations to data obtained in this region showed excellent agreement with the flow field predicted by the method of characteristics (ref. 17). At the outer edge of the shear layer, the static pressure is known to be equal to the ambient pressure so that a velocity determination from the pitot data was also possible. Between these extremes, the local stagnation pressure of the flow is not known due to the presence of shocks.

An estimate of the velocity distribution across the shock-shear region was obtained by assuming

$$\frac{u_o - u}{u_o} = \left[1 - (1-\eta)^{3/2} \right]^2 \tag{4-1}$$

where u = local velocity, u_o = velocity in potential region, and η = dimensionless location in the shear layer. This relation, originally due to Abramovich (ref. 26), constitutes a good approximation for the initial region of supersonic under-expanded jets (ref. 25).
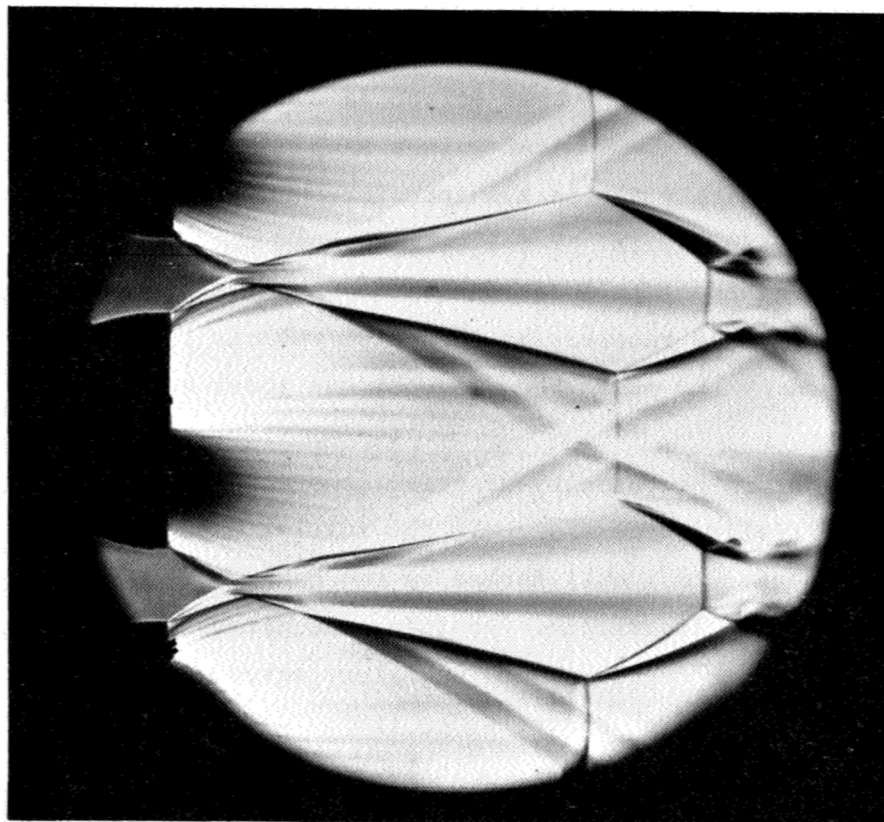
4-3

Figure 4-3. MULTIPLE JET INTERACTIONS FOR SATURN
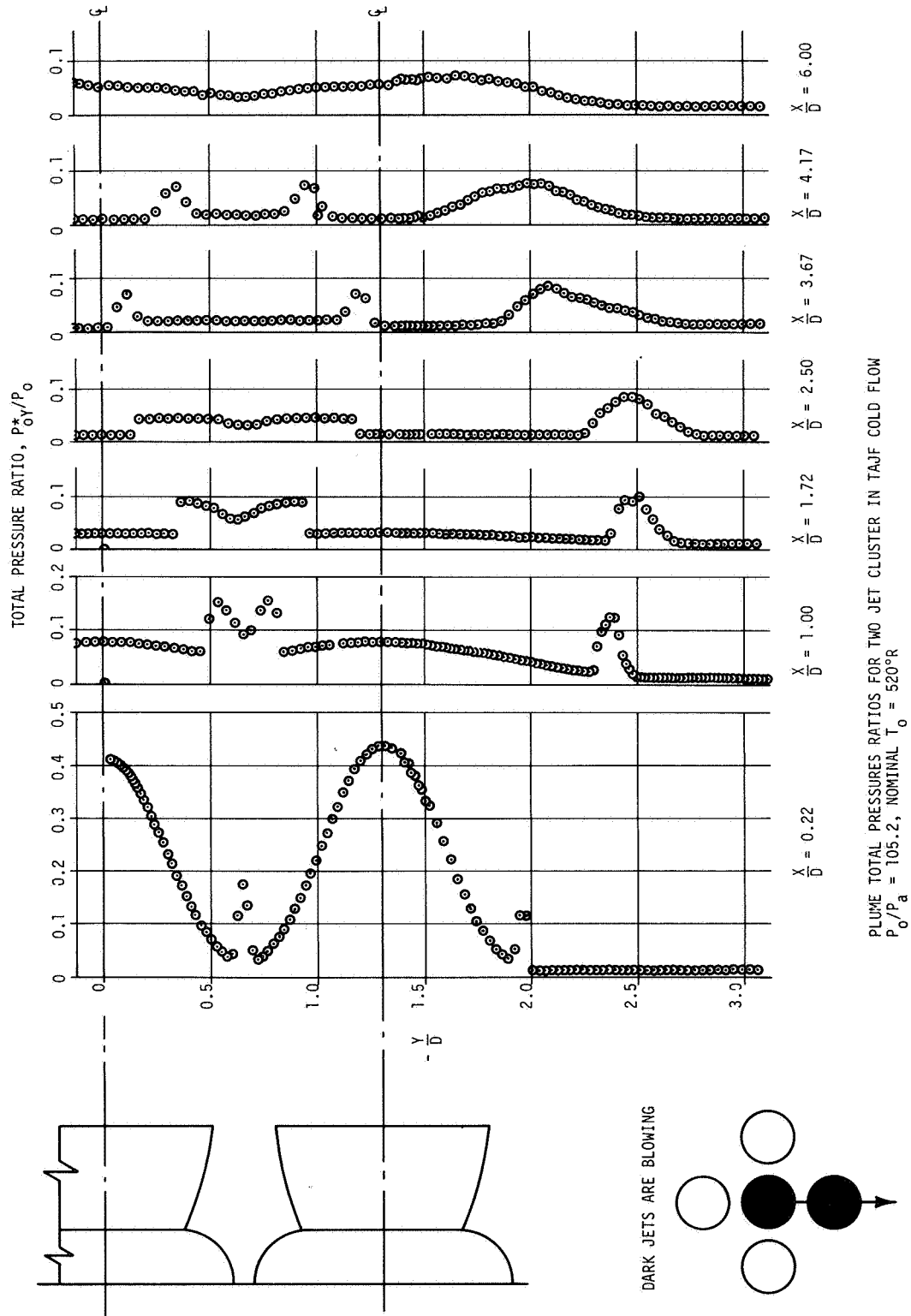CONFIGURED CLUSTER (P_o = 600 psig)

Figure 4-4. TYPICAL PITOT PRESSURE PROFILE ACROSS CLUSTERED JET (REF. 17)

The velocity profile resulting from the use of this relation in the viscous region, and isentropic relations in the potential core is shown for several axial locations in Figure 4-5. Non-uniformities noted in the velocity profile near the exit have nearly vanished within a diameter of the exit. This behavior was also noted at lower stagnation pressures.

Attempts to estimate velocity distributions in the subsonic portion of the jet (downstream of the Mach disc) were unsuccessful. The reason for this failure is that the static pressure in the subsonic region does not immediately obtain equilibrium with the ambient pressure. The study presented in reference 25 shows that pressures in this region oscillate around the equilibrium value by $\pm$ 50 percent for 10 to 15 diameters downstream of the initial shock cell.

An additional factor of interest for scaling of results from this investigation is the extent of the shear layer. Two means of correlating such data are the analytical relations due to Che-haing (ref. 25) and Korst (ref. 7). The latter was not used for the present study because it is, by assumption, only valid far from the nozzle lip (where the spreading is linear). The former expression, although applicable, was not used since it required scaling with the curvature of the jet boundary which is inconvenient to use. A simple empirical relation was obtained which describes the variation of shear layer thickness in these investigations. The thickness varies as

$$\frac{\delta}{D} = 0.02 + 1.44 \, \phi \qquad\qquad (4\text{-}2)$$

where

$$\phi = \left(\frac{X}{D}\right)^{0.565} \left(\frac{P_o}{P_a}\right)^{-0.435}$$

A comparison of the data and this relation is given in Figure 4-6. The linear variation of the thickness with the parameter ϕ is quite good for $X/D \le 2$.
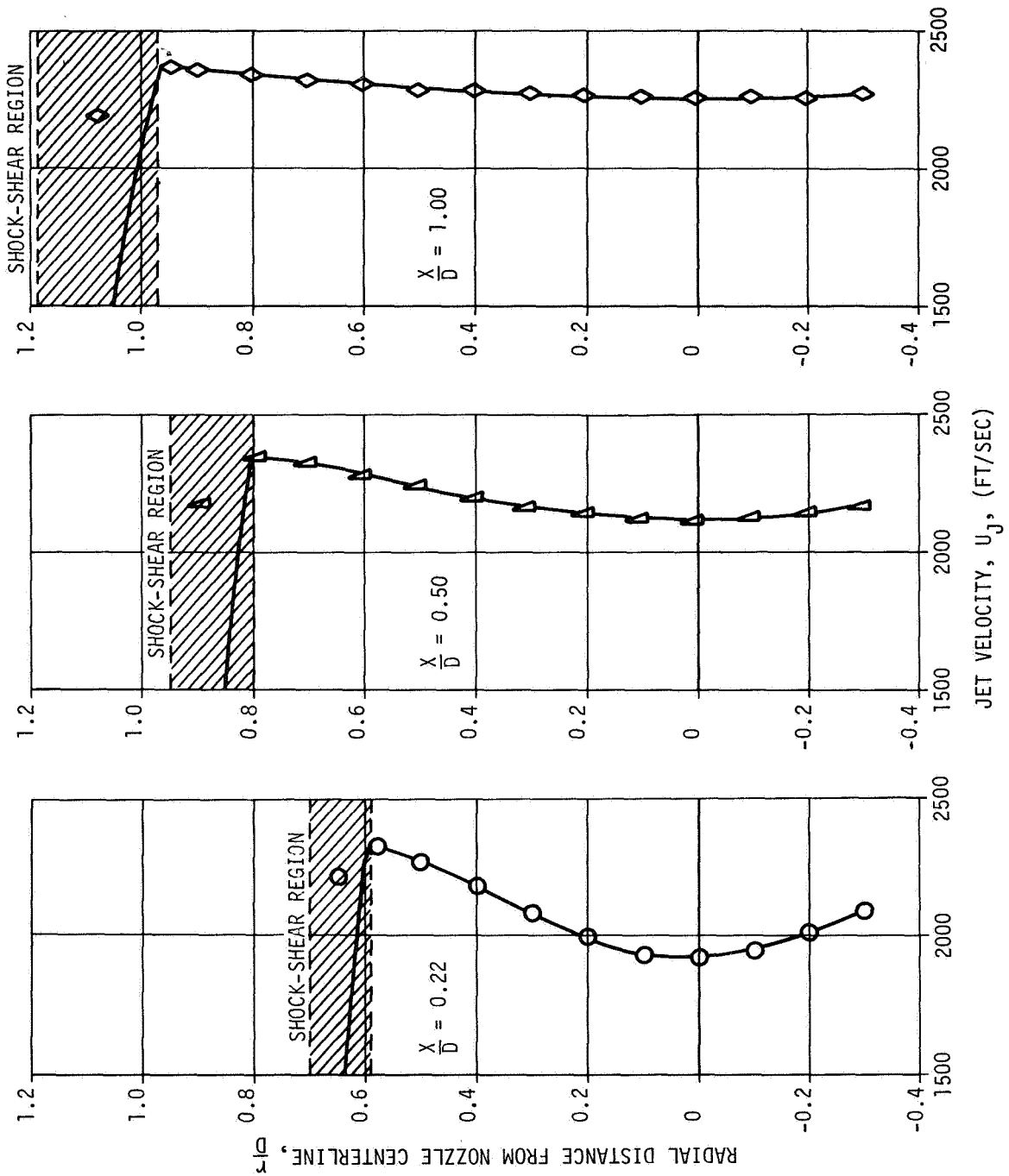
Figure 4-5. VARIATION OF JET VELOCITY FOR SATURN CLUSTER MODEL (P_o = 1500 psig)

STAGNATION - AMBIENT PRESSURE RATIO, $\dfrac{P_0}{P_a}$

   ○   35.7

   □   63.5

   ◇   105.2

$$\frac{\delta}{D} = 0.02 + 1.44\phi$$

Y-axis: APPARENT SHEAR LAYER THICKNESS, $\dfrac{\delta}{D}$

X-axis values: 0, 0.05, 0.10, 0.15, 0.20, 0.25, 0.30

Y-axis values: 0, 0.2, 0.4, 0.6, 0.8, 1.0

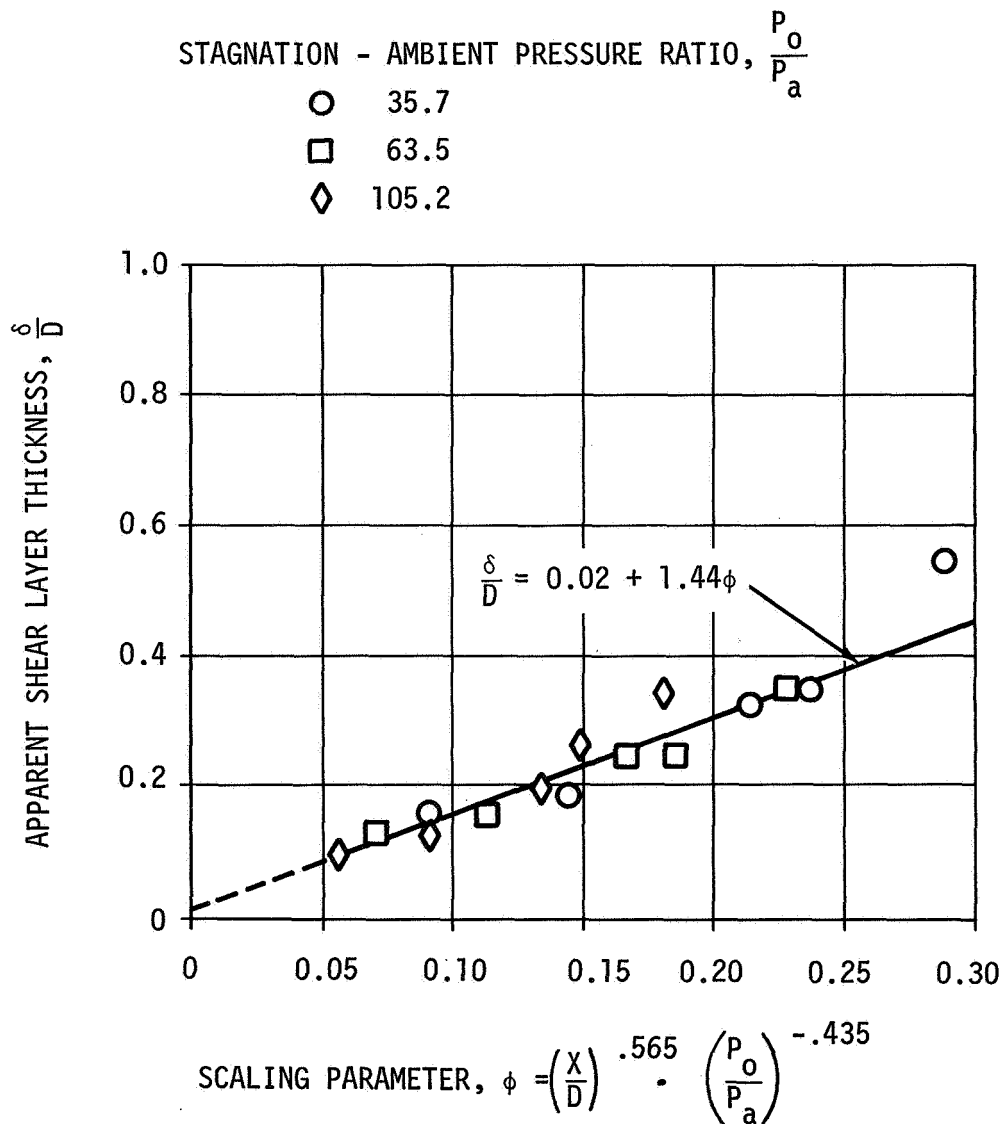$$\text{SCALING PARAMETER, } \phi = \left(\frac{X}{D}\right)^{.565} \cdot \left(\frac{P_0}{P_a}\right)^{-.435}$$

Figure 4-6. VARIATION OF SHEAR LAYER THICKNESS NEAR NOZZLE
EXIT PLANE

Far-field microphone data were taken at a single location relative to the model as noted in Section III. The root-mean-square acoustic pressure at that location is shown in Figure 4-7 as a function of chamber pressure for several configurations. The variation is seen to be a linear function of stagnation pressure and increases in level with additional jets blowing for Configurations I, IIA, and IIIA. This trend was not observed for the symmetric four-jet (IVA) and Saturn (V) configurations which show essentially identical sound pressure level trends.

It is of interest, in view of this latter result, to compare these data to empirically established trends. References 27, 28 and 29 indicate that the acoustic power radiated by a supersonic jet or rocket is proportional to the mechanical power of the exhaust. This power may be expressed (in watts) by

$$W_M = 0.67 \ F \cdot V_e \qquad\qquad (4-3)$$

where F is the thrust (lb_f) and V_e the exit velocity (ft/sec). For the Saturn Cluster Model the thrust may be approximated by

$$F = A^*N \ P_o V_e \sqrt{\frac{\gamma}{gRT_o} \cdot \left(\frac{2}{\gamma+1}\right)^{\frac{\gamma+1}{\gamma-1}}} \qquad\qquad (4-4)$$

For this cold-flow experiment the only significant variation in the parameters affecting mechanical power arises from the change in the number of engines exhausting, N, and the stagnation pressure.

The measured sound pressure levels are plotted against the mechanical power in Figure 4-8. The slope of the sound pressure level rise agrees with that proposed by Von Gierke (ref. 27) except at the highest power levels. In most cases, the values obtained for clusters of three or more rockets fall below the established trend. This indicates that clustered exhausts tend to interfere with one another, as is commonly accepted.

Microphone power spectra for the single jet configuration are shown in Figure 4-9. The power spectral density is seen to increase almost linearly on
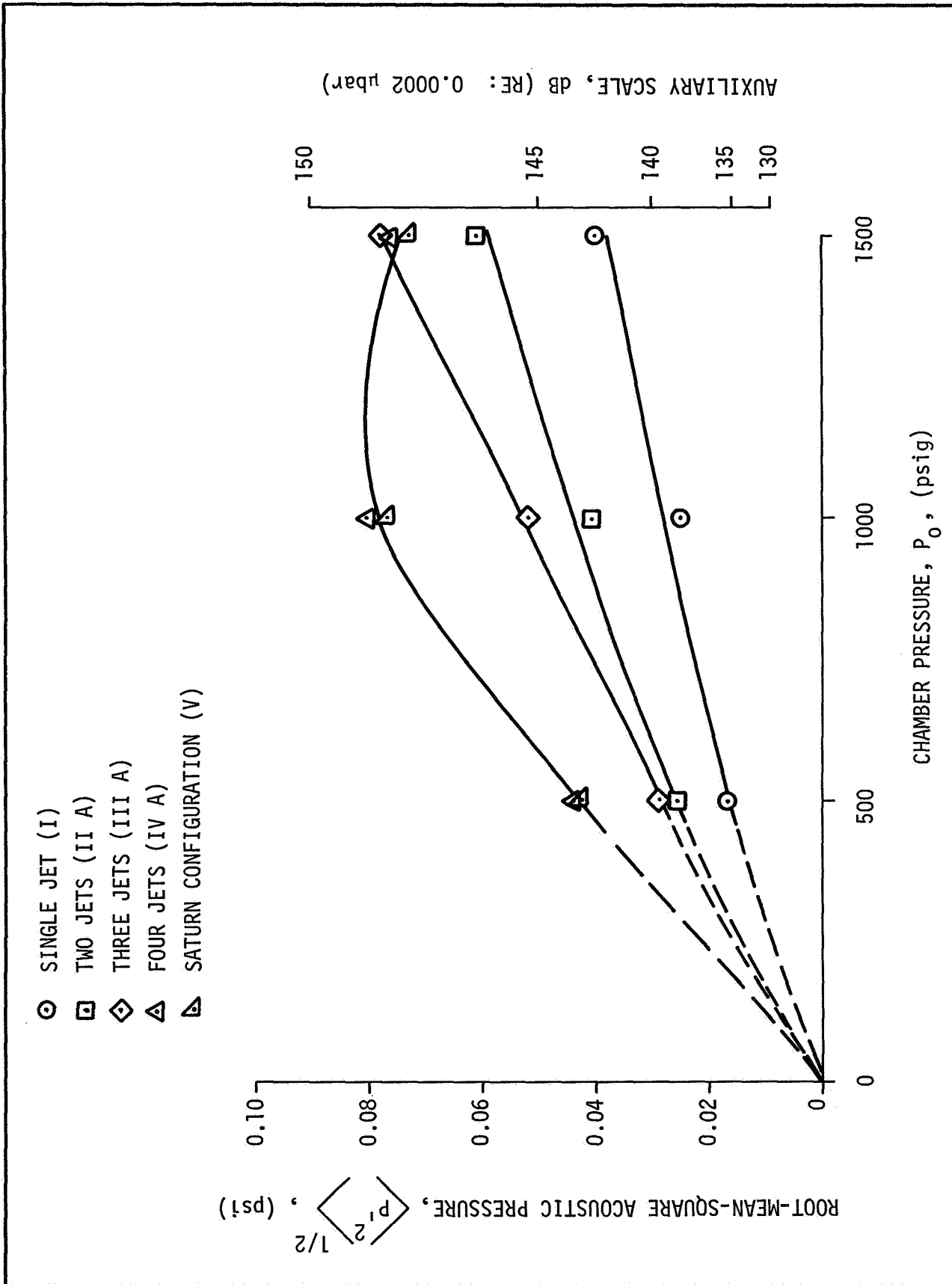
NORTHROP·HUNTSVILLE

Figure 4-7. VARIATION OF FAR-FIELD MICROPHONE PRESSURE WITH CHAMBER PRESSURE FOR SEVERAL CONFIGURATIONS
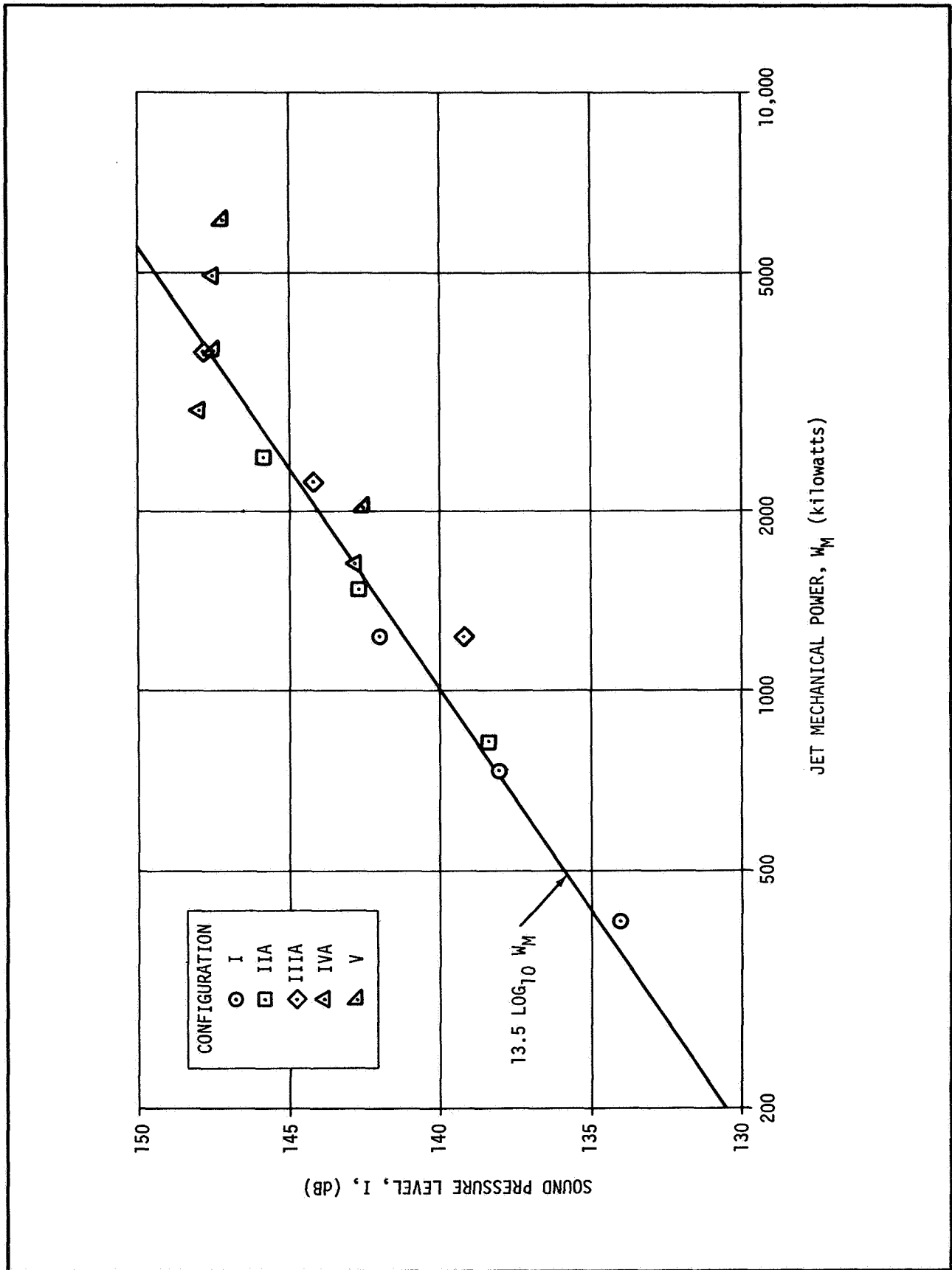
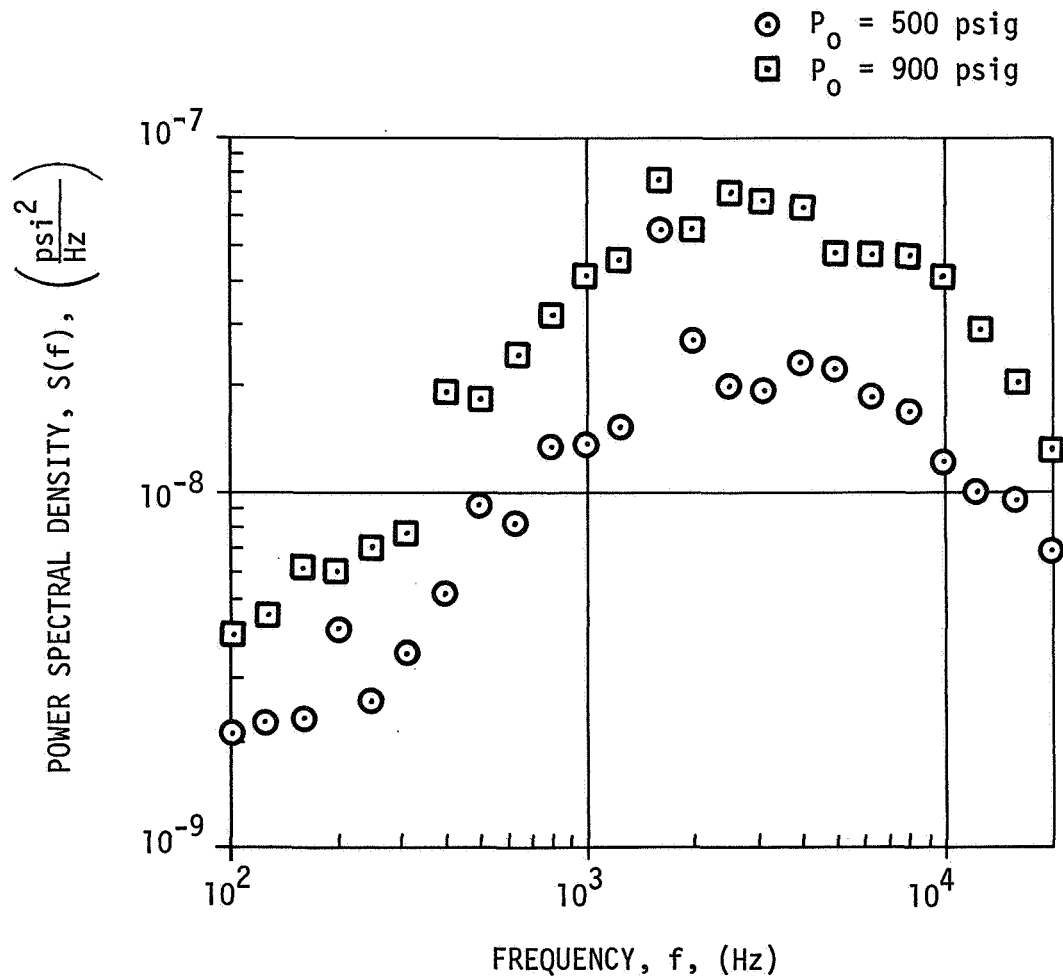Figure 4-8. VARIATION OF SOUND PRESSURE LEVEL WITH JET POWER

Figure 4-9. MICROPHONE SPECTRA FOR SINGLE JET EXHAUSTING
(CONFIGURATION I)

the logarithmic scale up to 1.0 kHz thus indicating a simple power law dependency at low frequencies (i.e., $S(f) \sim f^m$). The four-jet spectra, shown in Figure 4-10, do not exhibit such behaviors at low frequencies appearing more like a white noise signal over the entire frequency range. Spectra obtained for the Saturn configuration, Figure 4-11, appear similar to the four-jet case at the lower chamber pressure and similar to the single jet at the higher pressure. The microphone spectra display similar trends above, approximately 4 kHz, and, as will be shown later, the greatest contribution to the measured acoustic levels occurs above that frequency.

Comparisons of these data with conventional scaling parameters for supersonic jets were not successful. From the shadowgraph shown on Figure 4-12, it is seen that the microphone arrangement was such that the dominant factor influencing the spectra is Mach wave emission in the initial supersonic portion of the jet. Since frequencies tend to be highest in this initial region, it is to be expected that the spectra are effectively weighted to higher frequencies than would be normally expected. Some verification of this speculation may be gained from the dimensionless spectra of references 28 and 29. For both cases it was found that the acoustic power is down 20 dB from the peak value for a Strouhal number of 10. Applying the Strouhal number definition of reference 28,

$$S = \frac{fD^*}{C_a} \left(\frac{2}{\gamma+1}\right)^{\frac{\gamma}{\gamma-1}} \left(\frac{P_o}{P_a}\right)^{1/2} \qquad (4\text{-}5)$$

where D^* is the throat diameter and C_a, the ambient acoustic velocity, to the cluster model tests, one obtains a maximum Strouhal number ranging from 5 to 8.5 for the various chamber pressures of the investigation. In this range the acoustic power would be expected to be down by 12 to 18 dB from the peak value. It is obvious from the spectra measured that this was not the case.

A conclusion obtained from this discussion is that the rms pressures measured are appreciably lower than the true values. It will be seen later that the base pressure data also contain significant energy above the tape system cut-off frequency of 20 kHz although the amount occurring is less than in the
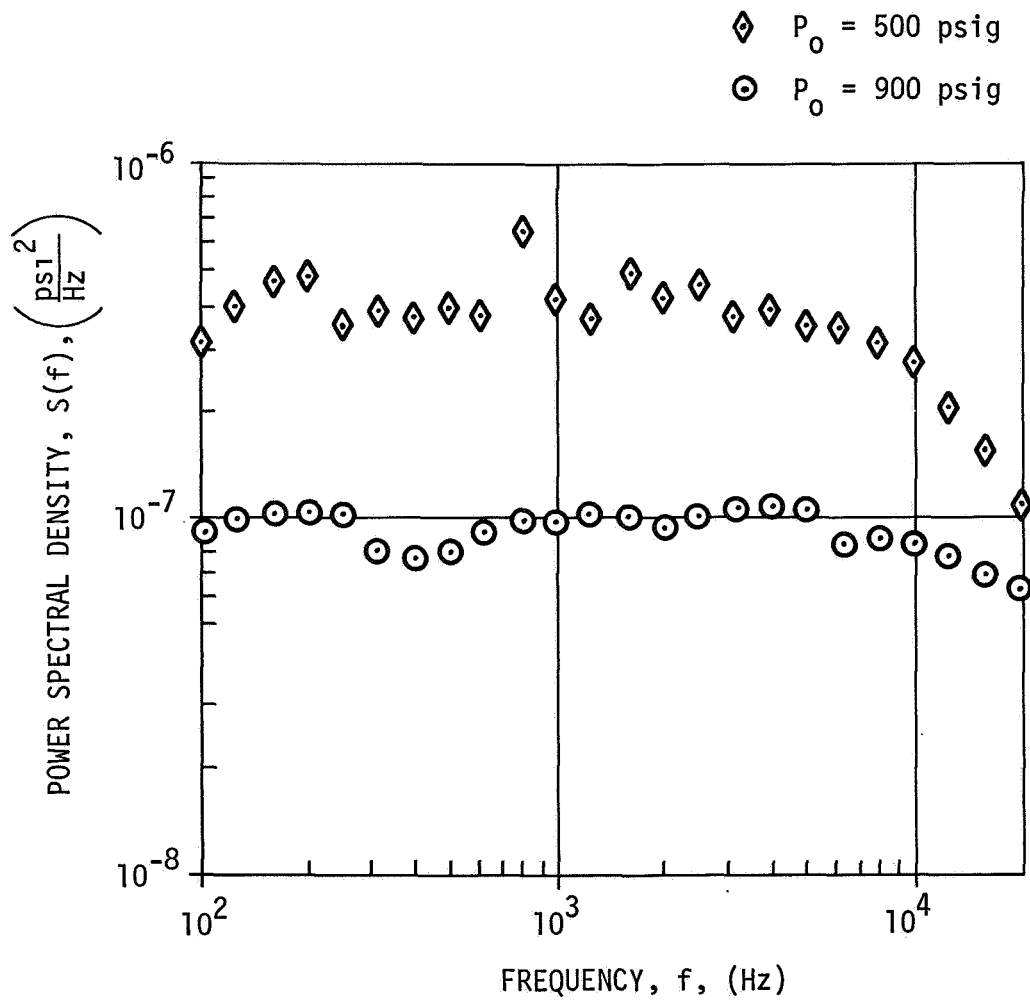
Figure 4-10. MICROPHONE SPECTRA FOR FOUR JETS EXHAUSTING
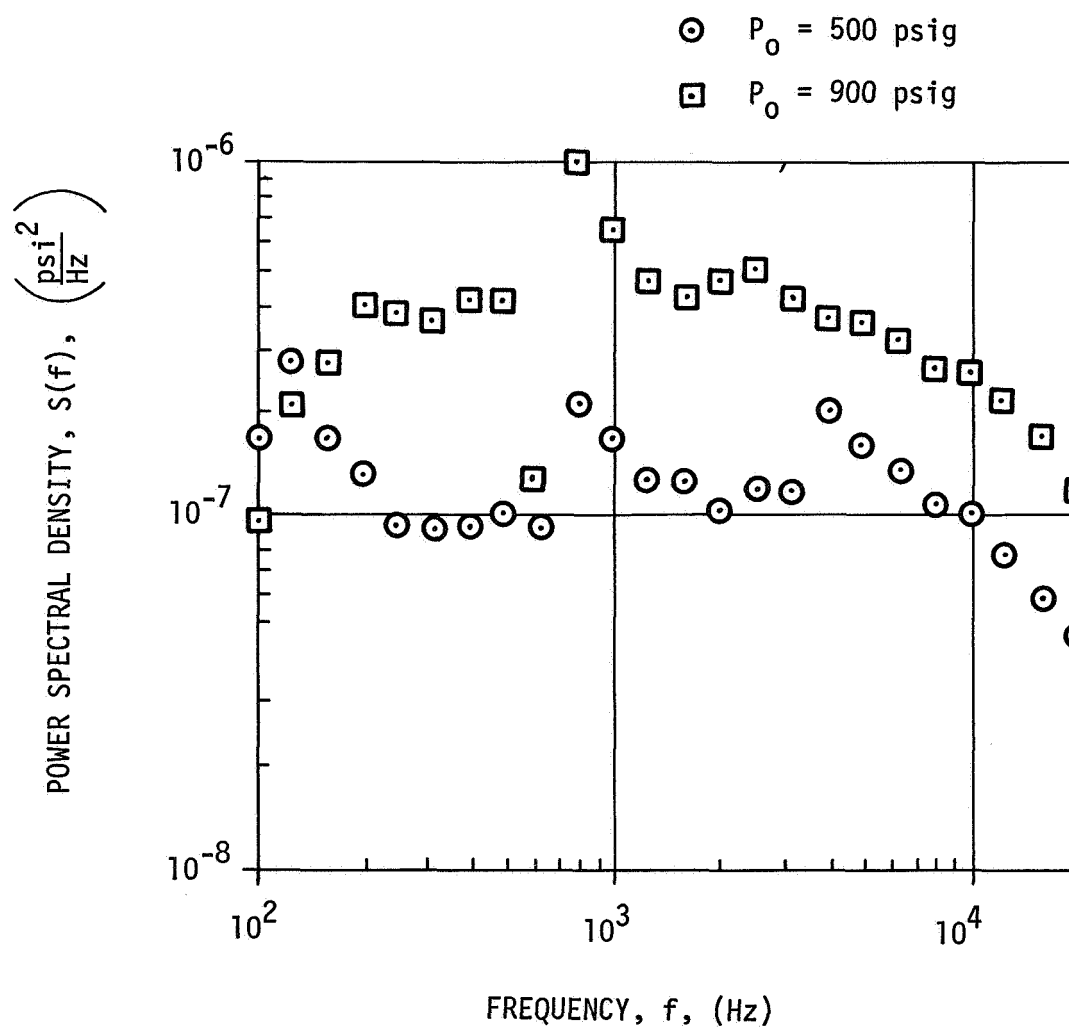(CONFIGURATION IVA)

Figure 4-11. MICROPHONE SPECTRA FOR SATURN CLUSTER EXHAUSTING (CONFIGURATION V)

Figure 4-12. SHADOWGRAPH SHOWING MACH WAVE PATTERN AND MICROPHONE LOCATION

microphone data. Finally, it is observed that this anomaly does not affect
the conclusion drawn earlier as the scaling of levels with jet power. Since
the spectral results for all cases are similar at high frequencies, It is
expected that only the absolute magnitude of the sound pressure level is affected,
but not the data trend.

4.2 LOADS AT THE BASE OF CLUSTERED JETS

Although a large body of mean static pressure data were taken in the test
series, departures from the ambient pressure were minimal in most cases. For
example, measurements taken for the single-jet configuration indicated $\overline{P}_b = P_a$
for all chamber pressures. The Saturn configuration measurements also showed
slight departures from ambient pressure with the differential, $\overline{P}_b - P_a$, ranging
from 0 to -0.1 psi at the P_o = 500 psig condition to -0.1 to -0.2 for P_o = 1500 psig.
Although the primary intersection of the plumes occur within a nozzle diameter
of the exit in the latter case, these results are quite reasonable, for signi-
ficant convection is not expected since the impingement zone is not fully closed.
The primary action of the plumes is, therefore, to produce an ejector effect, thus
accounting for the negative values of the pressure differential.

Significant departures from the near uniformity of base pressures were
observed, however, for the symmetric four-jet configuration (IV A). An approxi-
mate contour plot for this case is shown for P_o = 500 psig in Figure 4-12. This
figure shows that the pressure differential is -0.3 psia at the edge of the base-
plate, increases to -0.1 psi between the impinging jets, then decreases rapidly
to a value of -0.8 psi at the center of the base. This case contrasts greatly
with that observed for P_o = 1500 psig as seen in Figure 4-13. Here the pressure
differential decreases from zero to a -0.2 psi difference between the impinging
jets, then reverses and rises to a peak value of +0.7 psi above ambient near
the center of the plate.

In interpreting these results it should be recalled that the static pressure
transducer and recording system have an overall accuracy of approximately
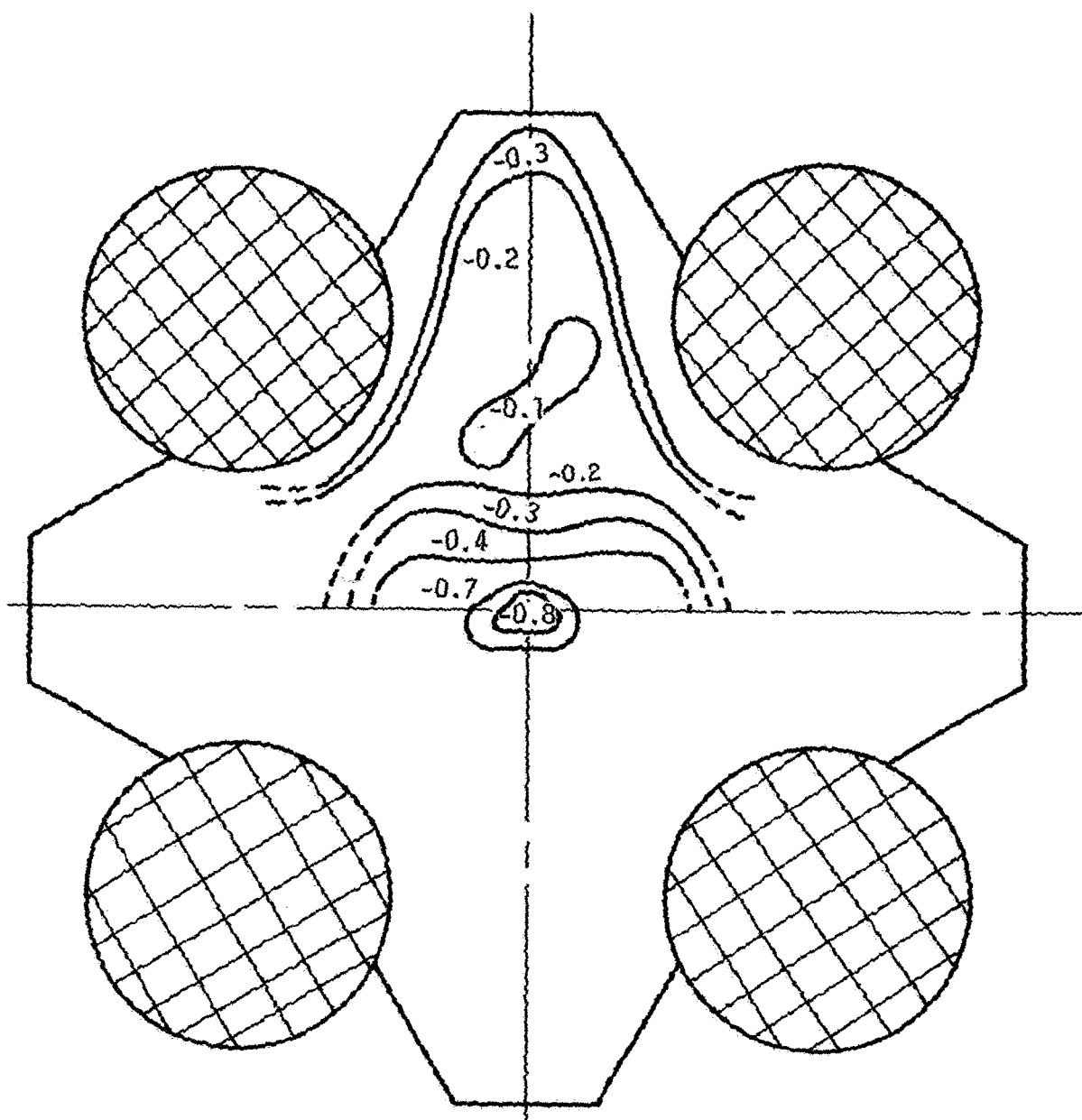$\pm$ 0.1 psi. Thus, little credence may be attached to data nearly at atmospheric

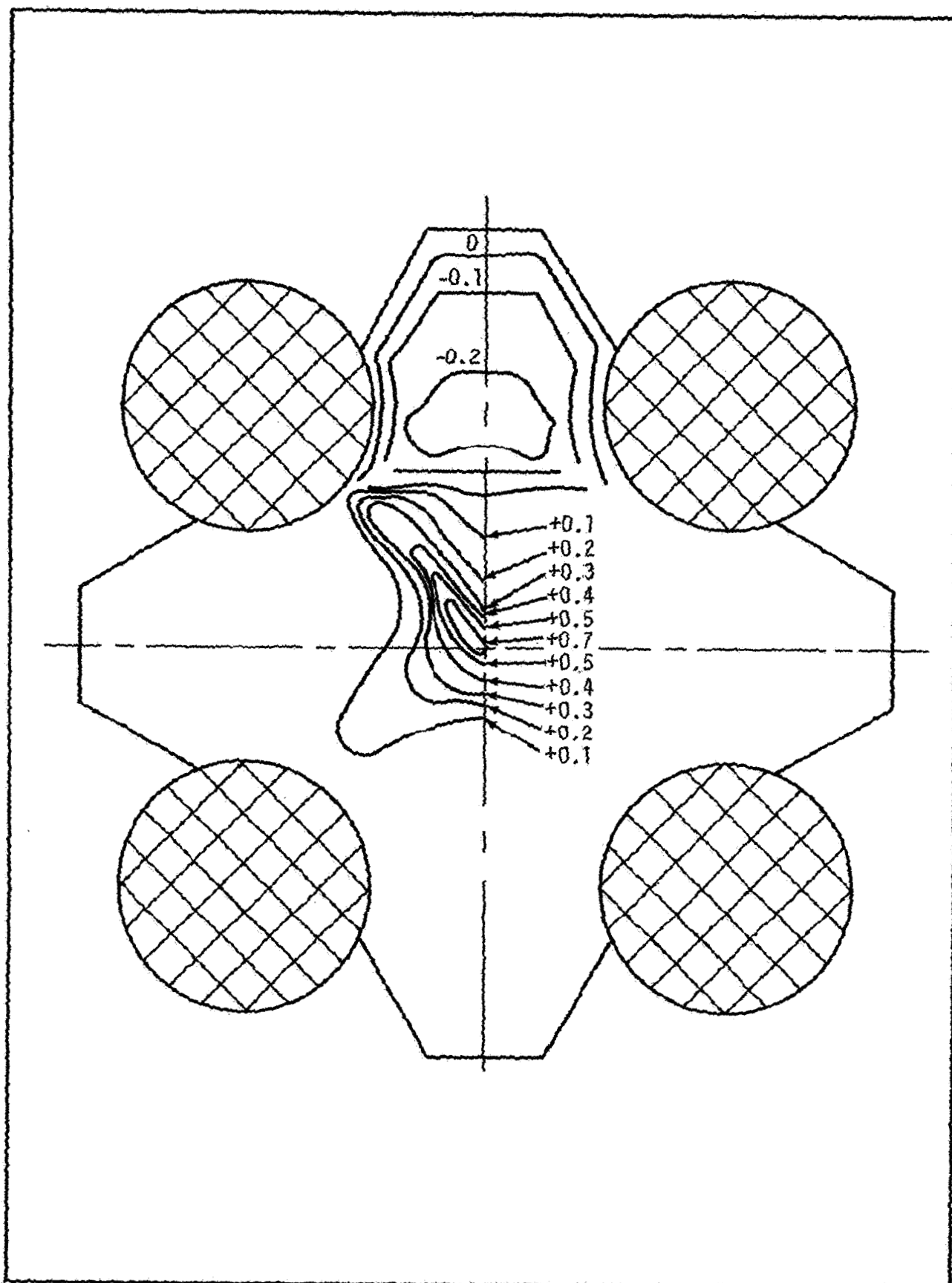Figure 4-13A. APPROXIMATE BASE STATIC PRESSURE $(\bar{P}_b - P_a)$ CONTOURS FOR CONFIGURATION IV A $(P_o = 500 \text{ psig})$

Figure 4-13B.   APPROXIMATE STATIC PRESSURE $(\bar{P}_b - P_a)$ CONTOURS FOR CONFIGURATION IV A $(P_0 \approx 1500 \text{ psig})$

pressure. The pressure extremes noted, however, are well within the capability of the system resolution and are accordingly considered as a physical manifestation of a jet induced flow along the baseplate. It is further noted that plume closure is possessed by this configuration at high stagnation pressures so that recirculation may be expected.

Pressure variations along the major instrumented axis of the model ($\theta=0°$, Table 3-3) are shown for the four-jet cluster in Figure 4-14. The appearance of these data near $r = 0$ suggests flow near a stagnation point at the highest chamber pressure and flow into a sink at the lowest. Similar trends have been noted with a four-jet cluster by Goethert (ref. 8). Assuming an incompressible stagnation flow (ref. 30) near the center of the baseplate, the flow velocity required to match the data in that region is approximately 50 ft/sec or less than 4 percent of the mean velocity in the shear layer. This velocity would necessarily be much higher in the vicinity of the engine bells if the flow model could be assumed valid in that region. It is likely, however, that air is drawn into the base region near the outer region of the plate due to the pumping action of the jets. If so, this action coupled with the recirculatory flow from the plume would cause a complex vortex pattern to exist above the baseplate at high stagnation pressures.

The rms dynamic pressures on the baseplate are shown for Configuration I in Figure 4-15. Virtually no variation was found between transducer locations for this single jet case. The values obtained are, moreover, only slightly influenced by chamber pressure indicating only a weak dependence on the jet power.

Four-jet cluster data are shown in Figure 4-16. The data for $P_o = 500$ psig and $P_o = 1500$ psig are similar in trends with a linear decrease from the high values noted in the center of the base to a nearly constant lower level between the outboard nozzles. It is further noted that the levels in the central region are preferentially higher along a line drawn through $\theta = 180°$. The rms levels at the intermediate pressure ($P_o = 900$ psig), however, show little variation and fall substantially below the levels noted for other chamber pressures.
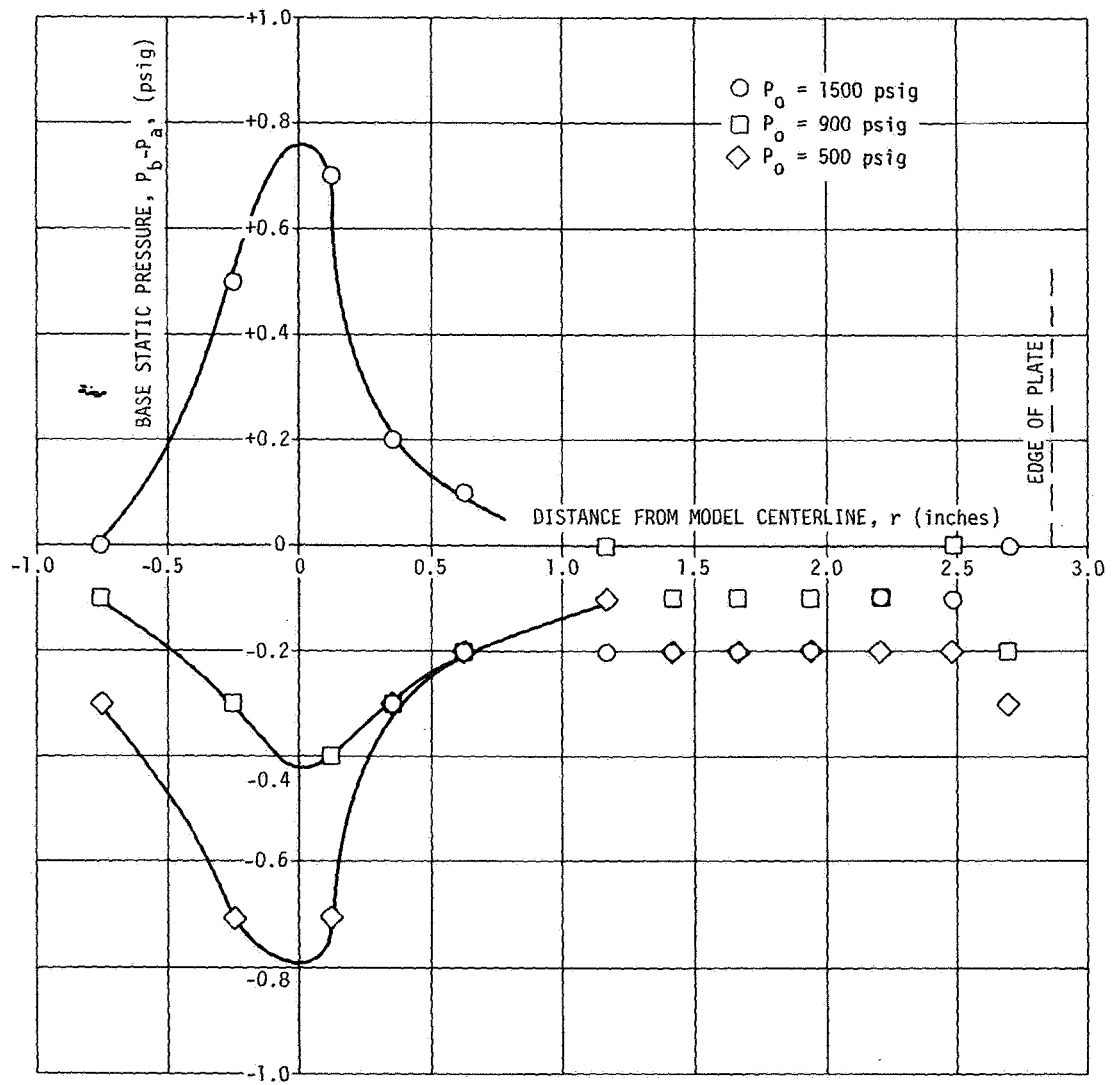
Figure 4-14. DISTRIBUTION OF MEAN PRESSURES FOR SYMMETRIC FOUR JET
CONFIGURATION
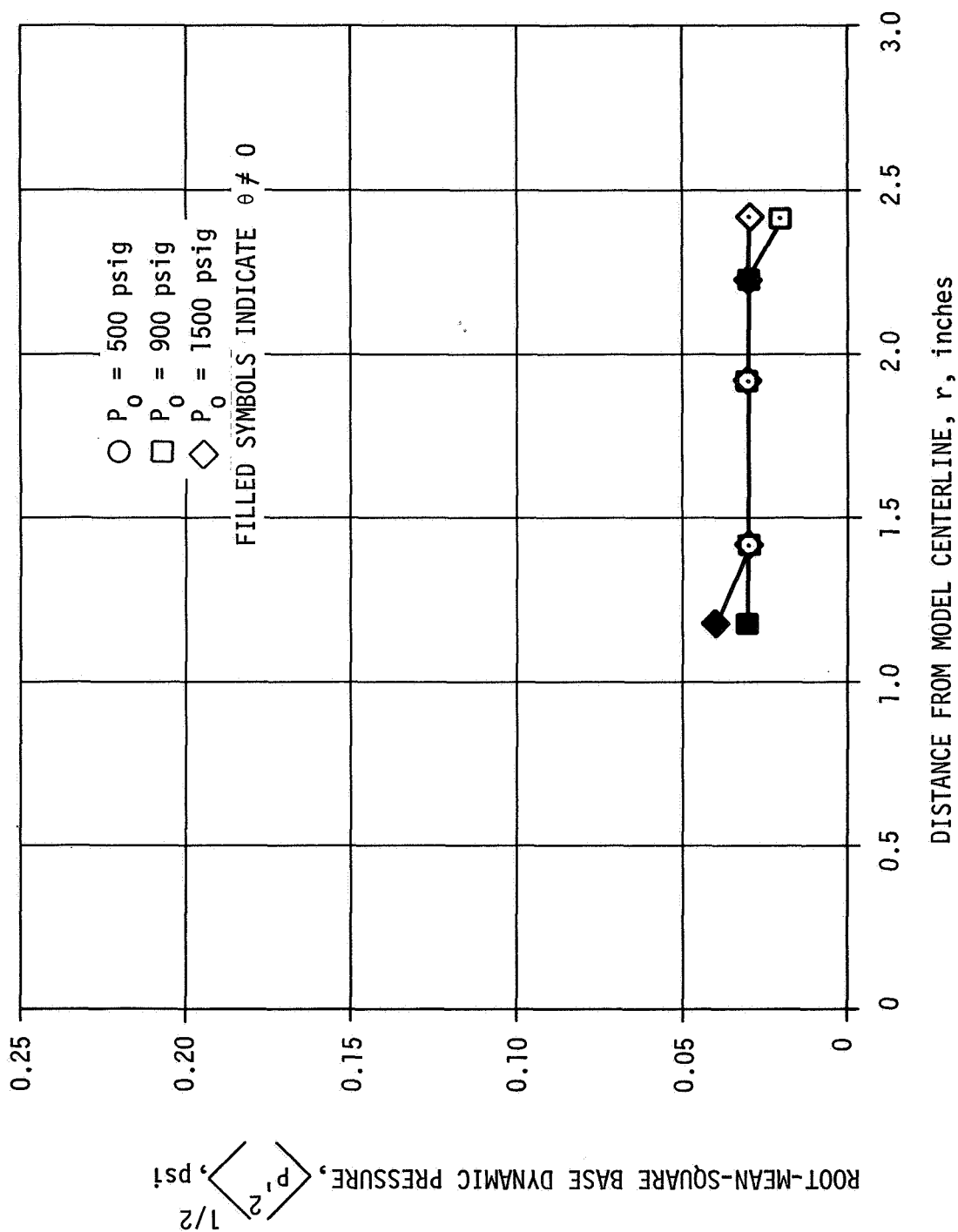
NORTHROP·HUNTSVILLE

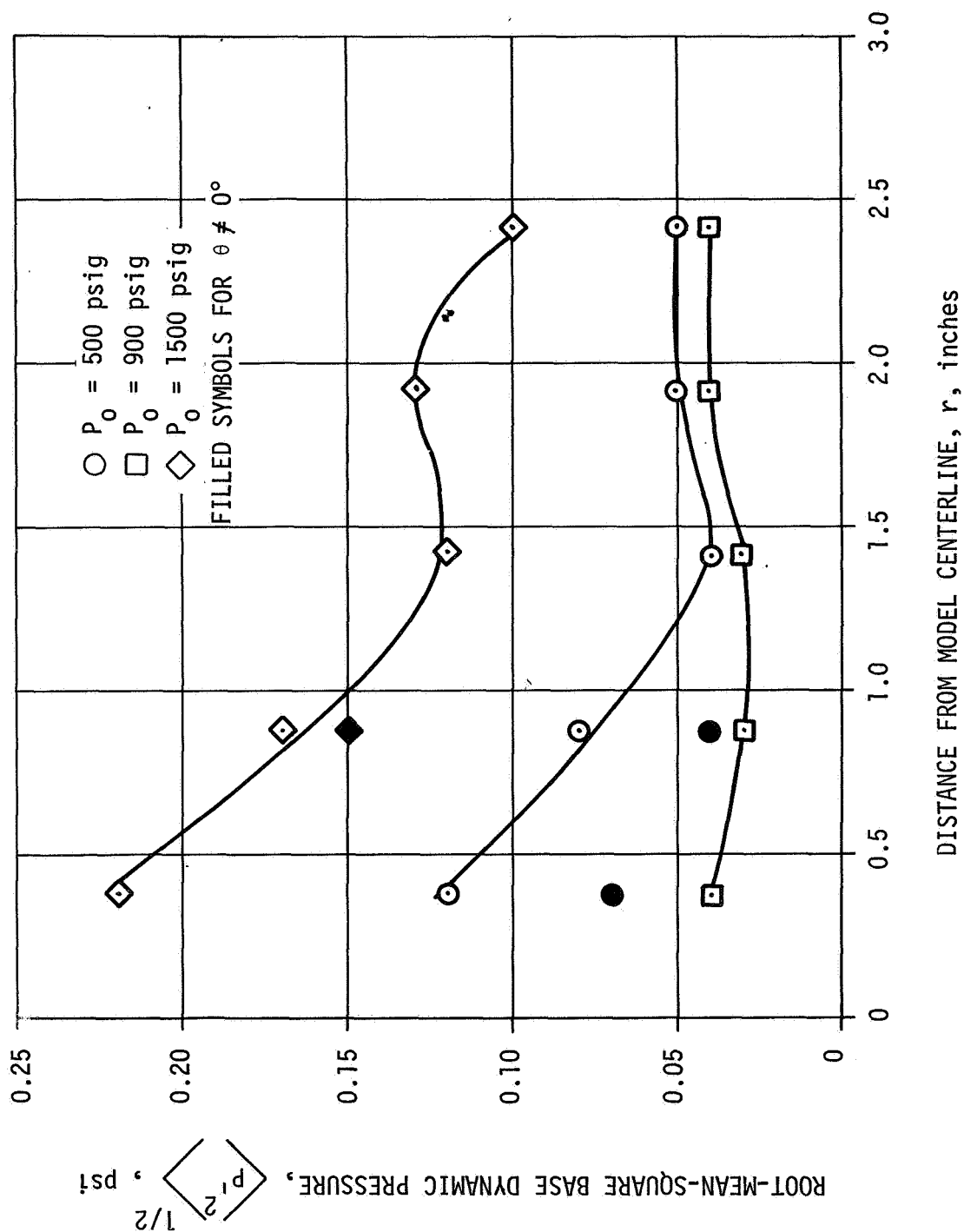Figure 4-15. ROOT-MEAN-SQUARE BASE PRESSURES FOR SINGLE JET CONFIGURATION (I)

Figure 4-16. ROOT-MEAN-SQUARE BASE PRESSURES FOR FOUR-JET CONFIGURATION (IV A)

This result is in sharp contrast to the mircophone data which show the rms pressure to be a maximum at this chamber pressure. It is probable in view of these results and those noted above for the mean static pressures that the transducers are being affected by a flow field not common to the other cases studied.

Turning to the Saturn configuration data, Figure 4-17, the variation of rms pressures with location on the baseplate is seen to be slight. The overall values clearly increase with increasing values of chamber pressure which is not completely evident in the cases presented above.

From these results and those obtained for other configurations, no definite conclusions could be reached for rms variations with chamber pressure or jet thrust. This is, perhaps, not surprising in view of the geometric variables introduced by various nozzle combinations and chamber pressures. For example, for a single nozzle an increase in chamber pressure increases the length of the initial supersonic portion of the jet as well as increasing the effective acoustic radiating area of the jet near the exit. Addition of a second nozzle causes intersection regions to be formed where shock-turbulence interactions may be important. As the pressure is increased for such multiple nozzle geometries these interaction regions come in closer proximity to the base but the jet is not free to expand in all directions which limits the effective radiation to the base. This line of thought may be extended to additional nozzle combinations but the complexity increases rapidly. Only the very general observation can be made, therefore, that the rms pressure level on the base tends to increase with the total jet thrust and the rate of increase appears greater at larger values of thrust.

Pressure variations with location on the plate may be more readily explained by the model presented earlier for acoustic waves of random incidence on a plane. Equation 2-14 shows that the rms level under such a loading condition would be independent of location. This conforms very nearly with the data presented for the single- and five-jet configurations. The four-jet configuration exhibits this result only near the edge of the plate and significant variation
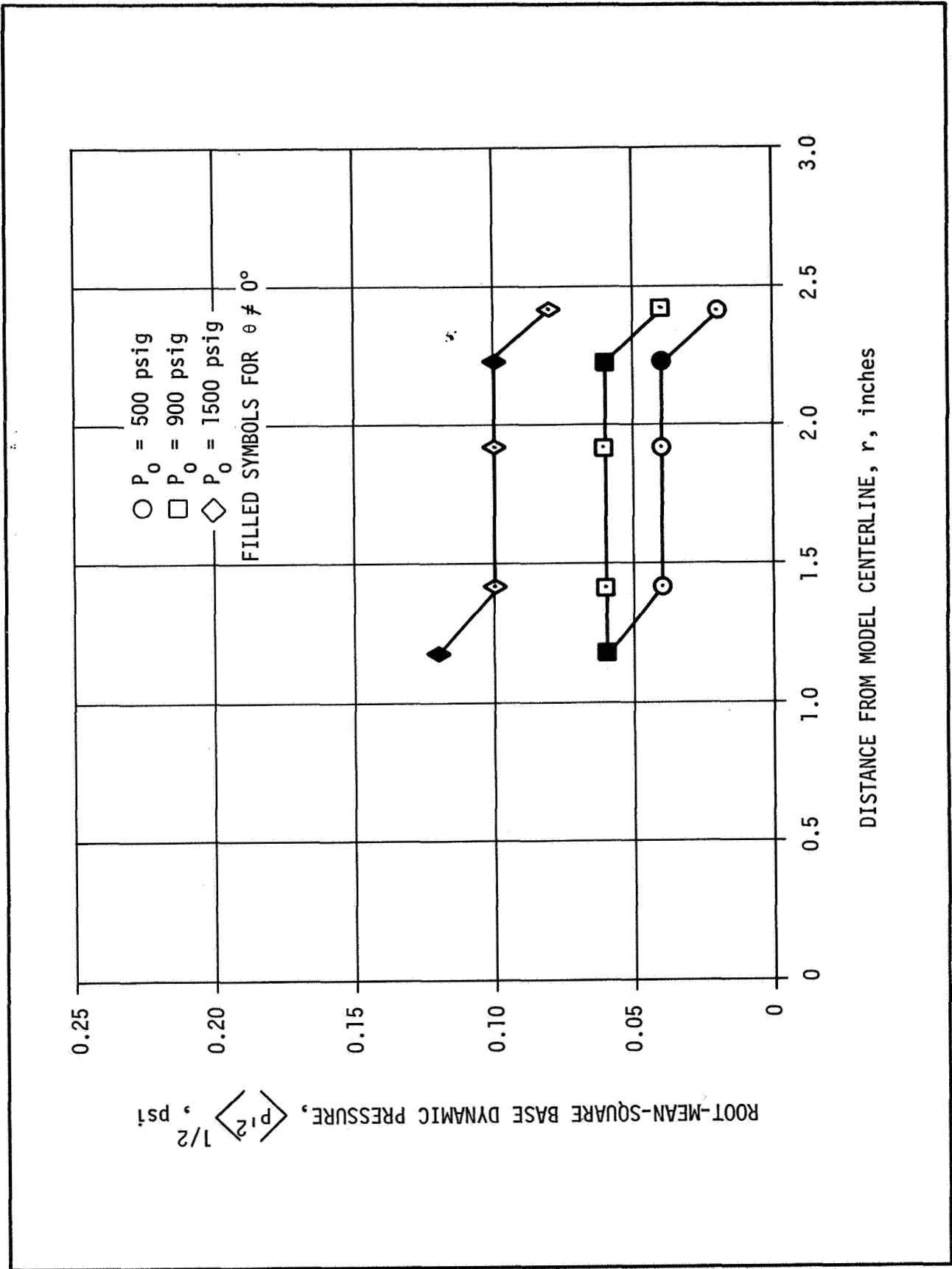
Figure 4-17. ROOT-MEAN-SQUARE BASE PRESSURES FOR SATURN CONFIGURATION (V)

is only seen in the center. A probable explanation for this departure from the theoretical trend is that flow existed in the central region of the plate as was discussed above. In regions of wake impingement an rms value of 10 percent of the impact pressure is common (ref. 24). Applying this to the present data, an rms increase of 0.08 psi would be expected at the center of the plate. This compares favorably with the approximately 0.10 psi rise observed on the four jet cluster at P_o = 1500 psig.

The power spectral density for a typical transducer (F4) over the range of chamber pressures is shown for Configuration I in Figure 4-18. The trends are similar for all pressures showing a somewhat linear rise on the logarithmic scale until a peak spectral density value is attained at 2 to 2.5 kHz. This behavior is similar to the microphone spectra for this configuration where the peak rise occurred at 1.6 kHz. Above the peak frequency, however, the transducers roll-off more rapidly than the microphone until the (tape system imposed) cut-off frequency is reached. A check was made to see if the spectral roll-off was induced by the (finite) size of the transducers. Using the techniques of reference 31, no appreciable error was found to be introduced into the spectra due to size limitations up to 20 kHz for the 0.125-inch transducers of this study.

A comparison of all transducer spectra for the single jet is shown in Figure 4-19. The data are seen to be consistent with results for the F4 spectra. A secondary peak may be clearly identified, however, in the 0.63 to 1.00 kHz range for P_o = 900 and 1500 psig. This result is not seen in the microphone spectra.

The spectra for transducer F4 are shown for Configuration IVA in Figure 4-20. An increase of the low frequency energy content over the single-jet case is noted at all chamber pressures. It may be inferred, however, from the P_o = 500 and 900 psig cases that the relatively narrow band component seen around 2 kHz still exists but is masked by the gains at lower frequencies.

Spectral results for those transducers located along the axis described by θ = 180° in the base coordinate system are shown in Figure 4-21. It is very
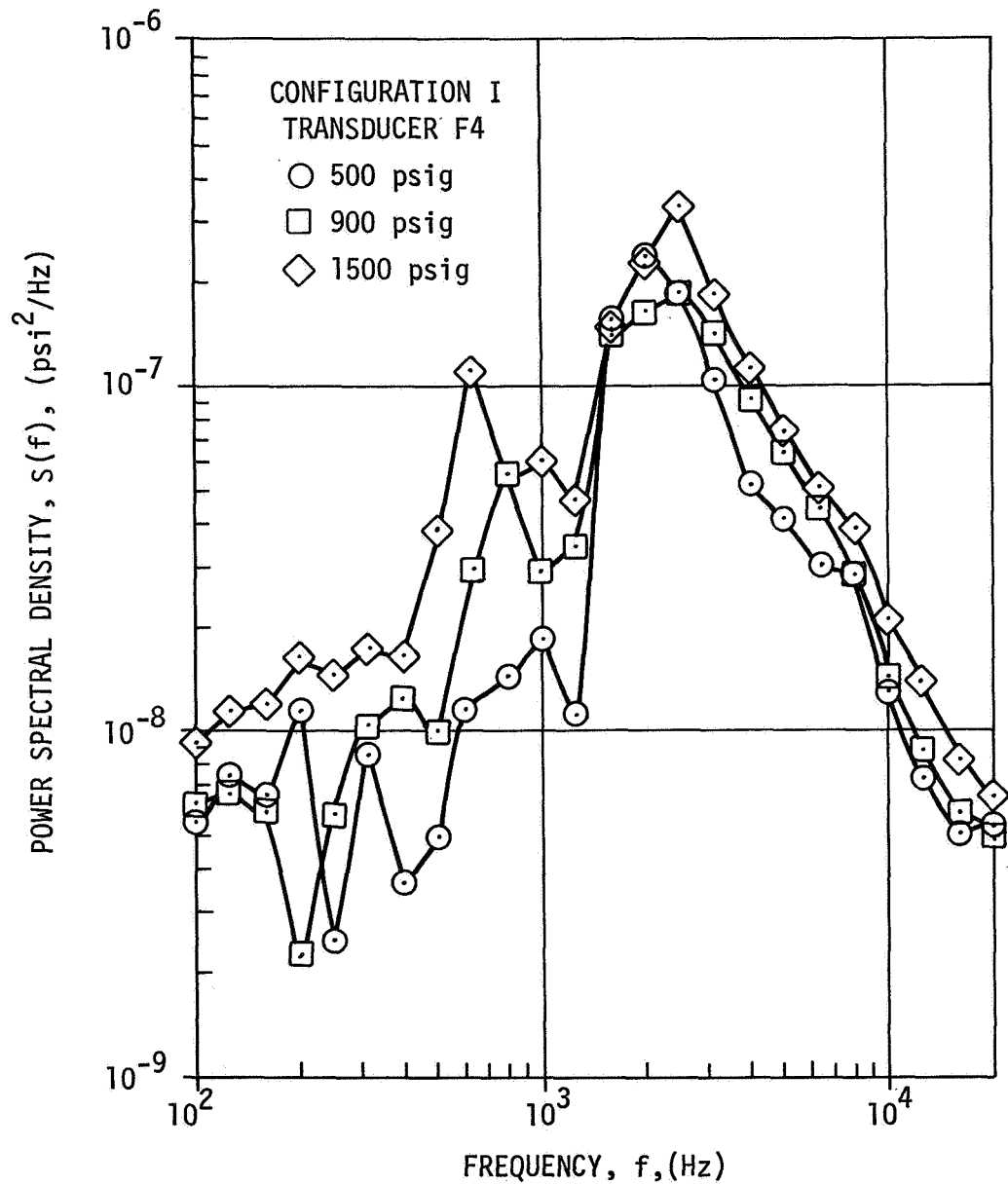
Figure 4-18. VARIATION OF TYPICAL TRANSDUCER SPECTRA WITH
CHAMBER PRESSURE FOR SINGLE JET

Figure 4-19A. SPECTRAL DISTRIBUTION FOR SINGLE JET CONFIGURATION (P_o = 500 psig)
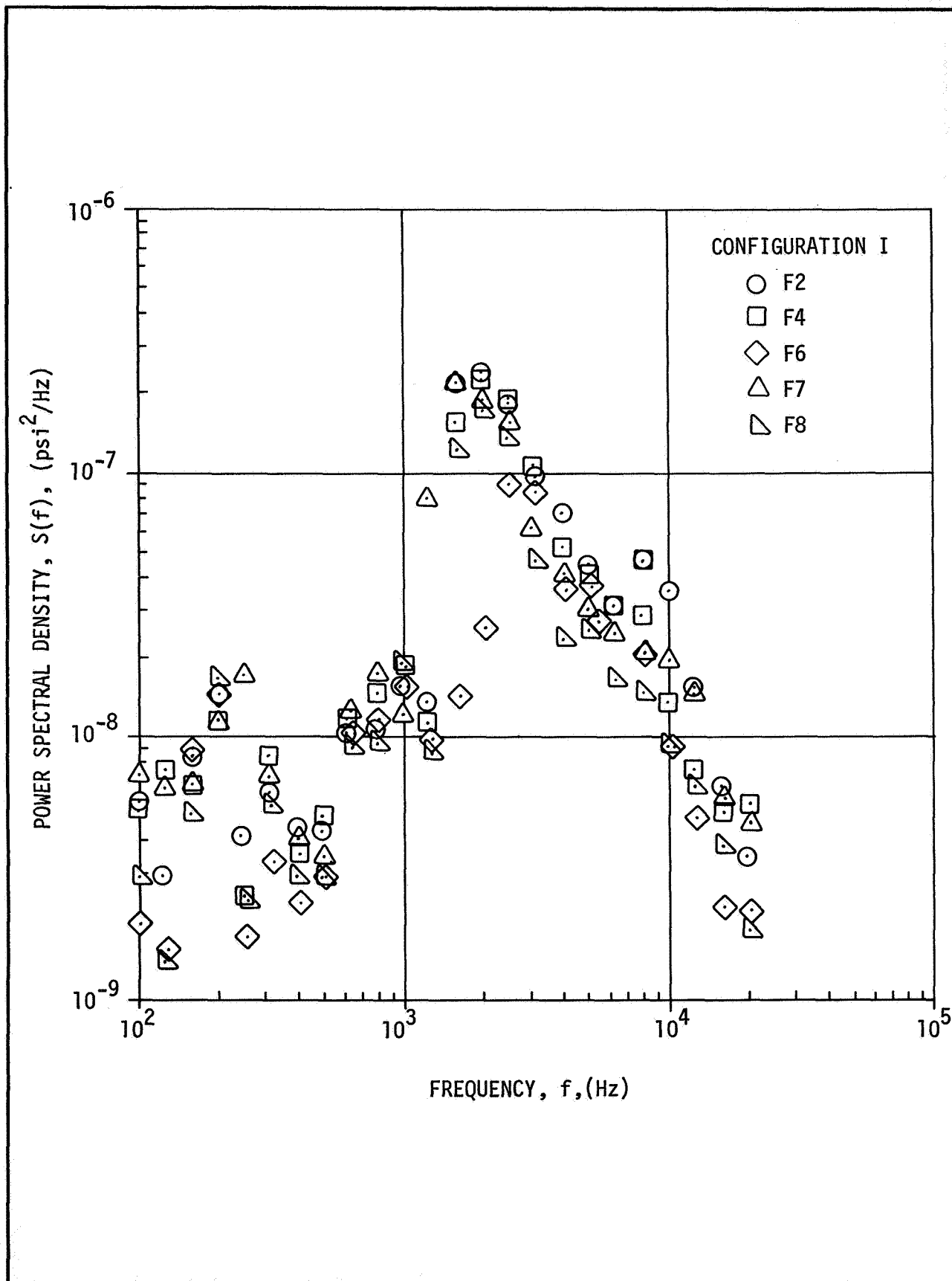
Figure 4-19B.   SPECTRAL DISTRIBUTION FOR SINGLE JET CONFIGURATION (P_o = 900 psig)

Figure 4-19C. SPECTRAL DISTRIBUTION FOR SINGLE JET CONFIGURATION (P_o = 1500 psig)

Figure 4-20. VARIATION OF TYPICAL TRANSDUCER SPECTRA WITH CHAMBER PRESSURE
FOR FOUR-JET CONFIGURATION
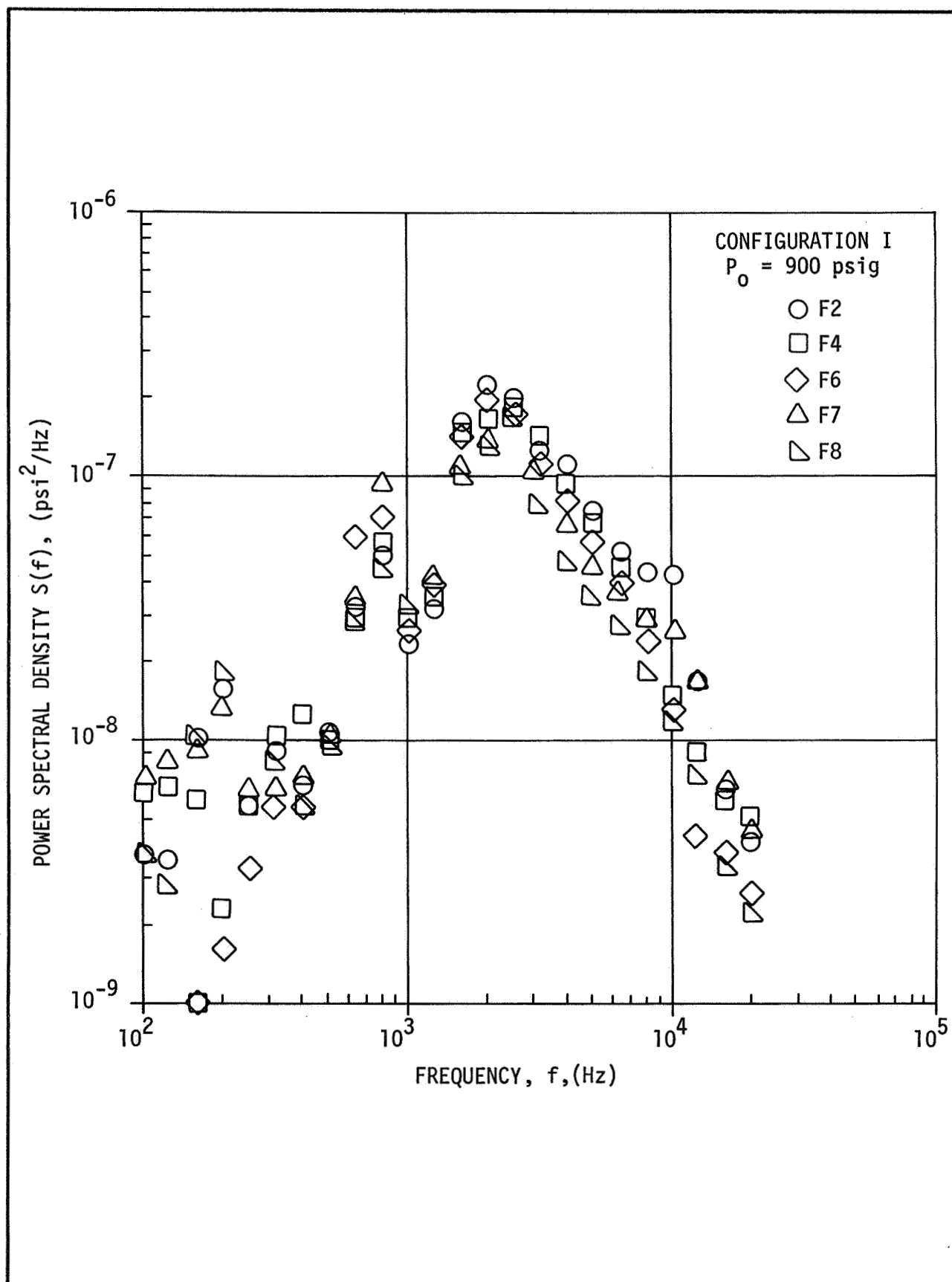
Figure 4-21A. SPECTRAL DISTRIBUTION FOR FOUR-JET CONFIGURATION (P_o = 500 psig)

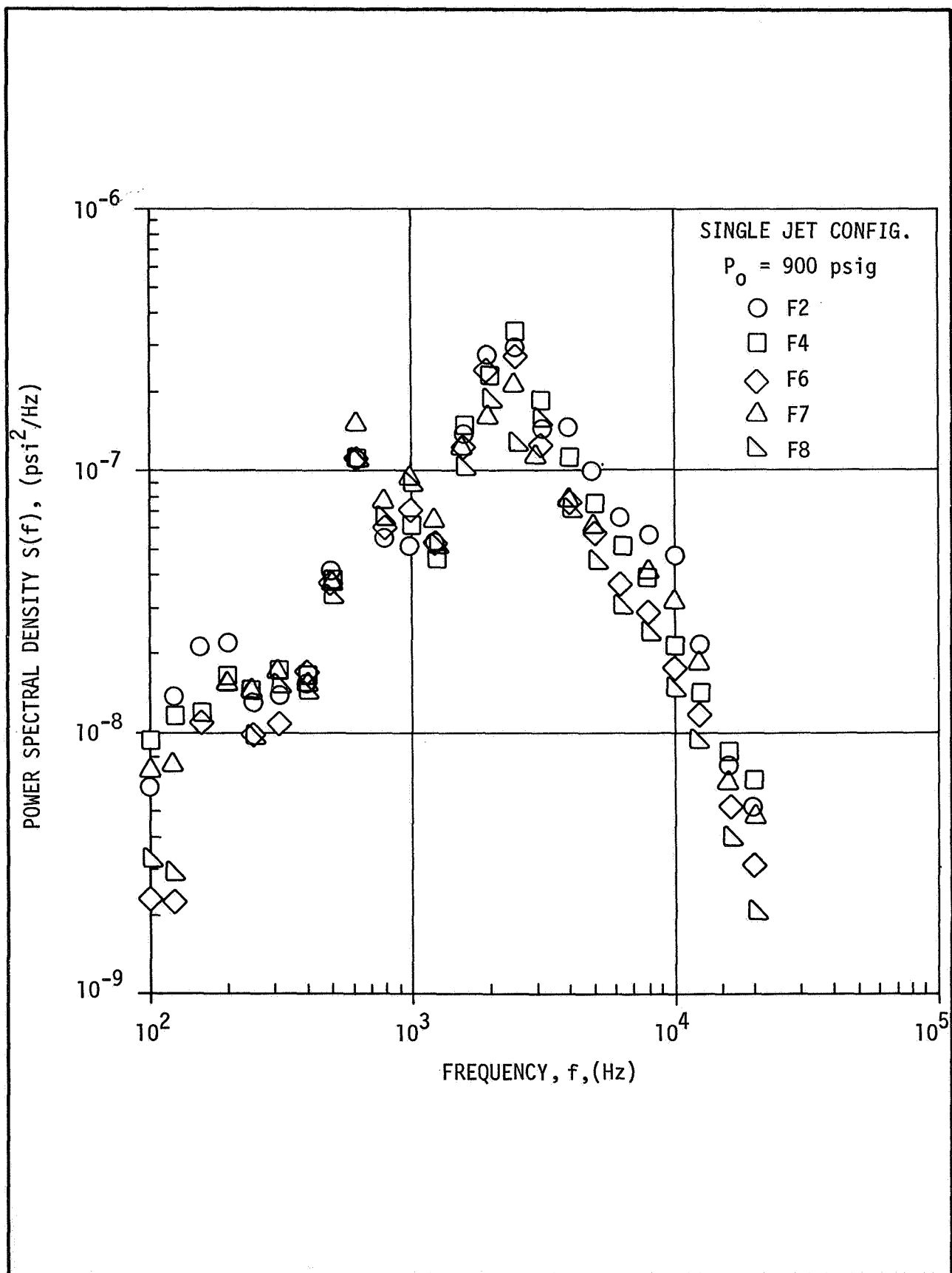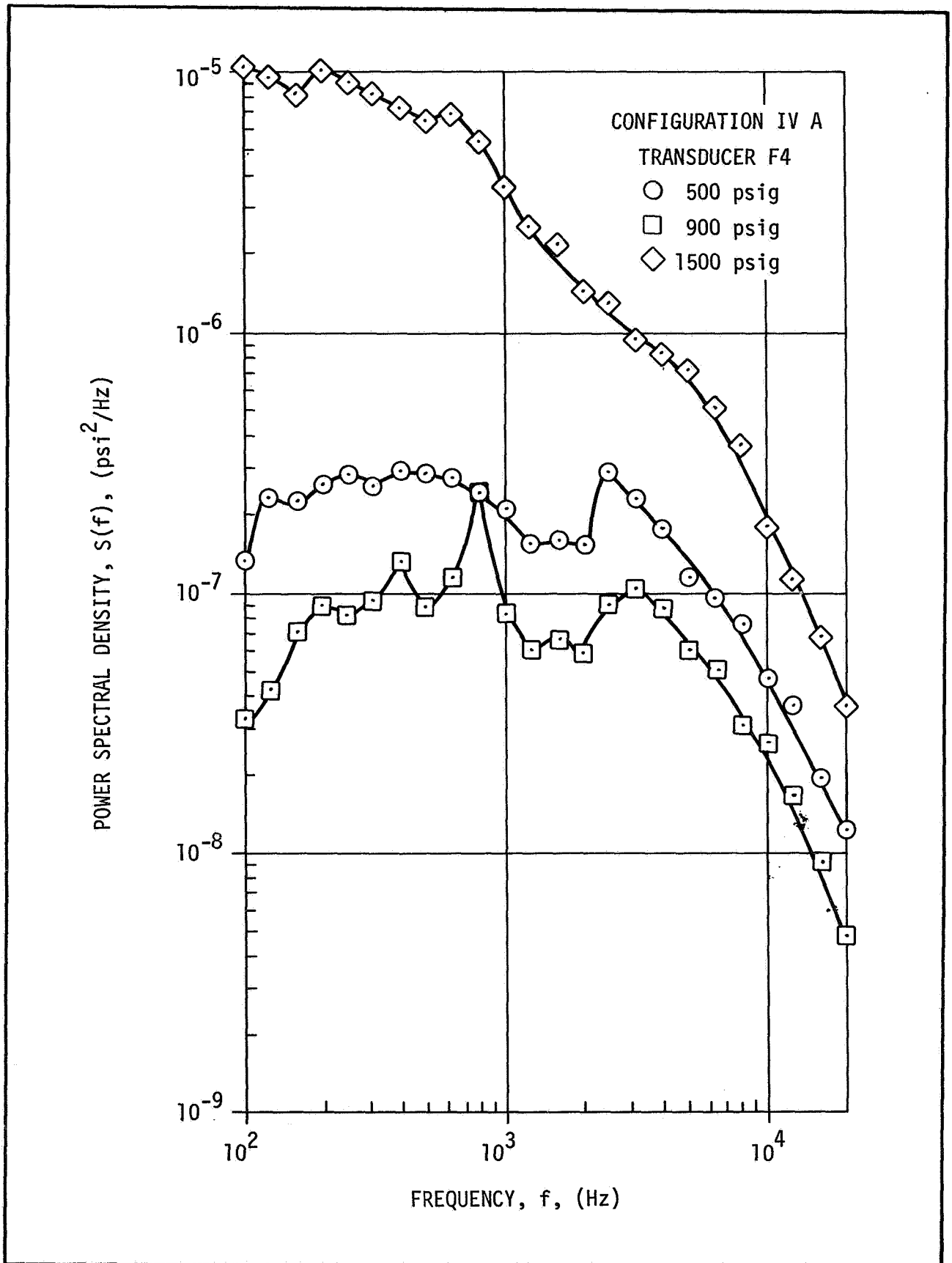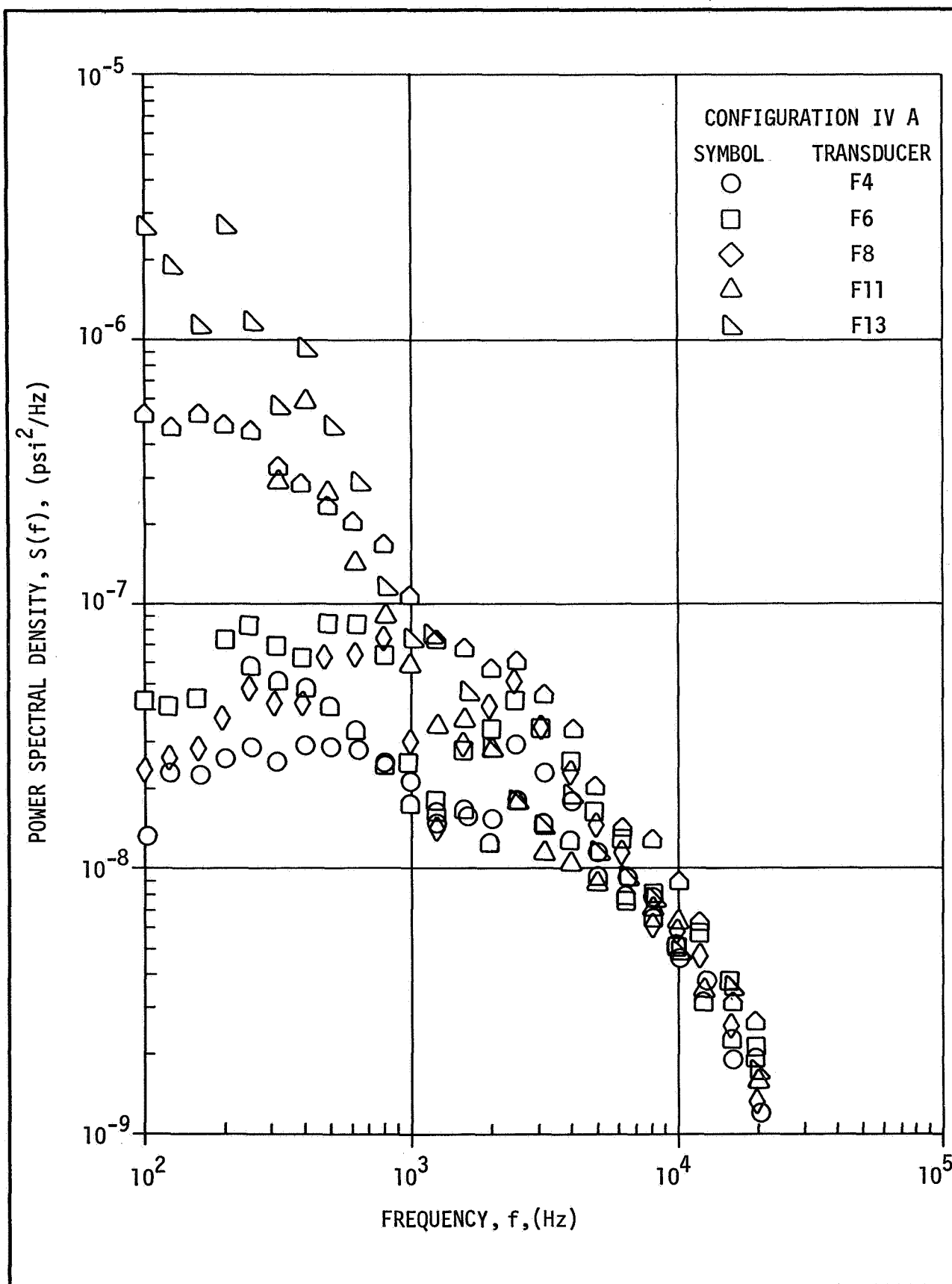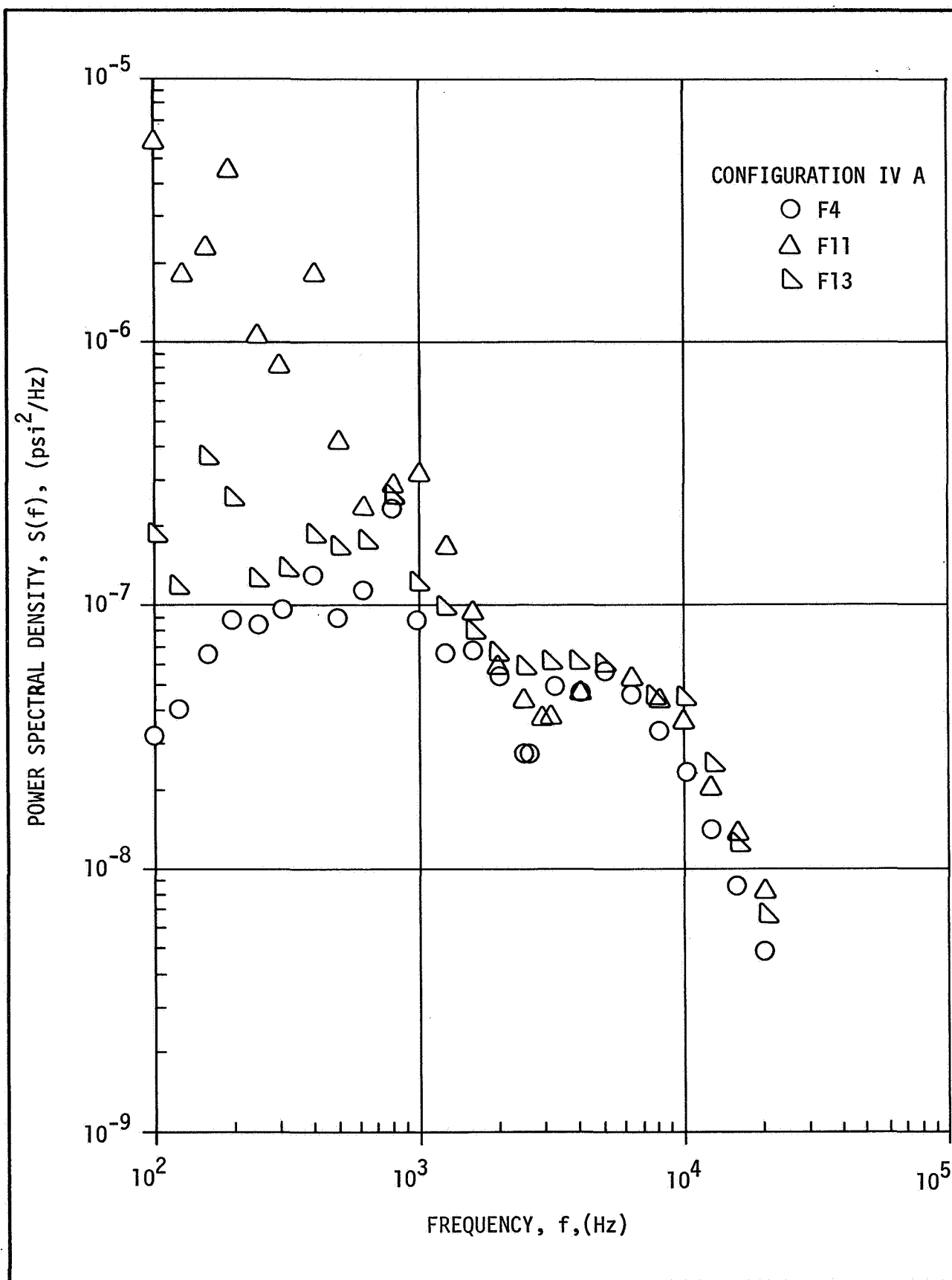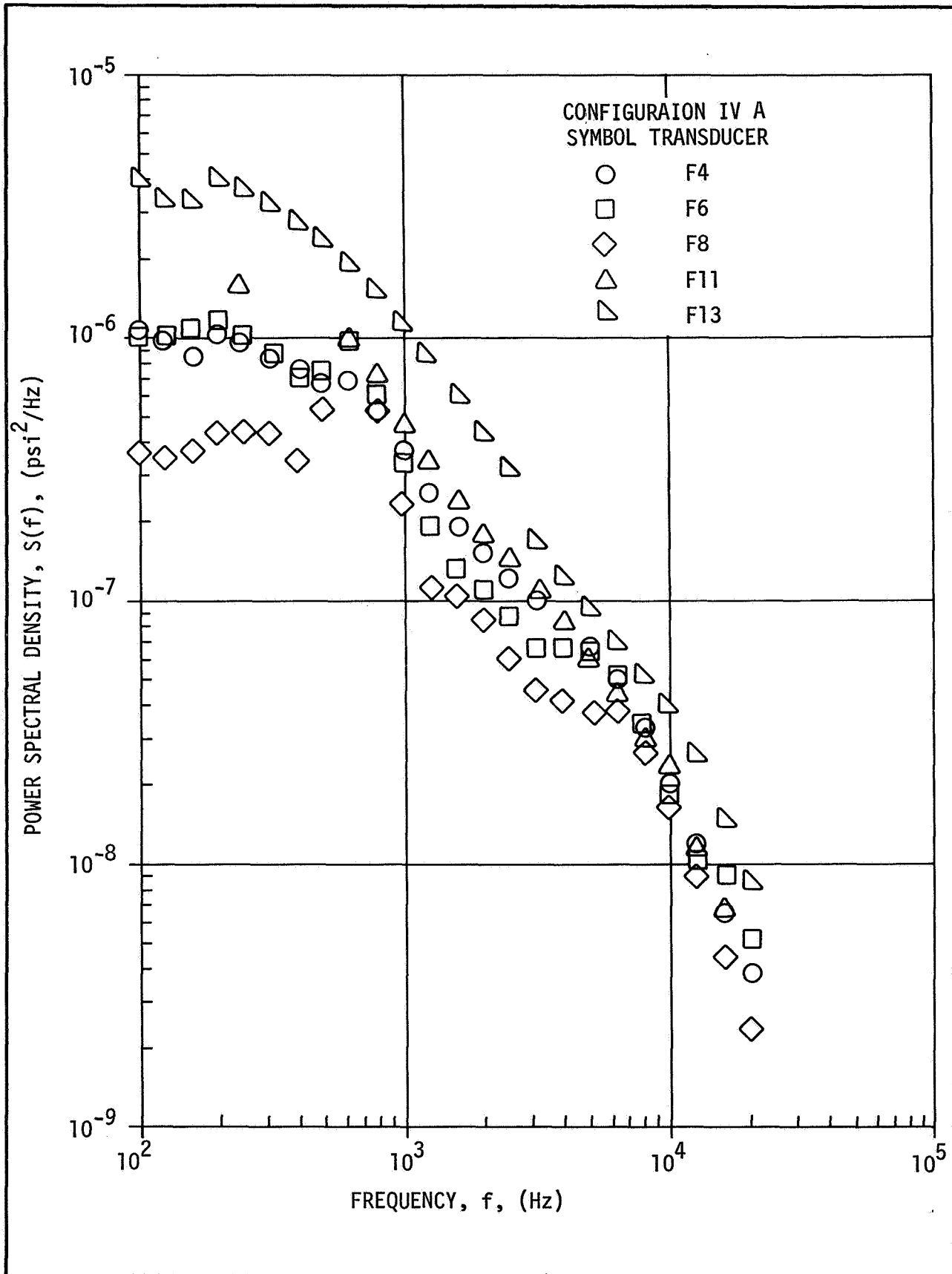Figure 4-21B. SPECTRAL DISTRIBUTION FOR FOUR-JET CONFIGURATION (P_o = 900 psig)

Figure 4-21C.   SPECTRAL DISTRIBUTION FOR FOUR-JET CONFIGURATION (P_o = 1500 psig)

apparent from these results that the large increase in rms pressure levels noted earlier in the central portion of the plate are due to increases at low frequencies. Transducer F9, located at the center of the model, was not included in these comparisons since the apparently high dynamic pressures at its location caused signal clipping. Also, the spectra seen in this case are similar to those commonly associated with flow phenomena. This is in agreement with conclusions drawn earlier from the mean pressure data.

Results for the Saturn configuration are shown in Figure 4-22 for the transducer F4 at all chamber pressures. At the lowest pressure, P_o = 500 psig, its characteristic shape is similar to that observed for the single jet although of greater magnitude. The P_o = 1500 psig curve, on the other hand, shows a similarity to the four-jet spectra, but the roll-off at high frequencies is much less pronounced. The curve for the intermediate pressure P_o = 900 psig, is dominated by a spectral peak centered at 0.63 kHz. This relatively narrow band component is some one to two orders of magnitude higher than the spectral values outside its influence. Although data taken for other configurations showed some influence near this frequency, the dominance of this peak is unique to this configuration.

A comparison of all available spectra for this configuration is given by Figure 4-23. The results for F4 are representative of those at other locations with the notable exception that at P_o = 1500 psig a single transducer (F8) exhibits the characteristic shape seen in transducer data at P_o = 900 psig. This is not an isolated occurrence as seen in Figure 4-24 where the power spectra are shown for another test at P_o = 1500 psig. For this case all available data show the dominant peak noted for the lower pressure condition. This "duality" of results implies that an instability in flow or acoustic generation mechanism exists. It is possible, therefore, that at some intermediate pressure the peak observed may be still more severe.

In order to make additional comparisons of these results, it is useful to present the spectra in a non-dimensional form. Potter and Crocker (ref. 28) have shown that far-field acoustic levels from tests of model rocket engines may
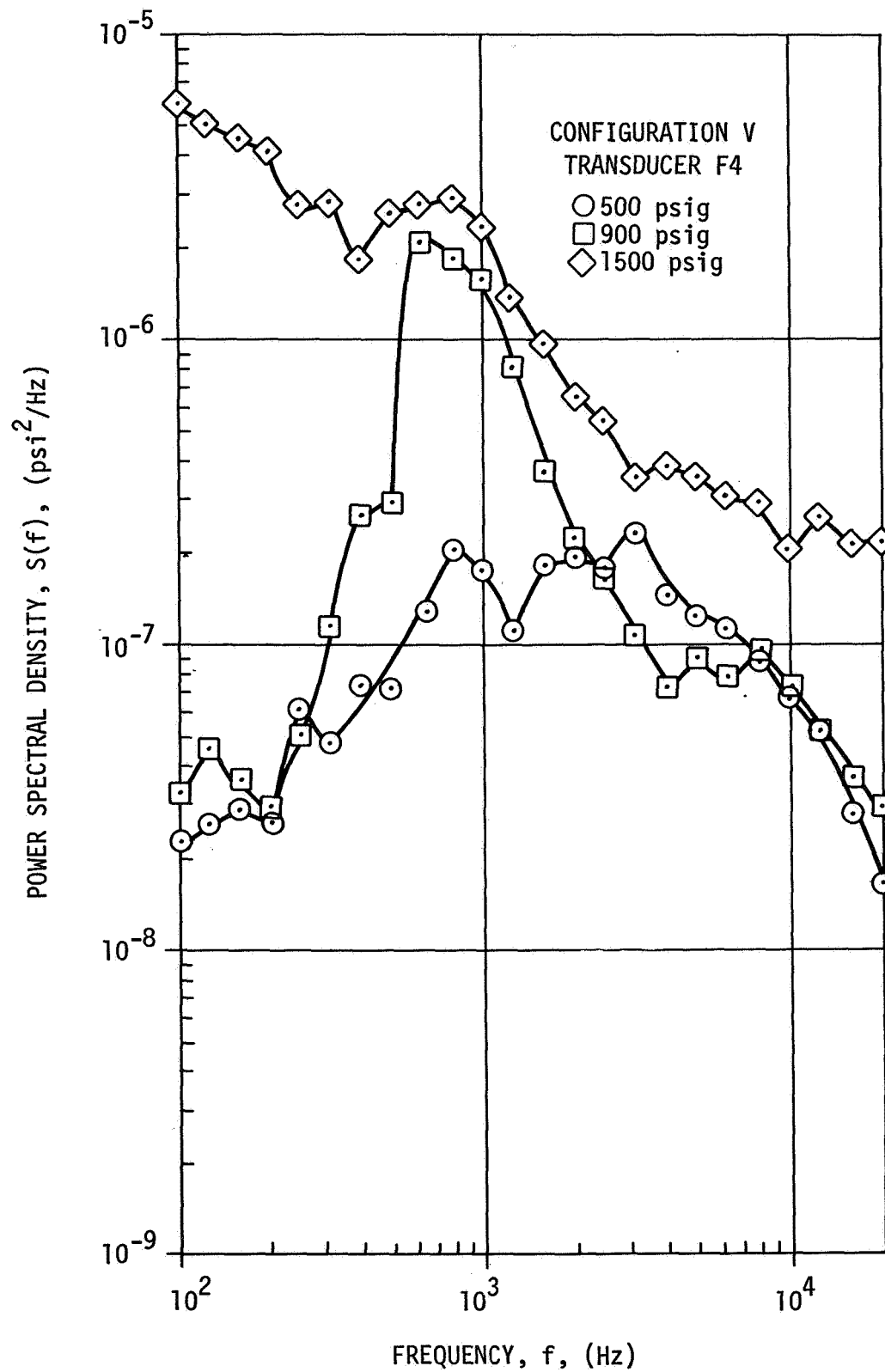
Figure 4-22. VARIATION OF TYPICAL TRANSDUCER SPECTRA
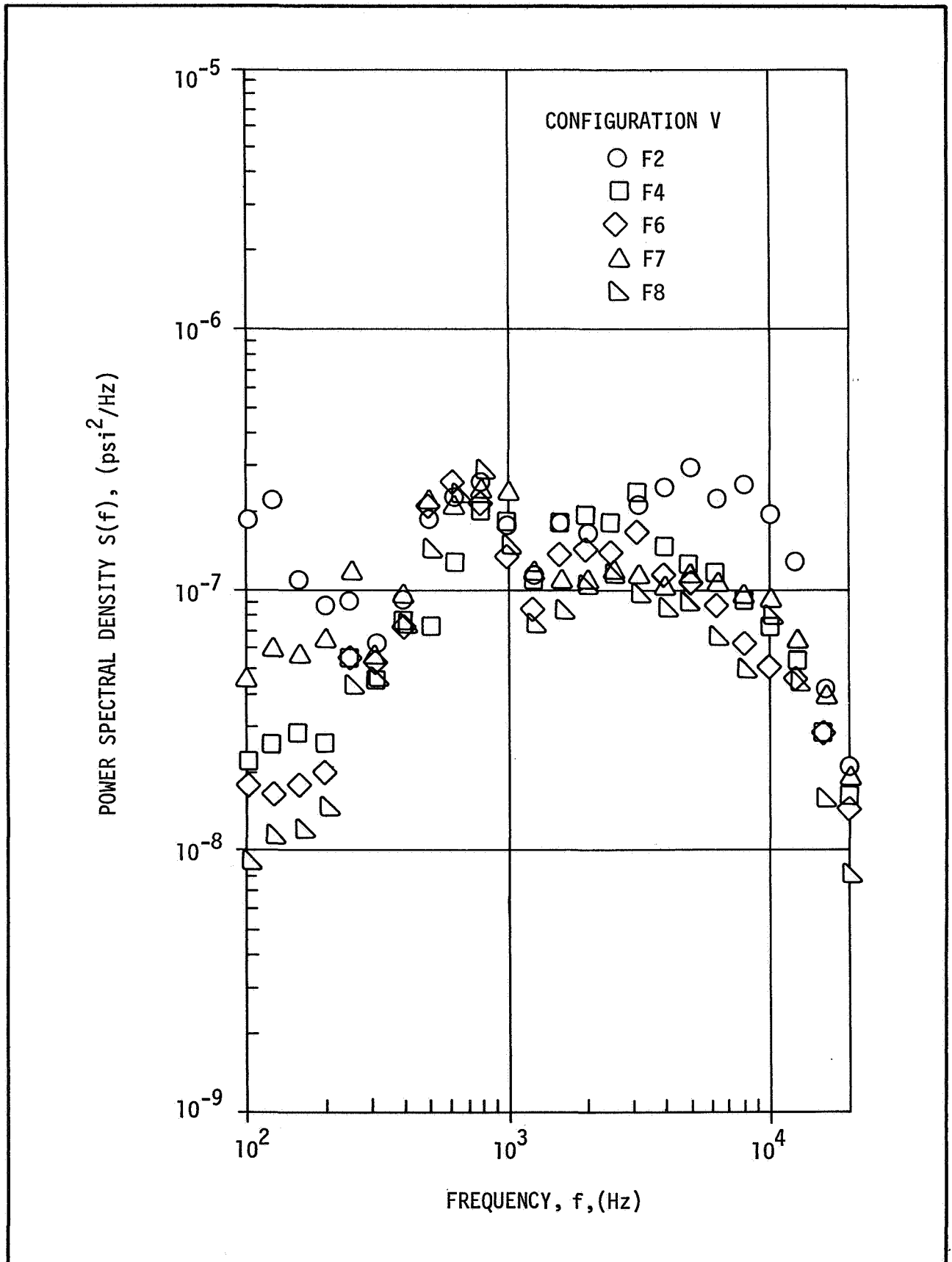FOR SATURN CONFIGURATION

Figure 4-23A.   SPECTRAL DISTRIBUTION FOR SATURN CONFIGURATION (P_o = 500 psig)
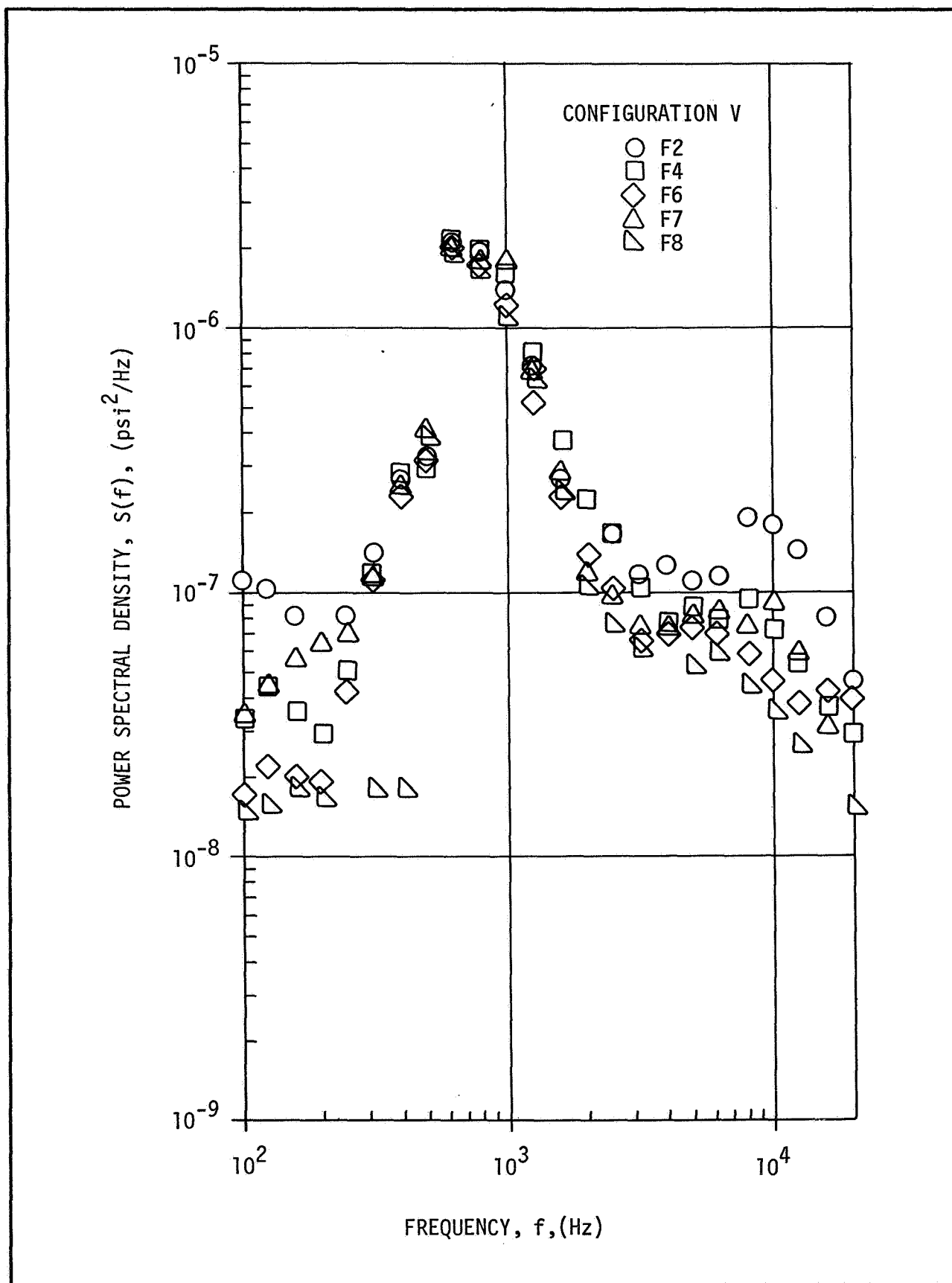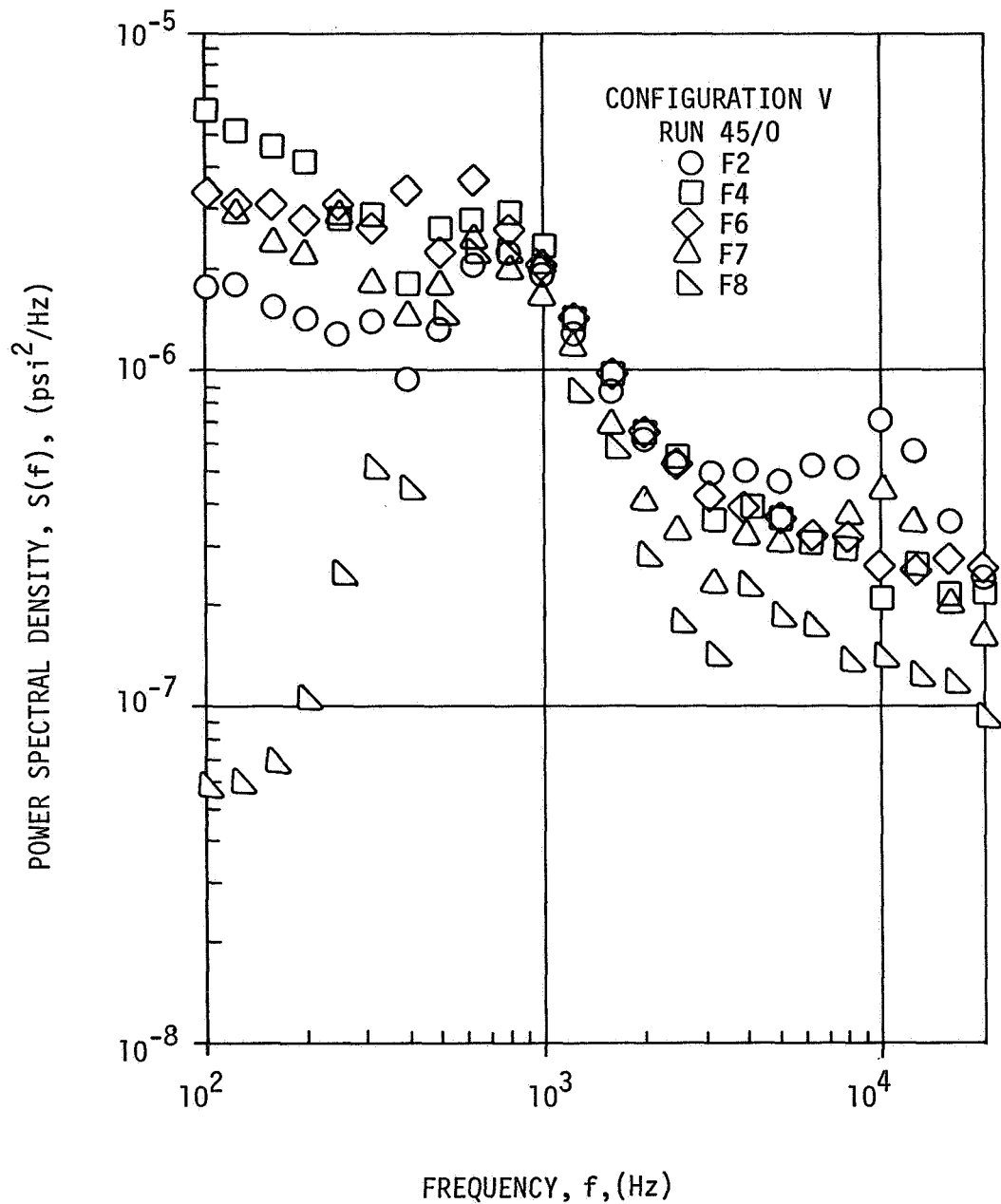
Figure 4-23B.   SPECTRAL DISTRIBUTION FOR SATURN CONFIGURATION (P_o = 900 psig)

Figure 4-23C. SPECTRAL DISTRIBUTION FOR SATURN CONFIGURATION (P_O = 1500 psig)
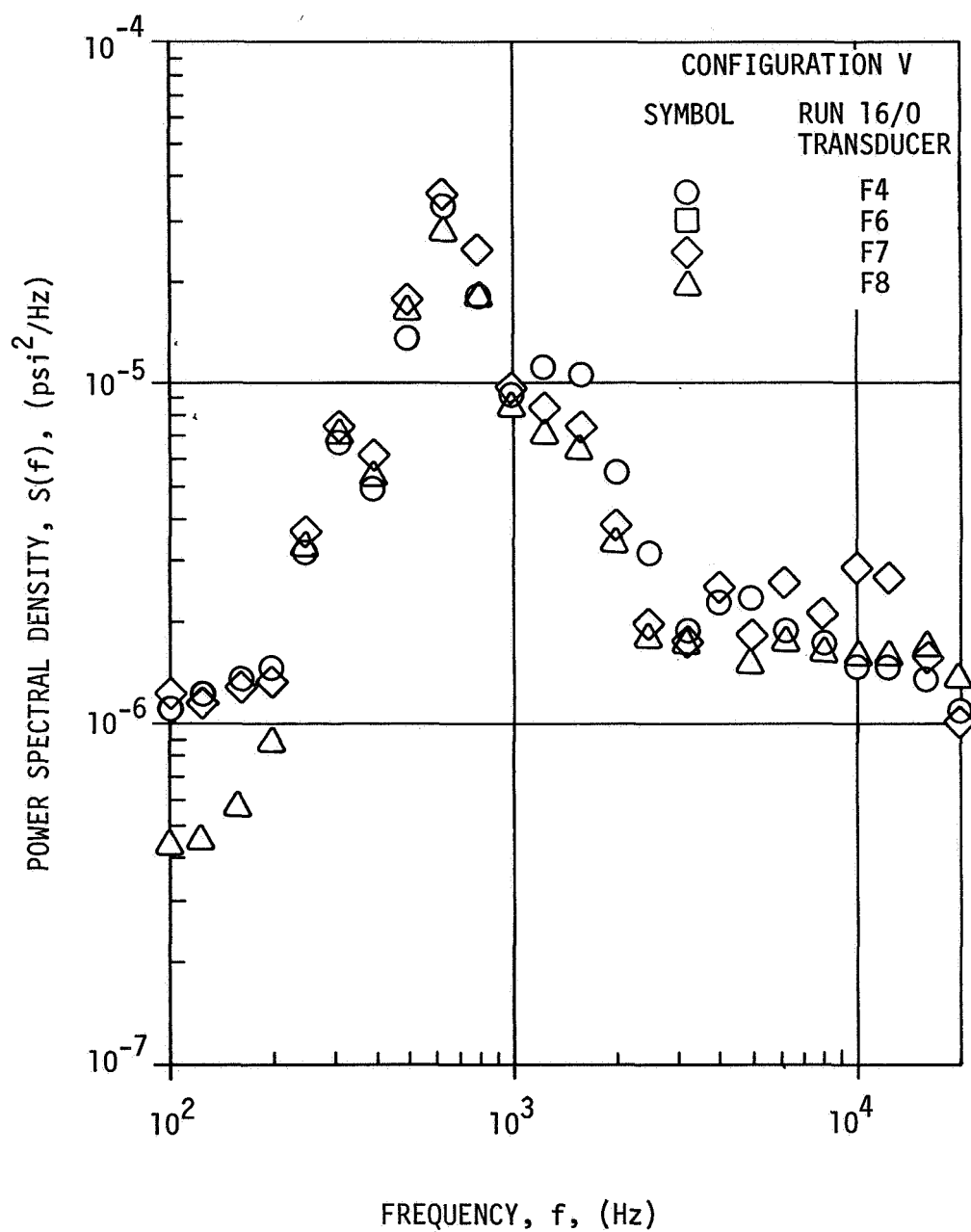
Figure 4-24. SPECTRAL DISTRIBUTION FOR SATURN CONFIGURATION

be effectively collapsed using the Strouhal number defined by equation 4-5 and a normalized spectral density of the form

$$K(f) = \frac{S(f)}{\langle p'^2 \rangle} \cdot \frac{C_a}{D^*} \left(\frac{P_o}{P_a} \right)^{1/2} \tag{4-6}$$

Figure 4-25 presents the normalized spectra for the typical transducer (F4) of the single jet runs. This type of data presentation is seen to be quite effective for this case where the dominant mechanism influencing the base loading is acoustic propagation. Attempts to reduce results for clustered exhaust runs by this method do not give a "similarity" profile for the spectral results because the spectra for different chamber pressures have differing characteristic shapes. This is, of course, to be expected in view of the different possible mechanisms that arise for the cluster configurations.

It is possible, on the basis of this normalization, to assign a dominant frequency to the spectra obtained in each case. For example for the single jet at P_o = 900 psig this peak spectral value occurs at a Strouhal number of 0.8 as is readily seen from the figure. A tabulation of the Strouhal number corresponding to such spectral maxima is given below

	"PEAK" STROUHAL NUMBER FOR CONFIGURATION:		
Chamber Pressure (psig)	I	IVA	V
P_o = 500	.48	.48	0.80
P_o = 900	.80	1.25	0.23
P_o = 1500	1.05	0.30	0.50

No trend is evident from such a tabulation but it shows that the criterion (ref. 28) that clustered exhausts have a lower peak spectral value than single jets is not satisfied in all cases by these data.

Dyer (ref. 32) presents a correlation relating source location to the observed frequency of an acoustic load. From that result, and the frequencies corresponding to the above values, it may be determined that the source of
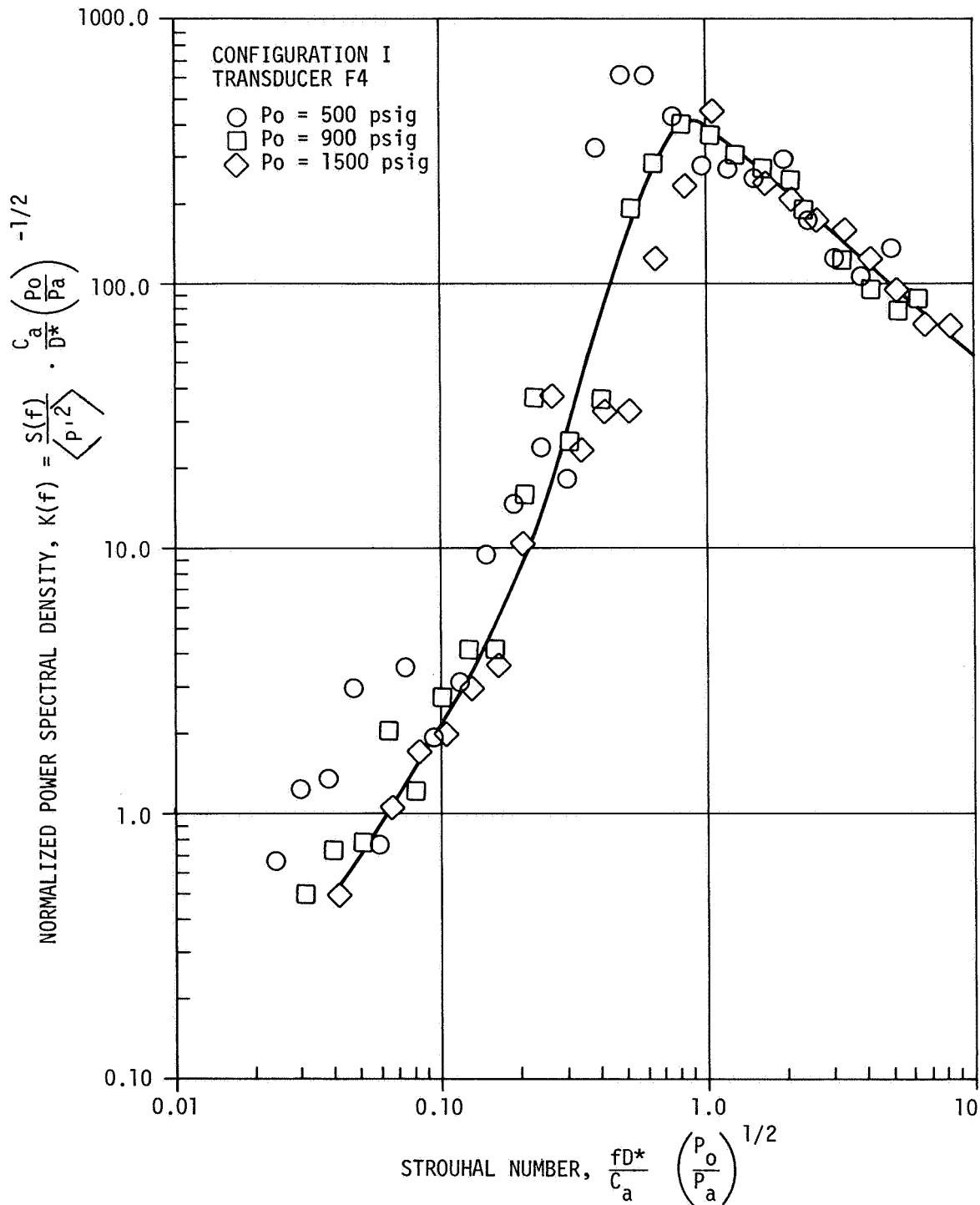
Figure 4-25. NORMALIZED SPECTRA FOR SINGLE JET CONFIGURATION

dominant excitation of the base occurs from 4 to 10 diameters downstream from the nozzle exit. It may be concluded, therefore, that in all cases the dominant excitation (if acoustically induced) has its origin in the subsonic portion of the jet.

A final comparison of spectral results is given in Figure 4-26 where normalized microphone and base transducer spectra of the present study are compared to the typical rocket exhaust spectra of reference 4-6. The weighting of the present microphone data to higher frequencies, cited earlier, is clear from this figure. It is noted, too, that the base spectra show greater high frequency content than the curve given in the referenced document. To some extent this is an anticipated result due to the proximity of the base transducers to the nozzle lip where higher frequencies would be expected. However, the above remarks on source location tend to negate that viewpoint. Inasmuch as the referenced data were obtained for hot flows in models of comparable size and exit Mach numbers to the present, it is reasonable to question whether a temperature dependence is the probable cause for the discrepancy noted for the Strouhal number range. It is noted in this regard that a Strouhal number modified by the factor $\left(\frac{T_o}{T_a}\right)^{1/2}$ would eliminate the disparity in these results. This question, however, can only be resolved by additional studies in hot flows.

It is apparent from Figure 4-26 that appreciable energy exists at Strouhal numbers in excess of 10. Since the data acquisition system used in this test precluded measurement in that range, it is useful to estimate the error induced in the root-mean-square pressures on the base due to this limitation. From the definition of the mean square one may write the ratio of true to measured values as

$$\frac{\left\langle p'^2 \right\rangle_t}{\left\langle p'^2 \right\rangle_m} = 1 + \frac{\int_{f_u}^{\infty} S(f)\,df}{\int_{o}^{f_u} S(f)\,df} \tag{4-7}$$

By considering the behavior of the spectral data presented in Figures 4-8 thru 4-24, it is found that the spectral roll-off at high frequencies corresponds to a $-5/3$ (or higher) power law. Assuming, for convenience, the spectra
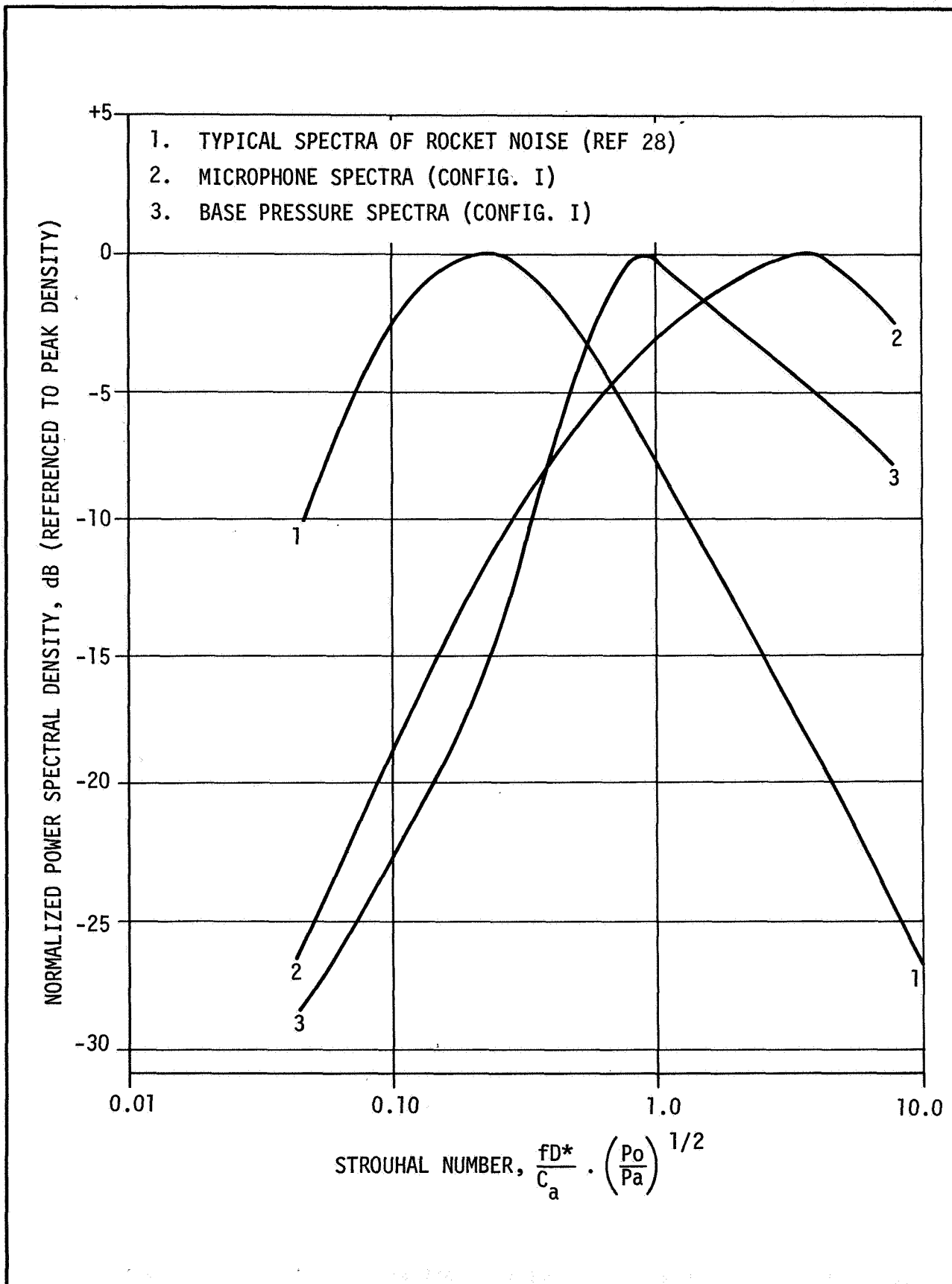
Figure 4-26. COMPARISON OF NORMALIZED MICROPHONE AND BASE PRESSURE SPECTRA

roll-off as f^{-2} above the cut-off frequency and noting the definition of the spectral density for third-octave analysis one may obtain

$$\frac{\langle p'^2\rangle_t}{\langle p'^2\rangle_m} = 1 + \frac{4.35\,\langle p'^2(f_u)\rangle}{\langle p'^2\rangle_m} \tag{4-8}$$

Evaluating this expression for the data shows that the measured rms values are from 2 to 9 percent below the true values with the majority of the data being about 7 percent low. These results are regarded as conservative but the use of a higher frequency cut-off system must be regarded as a major consideration in future tests in the Thermal Acoustic Jet Facility.

One objective of this test was to explore convected pressure fields at the base of engine clusters. Accordingly a considerable effort was expended in cross-correlation of dynamic data from various transducer pairs. Although over one thousand of the possible combinations were investigated, no conclusive evidence of recirculation was obtained from these correlograms for any configuration or test condition. Most correlograms, however, were limited to time delays of $\tau \leq$ 3ms. A convection speed significantly lower than the 50 ft/sec estimated from the mean pressure data could not be measured in this time frame. The determination of convection speed from cross-correlograms in the presence of a vortexing flow such as suspected in the tests of the four-jet configuration may also be cited as a contributing factor in the failure of the technique. No attempt was made to filter the data to eliminate the presumably higher frequency acoustic contributions.

Results typical of the cross-correlation of the base transducer data are shown in the correlograms of Figures 4-27 and 4-28 for the four-jet and Saturn configurations, respectively. Both sets of data are typified by a peak correlation coefficient occurring near zero time-lag. A second feature of the data is the reversal in sign of the correlation at zero-time lag, $R(\xi,o)$, for various separation distances.

The model presented in Section II for oblique plane waves of random incidence gives the cross-correlation coefficient as
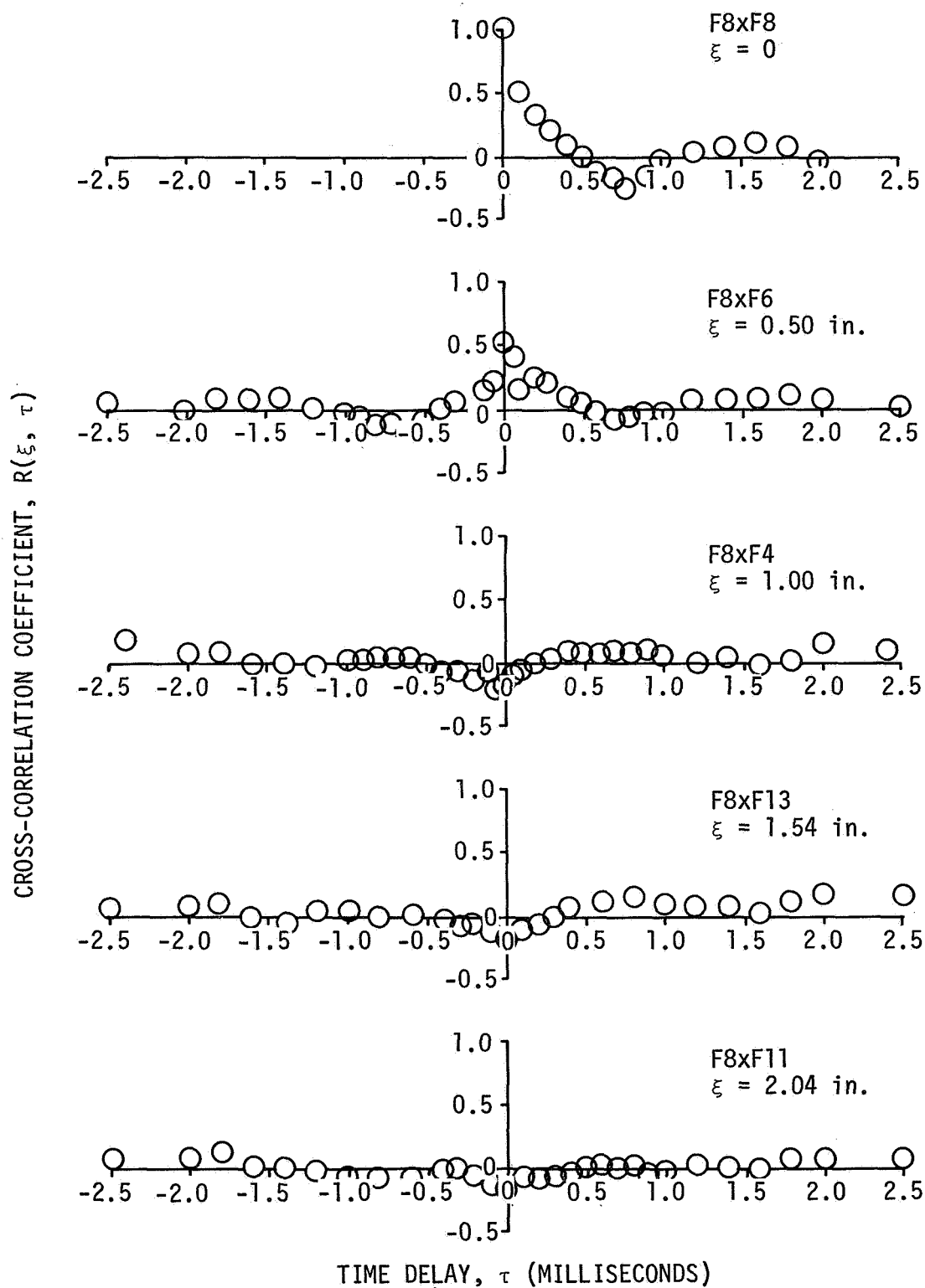
Figure 4-27.   BASE TRANSDUCER CROSS CORRELOGRAMS FOR SYMMETRIC
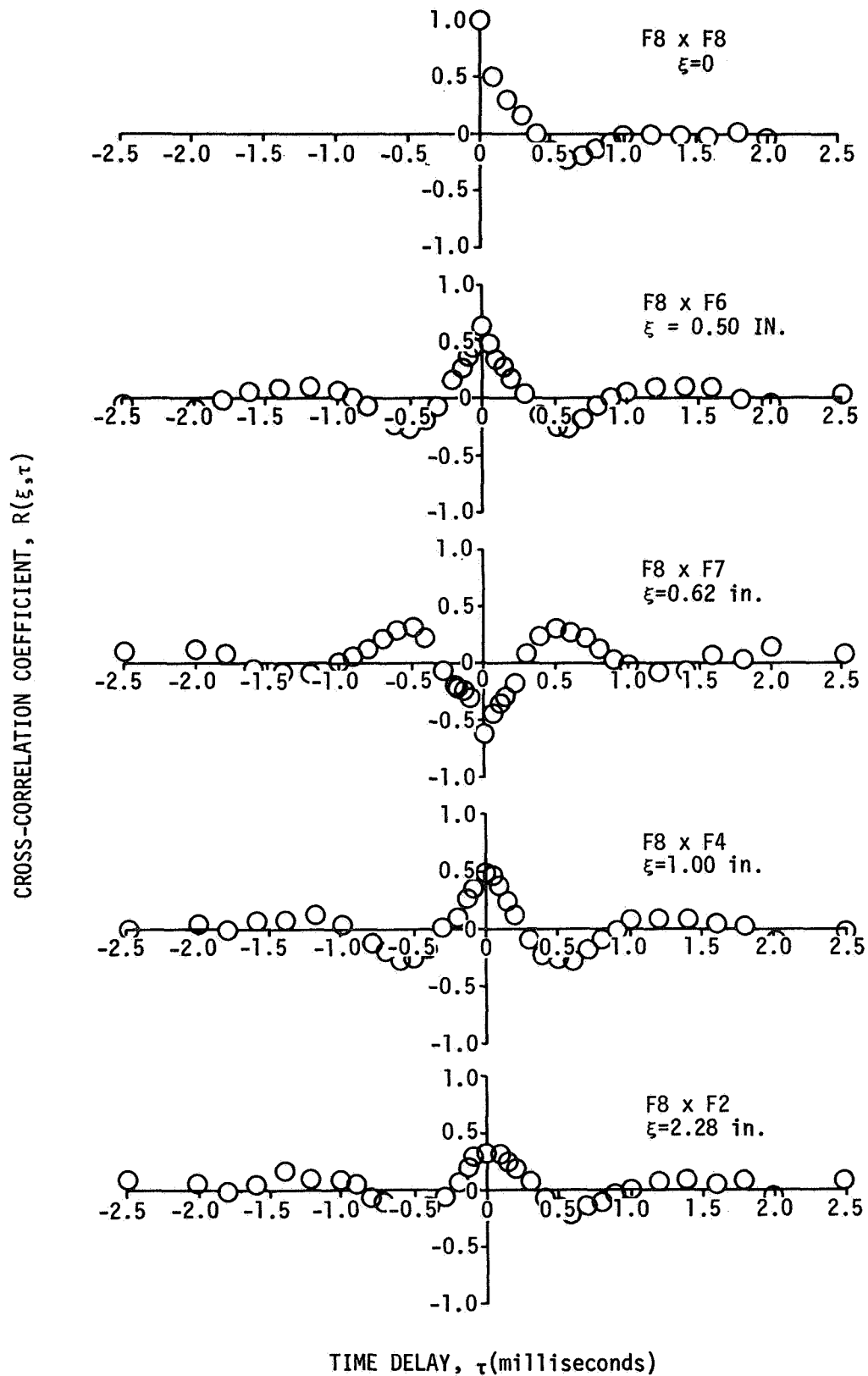FOUR-JET CONFIGURATION (P_o = 1500 psig)

Figure 4-28. BASE TRANSDUCER CROSS-CORRELOGRAMS FOR SATURN
CONFIGURATION (P_o = 900 psig)

$$R(\xi,\tau) = J_o(k_o\xi)\cos\omega\tau + \frac{4}{\pi}\sum_{n=o}^{\infty}\frac{J_{2n+1}(k_o\xi)}{2n+1} \qquad (2-19)$$

The cancellation property observed from the plots of correlation coefficient for increasing separation is predicted from this relation since

$$\lim_{\xi\to\infty} R(\xi,\tau) = 0 \qquad (2-20)$$

The relation can be used, moreover, to predict the behavior of the correlograms near zero time lag if a typical frequency is chosen. For a wave number of k_o = 5, i.e., f ~ 5 kHz, an evaluation was made for separation distances of ξ = 0, 0.1, and 0.2 foot. This range exceeds any transducer separation available on the Cluster Model baseplate. The behavior of the correlation coefficient near zero time lag as predicted from equation 2-19 is shown in Figure 4-29. It is seen that the peak value occurs for $\tau \leq$ 0.02 ms in the range of transducer spacings available in these tests. The observed existence of peak correlations near zero time lag is accordingly considered an acoustic manifestation.

The spatial correlation is defined by $R(\xi,o)$ and is given by

$$R(\xi,o) = J_o(k_o\xi) \qquad (2-21)$$

It is recalled that a condition for the derivation of equation (2-19) through (2-21) is that the pressure field be homogeneous. If so, the data from all transducer pairs may be plotted as a function of separation distance without other regard to their relative orientation. Such a comparison is made for the Saturn configuration in Figure 4-30. Considering the simplicity of the mathematical model used the agreement is good. This lends further credence to the assertion that the dominant loading mechanisms of these tests is essentially acoustic. It shows, moreover, that the reversals in sign of the peak correlation are a basic characteristic of transducer location.

The preceding results show the most characteristics of the dynamic pressure loads at the base of the engine clusters of this study can be explained as due to acoustic loadings. There is evidence, however, that recirculation exists in
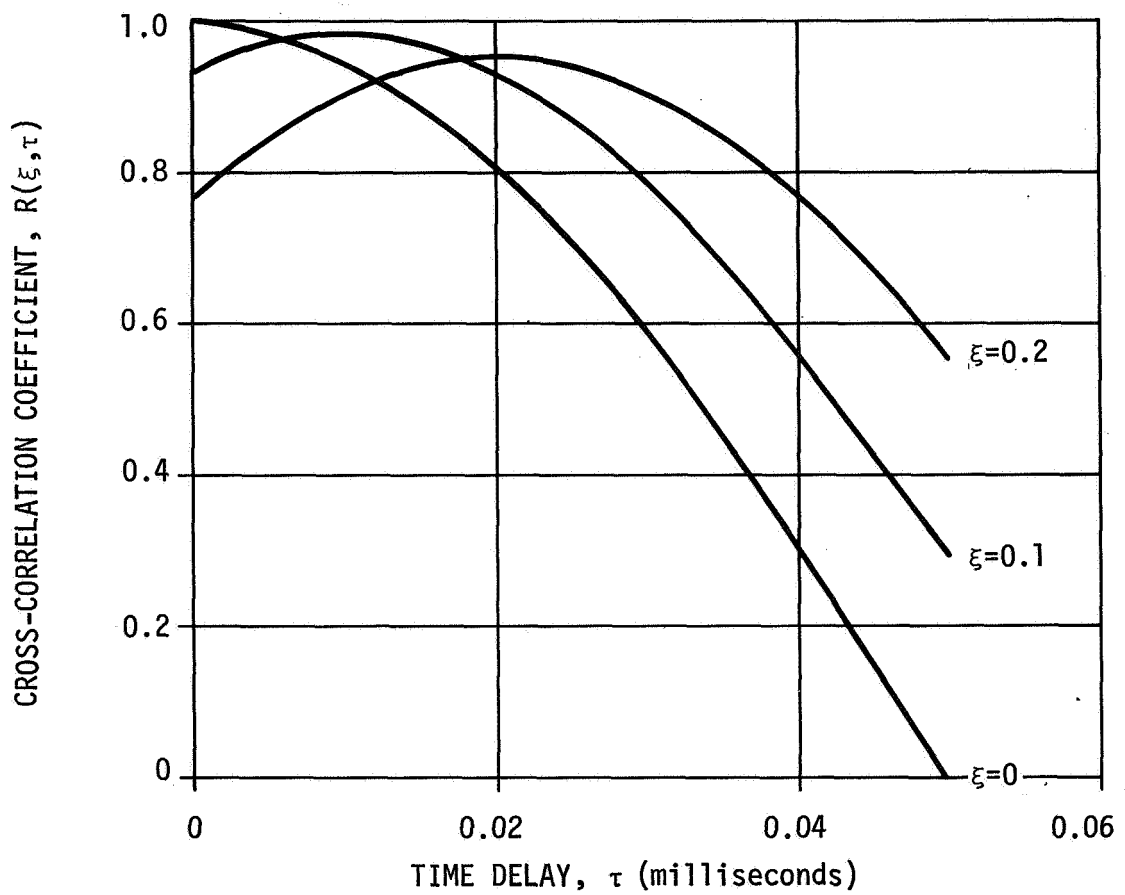
Figure 4-29. BEHAVIOR OF ACOUSTIC PROPAGATION MODEL CROSS-CORRELATION NEAR ZERO TIME LAG FOR A "TYPICAL" FREQUENCY OF 5 kHz
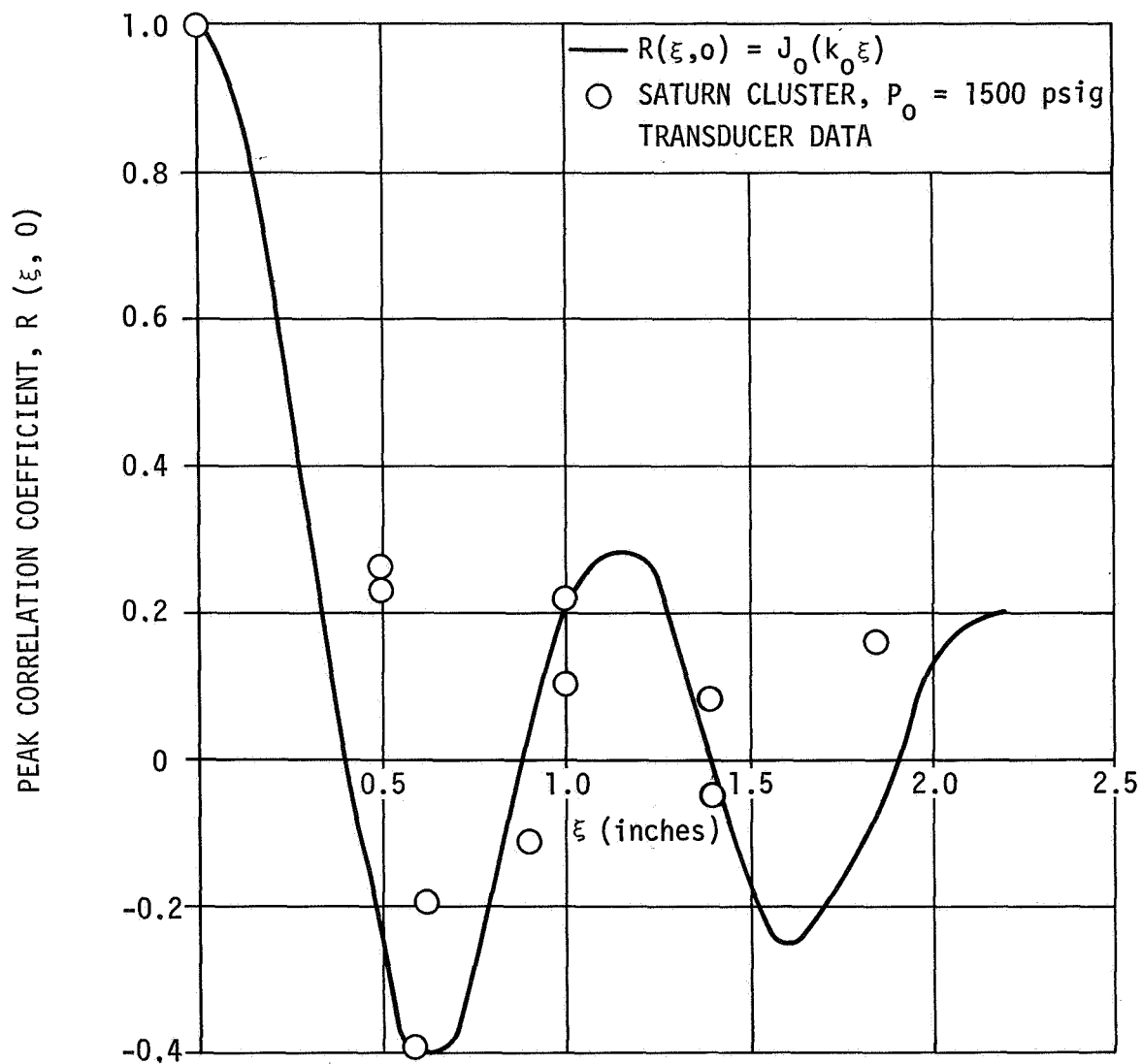
Figure 4-30. COMPARISON OF SPATIAL CORRELATIONS TO ACOUSTIC PROPAGATION MODEL

those tests where closure of the plumes is attained. Although the mathematical
formulation presented is an admitted simplification of the actual case where
waves of all frequencies exist, it appears that the approach taken could be ex-
tended to give a realistic model of the base pressure problem.

Section V

CONCLUSIONS

The preceding presentation of results revealed several important aspects of the loadings induced at the base of clustered rocket engines. In this section those observations will be summarized, the possible influence of facility associated factors on the data discussed, and some tentative remarks as to the influence of the findings on Saturn class vehicles presented.

5.1   SUMMARY OF SIGNIFICANT RESULTS

Two trends noted from mean measurements taken in the plumes near the nozzle exit plane were that the velocity profiles in the potential region are non-uniform and that the shear layer thickness is dependent upon the stagnation-to-ambient pressure ratio. Both of these factors may be of importance in the scaling of base load data from underexpanded flows. The former result implies that a higher mean velocity exists in the shear layer than would be experienced for uniform flow in the potential core of the jet. A shear layer thickness dependent upon pressure ratio implies that the scale of turbulence in the jet may be altitude dependent. This observation, however, must be tempered by the fact that no correction has been made for the curvature of the plume boundary.

Sound pressure levels as determined from far-field microphone data were found to scale directly with the total mechanical power of the exhaust flow. Clustered exhausts, however, showed a lower overall sound pressure level than would a single jet of the same mechanical power. Loads measured at the base of clusters did not exhibit such a well-defined behavior. Although the general trend was an increase of mean square dynamic pressure with jet power, there existed sufficient differences in the results to preclude the determination of an explicit relationship such as noted for far-field results. It appears, therefore, that the development of a general scaling relationship for base pressure loadings will require consideration of the individual sources of such loads including sound produced by turbulence, shock-turbulence interactions as well as convected pressure disturbances.

The power spectral density results, for both microphone and base transducers, appear to be weighted to higher frequencies than data obtained in hot flow models of size and exit Mach numbers comparable to the present model. It was noted that this discrepancy could be resolved if the Strouhal number definition employed was corrected by a ratio of stagnation temperatures between the hot flow and cold flow tests. This suggests that scaling of frequency results independent of jet temperature may be an oversimplification. Additional studies would be required to resolve this point.

Tests of the Saturn configuration showed spectral results that exhibited relatively narrow band components. At stagnation-to-ambient pressure ratios, of $P_o/P_a = 63.5$ and $P_o/P_a = 105.2$, the spectra showed a dominant peak at 0.63 kHz that was some two orders of magnitude higher than values outside its influence. It was found at the higher pressure ratio, however, that this result did not always occur. This anomaly is regarded as evidence of an instability in a sound producing mechanism. It is possible, also, that more severe cases of narrow band spectral components may lie between the pressure ratios tested.

In these tests the variation of the mean static and dynamic pressures on the base was found to be independent of location for most cases studied. It was shown that constant values of dynamic pressure are characteristic of acoustic wave propagation on the baseplate. For most cases tested, therefore, the dominant loading mechanism is believed to have been acoustic in nature. Use of a source location criterion due to Dyer (ref. 32) showed the probable dominant source location to have been the subsonic portion of the plumes.

Exceptions to the behavior noted above were found in tests of the symmetric four jet configuration. The results obtained showed the mean static pressures to vary from 0.8 psi above ambient to 0.8 psi below ambient at pressure ratios of $P_o/P_a = 105.2$ and $P_o/P_a = 63.5$, respectively. A definite gradient in mean and dynamic pressures were found with the extreme values noted at the center of the baseplate. The difference in results for this configuration is attributed to flow in the base region. Cross-correlation of transducer pairs did not, however, verify this convection hypothesis. On the basis of a stagnation flow model,

it was estimated that the observed pressure distribution in the center of the baseplate could result for a velocity of approximately 50 ft/sec, i.e., 4 percent of the mean velocity in the shear layer. The data indicate that recirculation, if the cause of these results, may present a more severe loading condition than pure acoustic radiation.

5.2 INFLUENCE OF FACILITY CHARACTERISTICS ON THE DATA

In the preceding sections, data obtained have been discussed in view of the probable physical processes resulting from jet noise and interactions. It is equally possible that the data obtained could be due, in part, to other influential factors. Although this is not believed the case, a brief discussion of two such factors is presented below.

Since the Thermal Acoustic Jet Facility has not been previously used for the present base loading application, the question arises as to whether the statistical characteristics of the base pressures are simply a manifestation of some facility disturbance. Accordingly, investigations of settling chamber dynamic pressures were made for chamber pressures from P_o = 200 to 2000 psig over a mass flow range from 15 to 75 lb/sec. These results are reported in reference 33. It was found that the spectral content of these signals peaked at frequencies of 200 Hz and 8000 Hz. A comparison of those results to the spectra of the nozzle mounted transducers used in the cluster tests showed the nozzle pressures possessed similar spectral distributions. The absence of such dominant peaks in the base pressure data indicates, therefore, that the chamber pressure spectral content was probably not an influential factor in the present tests.

Of much more concern in these experiments was the influence of extraneous vibrations of the model. It is well known that piezoelectric transducers are quite sensitive to vibrations and may effectively act as accelerometers. Two possible vibratory excitations to be considered then are the fundamental frequency of the facility at the plate location and that of the plate itself. This latter case was the subject of reference 34 where it was shown on the basis of experiment and a simple analysis that the first natural frequency of the base – plate was in excess of 12 kHz. In the case of the massive cold flow duct a

much lower frequency would be expected. The only significant excitation in the vicinity of the TAJF, however, is a large compressor in an adjacent building. This compressor does introduce noticeable facility vibrations but in view of the compressor speed (0.01 kHz) these vibrations are well below the lower cut-off frequency of the data presented. It is concluded, therefore, that extraneous vibrations were not an influential factor.

5.3 SOME IMPLICATIONS FOR SATURN CLASS VEHICLES

From the preceding discussion, it is apparent that any attempt to extrapolate the present results to vehicles of the Saturn class must necessarily be argumentative. There are, nevertheless, some facets of the data that are worthy of comment in the context of trends that may be expected in the flight of such vehicles.

The magnitude of the dynamic pressure at the base of the vehicle for the predominately acoustic loads of the Saturn configuration tests varied from 0.05 to 0.10 psi, increasing with the stagnation-to-ambient pressure ratio. This value was, moreover, essentially constant over the plate.

A simple scaling based on dynamic pressure ratios between the shear layers of the Cluster Model and the Saturn S-IC stage would indicate that pressure loadings should be comparable in each case. The heat shield of the S-IC stage would, accordingly, experience a dynamic load of 2500 to 5000 lbs during flight. It must be recalled in this regard that the present data indicate that pressure loadings tend to increase with jet mechanical power. Furthermore, conventional scaling laws for jet noise require the radiated power to vary with the cube of the jet velocity up to the eighth power of velocity. The value quoted, therefore, is undoubtedly conservative. It may also be noted that the larger load quoted above occurred at the highest value of stagnation-to-ambient pressure and, hence, the highest effective altitude. Similar considerations can, therefore, be made for the S-II stage of the Saturn vehicle.

Loads of these magnitudes pose no particular concern to a vehicle as massive as the Saturn V if fairly broad band in nature. The strong spectral peaks noted earlier for the Saturn configuration at intermediate to high stagnation pressures thus becomes of particular interest. Increases in stagnation-to-ambient pressure

ratio would correspond, for a given nozzle, to increasing flight altitudes.
It is possible, therefore, that the fairly broad band spectra of low altitudes
undergoes a transition until a narrow band spectrum is attained at some inter-
mediate altitude. It would, accordingly, be possible for the lower energy
modes of the structure to be excited by a concentrated load of 5000 lb at the
proper frequency.

A simple Strouhal number scaling has been attempted for the data of this
study. Defining the Strouhal number by

$$S = \frac{f\delta}{\overline{V}}$$

where δ is the shear layer thickness near the plume intersection point and $\overline{V}$
the mean velocity in the shear layer, an equivalent frequency to the 0.63 kHz
spectral peak of the data may be obtained for the Saturn S-IC stage. Estimating
the shear layer thickness from the spreading parameter given by Korst (ref. 7)
and the velocity from F-1 engine data results in an equivalent frequency of
12 Hz for the S-IC stage. Applying the temperature correction implied by the
data would reduce this dominant frequency even more. Such a result would be
transient, however, since the spectra return to an essentially broad band
characteristic shape at higher pressure ratios.

In closing, it should be noted that recirculation occurs on Saturn vehicles
(ref. 35). Although the present experiment did not show such effects for the
five jet cluster, the data imply that when recirculation is present the magni-
tude of the fluctuating base load may be greatly increased.

Section VI

RECOMMENDATIONS

The results of this investigation show that significant loadings may be induced at the base of engine clusters by underexpanded clustered rocket exhausts. From the data obtained it is concluded that acoustic radiation from the subsonic region of the plume is the dominant source of excitation. Only limited indications of recirculation were found in this study, possibly since the important interaction of the free stream with the plumes was not present. For that case where recirculation was suspected, the loading was found to be more severe than was observed for purely acoustic radiation.

The formulation used to relate the behavior of the dynamic pressure data to the properties of acoustic waves of random incidence was surprisingly successful. Such an approach may prove a useful tool for further analysis. It is noted in this regard that this model, developed for a discrete frequency, can be extended to random frequency distributions if sufficient knowledge of the spectrum function is possessed.

Future studies of the base loading problem appear warranted in view of the tendency of Saturn configuration spectra to approach a narrow band excitation at certain pressure ratios, to explore the possible influence of temperature on the measured results, and to resolve the uncertainty in scaling such results. In that event, consideration should be given to the use of a more versatile model. Since the use of a single type of nozzle precludes studies of the change in turbulent scales or jet velocity, future models should be capable of using interchangeable nozzles. Other variables requiring study include the influence of the set-back distance of the base from the nozzle lip and the effect of nozzle spacing. Instrumentation of the baseplate should be more complete than in the present study where transducers were confined to an octant of the plate. Such a restriction complicates the interpretation of data or, for cases where symmetry is lacking, renders interpretation impossible.

Recirculation, as noted above, may ultimately prove more influential on the base loading than acoustic propagation. Since these effects were only observed at high stagnation-to-ambient pressure ratios, future studies should extend the range to values of P_o/P_a = 150 which is within the capability of the Cold Flow Duct. A method for flow visualization such as using a smoke generator should be considered for the base region. Also worthy of consideration is the use of shrouds to simulate the free stream-plume interaction. Successful development of such a shroud would allow determination of the influence of that interaction on the establishment of reverse flows in configurations lacking closure.

Several procedural changes would be well advised for future studies. First, the determination of the acoustic field generated by the jet exhausts should be a major consideration in base loading tests. This can be readily ac-complished by making a complete microphone traverse as part of the test procedure. Secondly, the use of a Crossed-Beam (optical correlation) technique would be of use in determining the velocity (convection speed) distributions in the shear regions of the jet. Such results may ultimately be of more value than the pitot data of the present study. Finally, data acquisition should be extended to a higher frequency range than the 20 kHz upper cut-off frequency used. This fre-quency restriction was imposed due to the multiplexing system used in the study. Since cross-correlation of transducer records yielded little useful information, consideration should be given to relaxing the multiplexing requirement so that the frequency range of the data can be extended.

In view of the consistency of the data obtained and the general conformance to results obtained in similar investigations, the conclusion must be made that the Thermal Acoustic Jet Facility is well-suited for studies of acoustic loadings on missile structure. The experience gained from these tests, however, suggests that a more complete calibration of the facility should be made to determine the basic noise and acceleration levels in the facility area under no-flow con-ditions as well as with flow.

Section VII

REFERENCES

1. Bisplinghoff, R. L., Ashley, H., and Halfman, R. L., *Aeroelasticity*, Addison-Wesley, Reading, Mass., 1957.

2. Bull, M. K., Welby, J. F., and Blackman, D. R., "Wall Pressure Fluctuations in Boundary Layer Flow and Response of Simple Structures to Random Pressure Fields," U. of Southhampton, AASU Report No. 243; July, 1963.

3. White, R., "Structural Response of Beams & Structures," Acoustics Short Course, U. of Ala. in Huntsville, 1967.

4. Crandall, S. H., and Mark, W. D., *Random Vibration in Mechanical Systems*, Academic Press, 1963.

5. Fisher, M. J., and Krause, F. R., "The Crossed Beam Correlation Technique," Journal of Fluid Mechanics, V. 28, Part 4, June 22, 1967, pp 705-17.

6. Zumwalt, G. W., Analytical and Experimental Study of the Axially-Symmetric Supersonic Base Pressure Problem, PhD Dissertation, U. of Ill., 1959.

7. Korst, H. H., Page, R. H., and Childs, M. E., "Compressible Two-Dimensional Jet Mixing at Constant Pressure," U. of Ill. Engr. Experiment Station Report ME-TN-392-1, OSR-TN-55-99, Apr. 1955.

8. Goethert, B. H., "Base Flow Characteristics of Missiles With Cluster-Rocket Exhausts", IAS Paper No. 60-89, July 1, 1960.

9. Goethert, B. H., "Base Heating Problems of Missiles and Space Vehicles", ARS Reprint No. 1666-61, Mar. 1961.

10. Lighthill, M. J., "On Sound Generated Aerodynamically, I. General Theory," Proc. Royal Society (London), A211, pp 564-587, (1952).

11. Lighthill, M. J., "On Sound Generated Aerodynamically, II. Turbulence as a Source of Sound," Proc. Royal Society (London), A222, pp 1-32 (1954).

12. Richards, E. J., Mead, D. J., *Noise and Acoustic Fatigue in Aeronautics*, Wiley and Sons, Ltd. London, 1968.

13. Krause, F. R., "Wall Pressure Fluctuations and Skin Vibrations with Emphasis on Free Shear Layers and Oscillating Shocks", NASA TMX 53189, Oct. 1964.

14. Powell, A., "On the Response of Structures to Random Pressures and to Jet Noise in Particular," in *Random Vibration*, Wiley & Sons, Inc., New York, 1958.

15. Tidmore, W. C., "Data Report, The George C. Marshall Space Flight Center's Cold Flow Duct, Thermal Acoustic Jet Facility, Test No. TAJF-009", Nortronics-Huntsville Report, March, 1968.

16. Mallard, S. R., "Data Report, The George C. Marshall Space Flight Center Cold Flow Duct, Thermal Acoustic Jet Facility, Tests Numbers TAJF-010 and -011", Nortronics-Huntsville Report, April, 1968.

17. Barnett, D. O., "Plume Characteristics of the Saturn Cluster Model," Nortronics-Huntsville Memo No. 51, 23 December 1968.

18. Delaney, B. R., "Pretest Information for a Study of Five Clustered Nozzles", Nortronics-Huntsville Memorandum, 2 March 1967.

19. Barnett, D. O., "Pretest Information for Schleren Stills and Movies of S-II Cluster Model in TAJF", Nortronics-Huntsville Memorandum, 14 September 1967.

20. Barnett, D. O., "Pretest Plans for Base Pressure Determination on Saturn Cluster Model in TAJF", Nortronics-Huntsville Memorandum, 20 Sept. 1967.

21. Bush, H. T., "Check-out of Magnetic Tape and Multiple Equipment to be used for Cross Correlation Studies", MSFC Memorandum, 3 December 1965.

22. Bradford, J. W., Hinds, W. E., "Preliminary Evaluation of the Piecewise Correlation Program for Non-Stationary Data", Northrop Technical Report M-792-7-208, July 1967.

23. "Technical Manual Instructions for Model 9410 Time Delay Correlator," Honeywell Co., Denver, Colorado, May 1965.

24. "Catalog Specifications", Bruel and Kjäer Co., Naerum, Denmark, 1965.

25. Abramovich, G. N., The Theory of Turbulent Jets, M.I.T. Press, Cambridge, Mass., 1963.

26. Che-haing, Chiang, "Axially Symmetric Supersonic Turbulent Jets Discharged From a Nozzle with Underexpansion", in Turbulent Jets of Air, Plasma and Real Gas, Consultants Bureau, New York, 1969.

27. Von Gierke, H.E., "Aircraft Noise Sources", in Handbook of Noise Control, McGraw-Hill, 1957.

28. Potter, R.C., and Crocker, M.J., "Acoustic Prediction Methods for Rocket Engines, Including the Effects of Clustered Engines and Deflected Exhaust Flow," NASA Contractor Report NASA CR-566, October 1966.

29. Kolb, A. W. and Maurer, O.F., "A Brief Review of Noise Effects on Aerospace Structure", in Noise Generation and Suppression in Aircraft, U. of Tennessee Space Inst., 1968.

30. Schlicting, H., Boundary Layer Theory, McGraw Hill, New York, pp 78-83, 1960.

31. Corcos, J. W., Cuthbert, J. W., Von Winkle, W. A., "On the Measurement of Turbulent Pressure Fluctuations With a Transcuer of Finite Size," U. of Cal., Inst. of Engr. Research Report 82-12, Nov. 1959.

32. Dyer, I., "Estimation of Sound-Induced Missile Vibrations," in Random Vibration, Wiley & Sons, 1958.